Numerical simulation of the interaction between flow and flexible nets using a porous surface model

Sarath Krishnan Karumathil

Advisor: Manuel Jesús González Castro

Doctoral thesis

Programa Oficial de Doutoramento
en Enxeñaría Naval e Industrial

Ferrol, 2022

Dr. Manuel Jesús González Castro, Doctor by the University of A Coruña, certify that this doctoral dissertation, entitled Numerical simulation of the interaction between flow and flexible nets using a porous surface model, has been developed by Sarath Krishnan Karumathil under my supervision in order to obtain the International Doctor mention by the University of A Coruña.

Dr. Manuel Jesús González Castro, Doctor por la Universidad de A Coruña, certifca que la presente memoria, titulada Numerical simulation of the interaction between flow and flexible nets using a porous surface model, ha sido desarrollada por Sarath Krishnan Karumathil bajo su supervisión para optar al grado de Doctor con mención Internacional por la Universidad de A Coruña.

Ferrol, 2022.

Sarath Krishnan Karumathil	Dr. Manuel J. González Castro
PhD. student	Advisor
Estudiante de doctorado	*Director de tesis doctoral*

Acknowledgements

A doctoral thesis despite being a personal achievement, is a work which needs support in both personal and professional level for many years.

Firstly, I would like to express my deepest gratitude to my advisor, Prof. Manuel Jesús González Castro, for guiding me throughout all these years to complete this thesis and sharing his excellent passion for research and knowledge with me, without his help, this thesis and my stay in Ferrol might not be possible.

I would like to extent my sincere thanks to my colleagues at the Laboratorio de Ingeniería Mecánica (LIM) of the University of A Coruña : Javier, Miguel, Urbano, Daniel, Alberto, Emilio, Florian, Fran González, Fran Mouzo, Borja, Álvaro, Manu, Mario, Fran Bottero, David and Amelia for providing a great working environment and joyful moments we have shared together. I would like to acknowledge the help provided by Alberto for the help he provided to solve numerous technical problems starting from my first day at LIM.

Special Thanks to Barry accepting and guiding me during my research stay in Hirtshals, Denmark; Thanks to the whole DTU Aqua team in Hirtshals for the warmest welcome they have given me during my stay. It was a pleasure working with them.

Finally, I would like to express my heartfelt thanks to the closest people for all the personal support they have given me during the good and bad times. I would like to thank my father (kunjikrishnan), my mother (Rathy), My sister (Anju) and my friends back in kerala for supporting me from distance, I know it is very difficult and lastly to my friends here in ferrol for providing a home away from home.

Agradecimientos

Una tesis doctoral a pesar de ser un logro personal, es un trabajo que necesita apoyo tanto a nivel personal como profesional durante muchos años.

En primer lugar, me gustaría expresar mi más profundo agradecimiento a mi tutor, el Prof. Manuel Jesús González Castro, por guiarme durante todos estos años para completar esta tesis y compartir conmigo su excelente pasión por la investigación y su conocimiento en muchas areas. sin su ayuda, esta tesis y mi estancia en Ferrol no serían posibles.

Quisiera extender mi más sincero agradecimiento a mis compañeros del LIM de la Universidad de A Coruña: Javier, Miguel, Urbano, Daniel, Alberto, Emilio, Florian, Fran González, Fran Mouzo, Borja, Álvaro, Manu, Mario, Diego, Fran Bottero, David y Amelia por brindar un excelente ambiente de trabajo y momentos felices que hemos compartido juntos. Me gustaría remarcar la ayuda que me han dado por Alberto por la ayuda para resolver numerosos problemas técnicos desde mi primer día en LIM.

Un agradecimiento especial a Barry por aceptarme y guiarme durante mi estancia de investigación en Hirtshals, Dinamarca; Gracias a todo el equipo de DTU Aqua en Hirtshals por la más cálida bienvenida que me han brindado durante mi estadía. Fué un placer trabajar con ellos.

Por último, me gustaría expresar mi más sincero agradecimiento a las personas más cercanas por todo el apoyo personal que me han dado en los buenos y malos momentos. Me gustaría agradecer a mi padre (Kunjikrishnan), mi madre (Rathy), mi hermana (Anju) y mis amigos en Kerala por apoyarme desde la distancia, sé que es muy difícil y, por último, a mis amigos de aquí en Ferrol por brindarme un hogar lejos de casa.

Abstract

Computational simulation is getting more and more attention in the recent years in the areas of understanding and improving many aspects of fisheries. Fishing nets are a major component of a fishing gear and are one of the complex parts in order to simulating them. The objective of this thesis is to use Computational Fluid Dynamics (CFD) to simulate the hydrodynamics of the fishing nets considering them as porous surfaces. This method greatly simplifies the pre-processing when the problem has complex netting geometries, as in fishing gears. The thesis also presents a new method for finding the resistance coefficients of Darcy-Forchheimer equation for porous media, required for the porous surface method and investigate the importance of both inertial and viscous porous resistance coefficients. The developed model is applied to study bottom trawling and the effect of fishing nets on sediment transport. In this study, the effect of different parameters while towing a net close to the seabed is investigated to find their significance in mobilising the sediment and on hydrodynamic forces.

Resumen

La simulación computacional está recibiendo cada vez más atención en los últimos años en las áreas de comprensión y mejora de muchos aspectos de la pesca. Las redes de pesca son un componente importante de un arte de pesca y son una de las partes complejas para simularlas. El objetivo de esta tesis es utilizar la dinámica de fluidos computacional (CFD) para simular la hidrodinámica de las redes de pesca considerándolas como superficies porosas. Este método simplifica enormemente el procesamiento previo cuando el problema tiene geometrías de red complejas, como en los artes de pesca. La tesis también presenta un nuevo método para encontrar los coeficientes de resistencia de la ecuación de Darcy-Forchheimer para medios porosos, requeridos para el método de superficie porosa e investiga la importancia de los coeficientes de resistencia porosa inercial y viscosa. El modelo desarrollado se aplica para estudiar la pesca de arrastre de fondo y el efecto de las redes de pesca en el transporte de sedimentos. En este estudio, se investiga el efecto de diferentes parámetros mientras se remolca una red cerca del lecho marino para encontrar su importancia en la movilización del sedimento y en las fuerzas hidrodinámicas.

Resumo

A simulación computacional está a recibir cada vez máis atención nos últimos anos nas áreas de comprensión e mellora de moitos aspectos da pesca. As redes de pesca son un compoñente importante dunha arte de pesca e son unha das partes complexas para simulalas. O obxectivo desta tese é utilizar a dinámica de fluídos computacional (CFD) para simular a hidrodinámica das redes de pesca considerándoas como superficies porosas. Este método simplifica enormemente o procesamento previo cando o problema ten xeometrías de rede complexas, como nas artes de pesca. A tese tamén presenta un novo método para atopar os coeficientes de resistencia da ecuación de Darcy-Forchheimer para medios porosos, requiridos para o método de superficie porosa e investiga a importancia dos coeficientes de resistencia porosa inercial e viscosa. O modelo desenvolvido aplícase para estudar a pesca de arrastre de fondo e o efecto das redes de pesca no transporte de sedimentos. Neste estudo, investígase o efecto de diferentes parámetros mentres se remolca unha rede preto do leito mariño para atopar a súa importancia na mobilización do sedimento e nas forzas hidrodinámicas.

Contents

List of Figures

List of Tables

Chapter 1

Introduction

1.1 Motivation

Fish and other living organism in the sea plays a big role as a food resource for the world population. In different part of the world there exist many ways to both cultivate the fish for food and also to catch the fish from the sea. Bottom trawling and purse seine fishing techniques account for the 53 % of the global fish catch and bottom trawling causes over 60 % fish discards [4]. The recent decades were crucial for both fisheries and aquaculture industry since the demand for the fish has increased exponentially and also the need for making these industries more eco-friendly. The Food and Agriculture Organization of the United Nations (FAO) imposed landing regulations demanding fisher folk to improve their fishing gear selectivity in order to conserve and revitalize the fisheries [5]. Improving selectivity of fishing gears and finding regulations for the fishing gears according to the target species need many investigations including experiments in flume tanks and sea trails for the changes we make in a fishing gear. There are notable developments in the computational power available during the last decades and thus inviting more investigations on computational simulation of fishing gears to improve the selectivity, reduce the environmental impact associated with different fishing techniques. Fishing net being the major part of a fishing gear, being flexible in nature is a challenging part to simulate in trawling fisheries.

This thesis intends to improve the existing methods for the simulation of fishing nets using computational fluid dynamics, in order to deal with complex shapes which can be seen in real life fishing gears. The previous researches on simulation of fishing nets were mainly focused on aquaculture cages and have used a method that models the net as thin solid. Applying that method to complex fishing gears need a lot of pre-processing work and is prone to human errors. In this thesis, a new method of modelling netting panels as porous surfaces is developed as a solution to deal with complex shapes which can be seen in fishing gears.

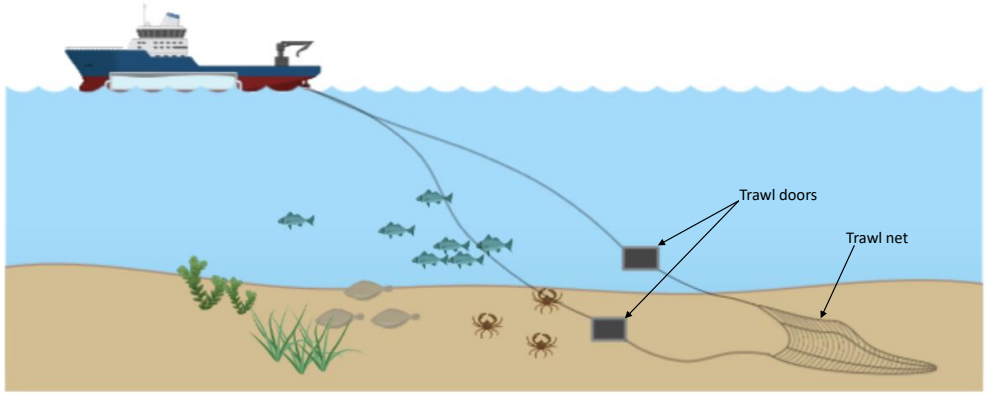

Figure 1.1: Bottom trawling to catch species living near the seabed.

1.2 Background

Fishing industry and aquaculture are facing many challenges demanding more research and innovation. Different landing obligations around the world to protect the fish stocks force fisherfolk to improve the selectivity of the fishing gears. Regarding the environmental aspect of fishing techniques, improving the efficiency is always a goal anglers seek to achieve. Fishing techniques like demersal trawling are famous for their impact on the seabed and research in these areas are important for a better ans selective catch without destroying the benthic environment in the seabed. In case of aquaculture, the increasing need of fish as a food source are forcing the industry to implement more cages in places where there are high current flows.

Demersal trawling, often referred as bottom trawling is a fishing technique where the fishing gears are trawled along the seabed in order to catch the marine species living in the bottom of the sea. The fishing gear used in this type of fishing includes otter boards (trawl doors), floats, bridles, sweep, floats, sinkers etc. Some of these parts can come in direct contact with the seabed while others move close to the seabed. This method of fishing is widely discussed because it produces a significant amount of bycatch, disturbs the seafloor, and damages other seafloor living things. Fishing net is the major component of the fishing gear and contributes to around 85% of the drag produced while trawling. Additionally, it has a significant impact on bycatch in terms of species and size of the fish, demanding more research in improving them for sustainable fishing. The research includes experimental studies in flume tanks of scaled fishing gears, sea trails of fishing gears with force sensors for finding the hydrodynamic forces caused, cameras for capturing the fish movement before the fishing gear and also inside the gear for understanding the areas where the modifications can be made for improving the selectivity. On field experimental investigations in these areas are time consuming and costly. A sea trail in order to find

the selectivity of a fishing gear might take weeks and even months to deduce results which demands for numerical experiments in advance. Increasing computational power in the recent years allow us to use computational simulations for analysing many related physics which may be difficult to understand with experimental investigations. Numerical simulations on real scale fishing gears and aquaculture net cages can help us to understand the hydrodynamics and to improve their efficiency in many areas. The main component in both of these cases is the fishing nets. Computational simulation of fishing nets in water is a fluid structure interaction problem. The fishing nets are flexible in nature and they change their shapes in the water.

1.3 Previous technical works

Study on behaviour of fishing nets in water is mainly focused on two main areas, Fisheries and Aquaculture. Nets are the major component in both fishing gears used in fisheries and net cages used in aquaculture industry.

1.3.1 Developments related with fisheries

The study of fishing nets began many decades ago with the primary goal of increasing the efficiency of fishing gear and reducing fuel consumption. This is primarily due to the drag forces generated while trawling the fishing gear. The net, which is the most important part of the fishing gear, has a significant impact on the hydrodynamic forces. Many studies have investigated analytical methods for finding the hydrodynamic forces caused by the fishing net in a water flow considering the effect of whole net twines and knots as the superposition of them individually. One of the oldest studies were done by [6] where they divided the net in the fishing gear into 4 different parts and calculated the drag individually to find the total drag caused by the fishing gear and validated the developed analytical model with experimental results conducted on a 50 feet flat shrimp net in the sea.

Investigations on fisheries in the earlier stage were mainly focused on the structural part of the coupled problem and finding the hydrodynamic forces from the Morison force models. Regarding the structural behaviour of netting, many contributions have been published in the last three decades: analytical models for twine deformation [7] and for nets with axisymmetric shape [8], lumped mass models of different types [9–12],finite-element models of twines [13] and netting [14], and methods to improve the efficiency of the numerical simulations [15, 16]. Procedures to measure the mechanical properties of netting have also been proposed in order to calibrate the numerical models [17–19].

[20] introducing a source term for representing the impact caused by the net. The source vector which depends on the velocity was resolved using the following formula written in conservative form:

$$U_{n+1} = U_n + \frac{\partial F}{\partial x} + S\left(U_n\right) \tag{1.1}$$

where U is the vector of conservative variables and F physical flow in one direction. Similar to this way of modelling fishing nets by adding the additional effect of fishing

nets in the source term of the Navier-Stokes equation, researchers later started using porous media to represent the net in water [1, 21, 22]. [23] used a porous media method in order to simulate the hydrodynamics of flow through plankton nets. [24] investigated the hydrodynamics around a scaled fluttering codend. find out that the fluttering motion is a low frequency activity which changes the fluid forces acting and the porosity of the codend. For the experiments, they predicted a vertical motion in the codend with an order of tenth of the diameter of the codend. Also demonstrating the complex fluid structure interaction resulting the wake hydrodynamics of the codend structure and the fluttering motion of the codend. [25] introduced an adaptive mesh refinement to model water flow around fishing nets and applied fluid structure interaction for predicting the behaviour of underwater nets for applications in fisheries. They have used a fluid model, which is a resolution of psuedo-compressible adaptation of Navier-Stokes equation. [26] investigated on fluid structure interaction simulation on a scaled bottom trawl and compared the results with flume tank experiments. Hydrodynamic forces were calculated same as in [27] as the superposition of forces acting on each twine bar and finite element approach for structural solver. They carried out studies on two different material nets, a dyneema multifilament and nylon monofilament with increased mesh size and decreased twine diameter respectively and found out a decrease in drag of around 2 times compared to a polyethylene net trawl. Experimental works on bottom trawls with different designs including mouth opening, twine diameter, material were conducted for understanding the effect of them on hydrodynamic forces [28].

[29] studied the deformation characteristics of a knotless polyethylene net, representing net as cylinders using the non slip boundary condition and a one way FSI coupling. They found a bigger relative error between the simulations and experiments for nettings with smaller solidities.

[30] did experiments on netting panels with different type of twine materials, knots and weave patterns at smaller angles of attack. Their experimental setup is different from the traditionally used experimental setup ([1, 3]) allowing them to effectively measure the hydrodynamic forces at smaller angles of attack avoiding the bigger influence of frames on the results. Experiments demonstrated that the drag generated by the knots account over 20% of total drag of a netting without knots. Later [31] used porous media model coupled with a non linear FEM for simulating the hydrodynamics of various nets at smaller angles of attack for unsteady flows at low Reynolds numbers.

1.3.2 Developments related with aquaculture

With increased demand for seafood, aquaculture is getting more and more attention these years and are also in need of expanding from the coastal zones to further offshore high current areas. Offshore farms are an emerging approach that needs stronger cages able to withstand the high energy of the environment to avoid damage of the structure and fish escapes [32]. Implementing net cages in these difficult conditions also require study on net cages and its movement in water. The study on the flow through these cages are important to determine the health of the fish in the cages. It is a normal practice to have more than one cages in the same

current and it is important to find whether the cages in the wake of other cages are getting enough flow through them since the flow determines the oxygen passage and thus the health of fish.

Various investigations on fishing nets are from the fish farming industries where they use cages to grow fish in still water or in open sea. This technique of fish farming are very old and with an increasing demand of fish as a food source, there were more research in the past 4 decades. [33] did an extensive review of investigations on hydrodynamics inside and outside of aquaculture cages.

[27] investigated on fluid structural numerical simulations on submerged supple nets breaking the net into rigid cylindrical bars. Hydrodynamic forces were calculated by Landweber and Richtmeyer hypothesis which is an adaptation of the Morison equations. [34] combined theoretical and experimental work to derive formulae to calculate drag and lift coefficients of netting as a function of its solidity ratio, and to estimate the velocity reduction in the wake after a netting panel. [35] used a similar methodology to propose empirical and semi-empirical formulae for the same purpose, in some cases related to the Reynolds number. [3] carried out experiments on flat and circular net panels to develop analytical models for predicting drag forces and the influence of Reynolds number, net solidity, mesh pattern and flow direction on drag force accounted by the fishing net.

Three-dimensional Computational Fluid Dynamics (3D CFD) is a promising approach to study the interaction between the netting and the water flow. Detailed small-scale CFD simulations of aquaculture cages or fishing gear would be impractical, since the large size of the netting panels and the small size of meshes, twines and knots would result in an enormous number of cells that would require too many computational resources. To solve this problem, [1, 21] proposed to model the netting as a thin porous media volume and validated their model with flat net panel experiments. The flow through this porous media was described with the equations proposed by [36] and [37]. The porous media coefficients were calibrated from tow tank measurements of drag and lift forces on a net panel at different angles of attack. The predictions of this numerical model had good agreement with experimental measurements.

[35] measured hydrodynamic loads on plane net samples in steady and oscillating flows modelling the net as lumped masses and springs and came into a conclusion that drag coefficient for a net can be found by considering twines as cylinders and knots as spheres for steady flows. for unsteady flows, the drag coefficients depends on particle velocity and period of the wave and net porosity. [38] studied the effect on drag coefficients for a copper netting compared to traditional nylon nets and found out that copper nets in current shows significant reduction in drag forces.

[39] made FSI simulations using a porous media model for simulating the flow field and a lumped mas model for representing the flexible fishing net plane in steady current. The co-simulation algorithm introduced by them was by evaluating the flow field on the plane net to later finding the drag forces to get the new net configuration. The velocity field was applied again on the new net configuration for finding the new drag forces and net configuration, iterating this step until a convergence criteria for obtaining the final result. the porous media model used in this research was also modelled the fishing net as a solid porous volume with pressure drop equations

governed by [36, 37].

[40] developed the numerical model for flow through and around aquaculture cages, fluid flow field was found using the porous media governing equations given by [41]. They simulated a floater net system in current and waves, coupling a lumped mass model for the structural solver and considering net as dynamic porous zones for the fluid part. The application of this study was intended towards the aquaculture cages, which has a rigid floated ring controlled by mooring lines [42]. They have also carried out extensive investigations on finding porous coefficients by transformation of Morison type load model [43].

1.4 Objectives

The main objective of this thesis is to develop a method to numerically simulate the flow through fishing nets which can be applied to real scale fishing gears used in different fisheries around the world. This main objective can be itemized to the following parts:

- Computationally simulate the fishing nets modelling net as a porous surface in order to deal with complex shapes of netting which can be seen in the fishing gears.
- Investigate on the ways to find the porous coefficients of a given type of fishing net.
- Validate the methods developed using previous researches and experiments.
- Apply the method developed in problems related with fisheries and understanding the hydrodynamic influence of fishing nets on fishing techniques.

Given the previous objectives, the main contributions of this work are outlined as follows:

- A method of modelling the net as a surface to apply porous media models to simulate fishing gears, validated against experimental data.
- A new and efficient approach for finding the porous media resistance coefficients of a given fishing net using experimental measurements and 2D CFD simulations.
- An in-depth study on the effect of fishing nets trawled close to the seabed to understand and improve demersal trawling using numerical experiments using the surface modelling approach.

1.5 Thesis structure

This thesis has been organized in 5 chapters with the main three chapters (2,3,4) written as independent documents including the methodology, results and conclusions:

Chapter 1 present the introduction to the thesis including the background of the study, state of art discussing the recent development in the area and the motivation of the thesis and objectives wish to complete with the thesis.

Chapter 2 describes the implementation of a porous surface model and the validation with experiments from previous research.

Chapter 3 describes a new method to calculate the resistance coefficients of a porous media from experimental data.

Chapter 4 shows the usage of the model described in 2 for investigations and better understanding of effect of trawling the fishing net close to the seabed and the study of sediment entrainment due to fishing net being towed near to the seabed.

Chapter 5 concludes the works carried out in the thesis and also proposes the future research lines.

Chapter 2

Modelling net panels as porous surfaces

Fishing industry and aquaculture fields are facing more challenges in the recent years which requires accurate prediction of the response of flexible fishing nets in water. This flexible net in water is a fluid structure interaction problem. A detailed modelling of the netting as a solid structure with twines and knots for solving the fluid part of this fluid structure interaction problem is computationally expensive to simulate. As a necessary consequence, a porous media approach is used interpret the effect caused by the net, with the net modeled as a thin solid porous medium and the pressure drop across the net evaluated using the Darcy-Forchheimer porous media model. For real scale fishing nets, modelling netting as a thin solid porous media is still computationally expensive and difficult to model for complex netting shapes. In this research a new method is implemented where net is modelled as a surface and the cells close to the surfaces are grouped according to their orientation for applying the porous media resistance. This surface modelling approach not only minimizes the difficulties to model complex shapes but also reduces the computational expense by not having to mesh very fine across the thickness of the netting. It also aids for an easy coupling between solid solver and the fluid solver since nets are modelled as triangulated surfaces.

The current method has been validated with past experimental researches and a good fit was obtained between the results.

2.1 Introduction

Fishing and aquaculture industries are facing multiple challenges that demand new research and innovation. Recent regulations that aim to ensure the sustainable exploitation of fish stocks, such as the EU landing obligation introduced by the [5], foster the development of more selective and efficient fishing gears to reduce by-catches and minimize the impact of fishing on the marine ecosystems and environment [44]. In aquaculture, offshore farms are an emerging approach that needs stronger cages able to withstand the high energy of the environment to avoid damage of the structure and fish escapes [32]; in addition, water motion inside the cages is important for the fish health because it affects the distribution of nutrients and oxygen. Sea trials

of new fishing gears and aquaculture cages are very costly and time consuming, and therefore computational simulation is a valuable tool to design and optimize such underwater structures. Netting is the main component of these structures, hence computational models for netting are required to accurately predict both the structural and the hydrodynamic behaviour of the structure.

Regarding the structural behaviour of netting, many contributions have been published in the last three decades: analytical models for twine deformation [7] and for nets with axisymmetric shape [8], lumped mass models of different types [9–12], finite-element models of twines [13] and netting [14], and methods to improve the efficiency of the numerical simulations [15,16]. Procedures to measure the mechanical properties of netting have also been proposed in order to calibrate the numerical models [17–19].

Regarding the hydrodynamics of netting, a review of the hydrodynamic inside and outside aquaculture cages can be found in [33]. Early researches were focused on calculating the hydrodynamic drag on netting, without studying the effect of netting on the flow field. Netting geometry was modelled by a collection of simple parts, where twines and knots were represented as cylinders and spheres; then drag forces on each part was calculated with standard formulas and added up to obtain the total drag force on a net panel [45]. This simple approach is still used in structural models of fishing gears and aquaculture cages based on lumped-masses or finite-elements [9, 10, 14], where drag coefficients are calibrated for a specific netting from model tests or sea trials. A more detailed approach was to study the drag and flow around a cruciform cylinder, the basic element of knotless netting used in most aqua culture cages. [34] combined theoretical and experimental work to derive formulae to calculate drag and lift coefficients of netting as a function of its solidity ratio, and to estimate the velocity reduction in the wake after a netting panel. Other authors used a similar methodology to propose empirical and semi-empirical formulae for the same purpose, in some cases related to the Reynolds number [3, 35].

Three-dimensional Computational Fluid Dynamics (3D CFD) is a promising approach to study the interaction between the netting and the water flow. But detailed small-scale CFD simulations of aquaculture cages or fishing gears would be impractical, since the large size of the netting panels and the small size of meshes, twines and knots would result in an enormous number of cells that would require too many computational resources. To solve this problem, [1] proposed to model the netting as a thin volume of porous medium. The flow through porous media was described with the equations proposed by [36] and [37]. The resistance coefficients of the porous medium were calibrated from tow tank measurements of drag and lift forces on a net panel at different towing velocities and angles of attack. The predictions of this numerical model had good agreement with experimental measurements. The same approach was proposed by [21].

Other reseachers have used this method to simulate the interaction between net panels and the flow field, and in some cases the porous media model was coupled with a lumped-mass structural model of the netting to account for fluid-structure interaction: [22, 46] simulated the fluid-structure interaction of net panels in steady current, [40] simulated a complete aquaculture cage, [47] and [42] studied the interaction between net cages and waves, and [43] proposed a new method to

calibrate the porous media coefficients from experimental data.

Modeling the netting as a thin volume with porous media properties has proved to be a very efficient method to apply CFD in aquaculture applications, since aquaculture cages often have very simple shapes: most of them consist on a cylindrical side net with its upper edge attached to a floating collar and its bottom edge attached to a circular or conical bottom net with sinkers. Modelling such simple net geometries as thin volumes is easy. However, the application of this technique to fishing gears is more difficult, because the shape of modern industrial trawl gears is becoming more complex due to the introduction of modifications to increase its selectivity, such as escape windows, separator panels, tapered sections, netting grids or multiple codends [44]. These complex netting geometries raise several difficulties:

1. Net panels in trawl gears are not flat. Porous media models need to be described with a set of resistance coefficients in the global coordinate system. Therefore, curved net panels need to be divided and approximated by a set of smaller flat net panels, each of them represented by a thin solid with porous properties adjusted according to its orientation. This process can be automated for cylindrical nets used in aquaculture cages, but it involves a considerable pre-processing work for curved nets with arbitrary shapes.

2. They often have complex intersections where three or more netting panels share a common edge. Modeling these netting geometries as thin solids is more difficult and prone to errors. Moreover, in a fluid-structure interaction approach, where the shapes of net panels change along time, it would be very difficult to automatically update the shape of the thin solids that represent the net panels without causing geometrical errors such as overlapping volumes or voids.

3. Dealing with large deformations in nets. [40, 48] have pointed out the problem that representing net panels as thin solids will introduce missing cells when simulating nets with large deflections. [49] developed an improved topological method to avoid missing cells, at the cost of increasing the complexity of implementing the porous media approach.

To solve the above-mentioned problems, we propose to model the geometry of net panels as 2D surfaces instead of 3D thin volumes, and then automatically apply porous media properties to the mesh cells that surround the surfaces. Hence, we call this method the porous surface method to differentiate it from the porous solid method. The resulting numerical model is similar, but this method greatly simplifies the pre-processing when the problem has complex netting geometries. In this paper, net panels are considered rigid and not affected by the flow across and around it, but the proposed method can also be applied to fluid-structure interaction problems where netting is deformed due to the effect of hydrodynamic forces.

This paper is organized as follows. Section 2.2 describes the numerical model used to simulate the flow through and around the netting. Section 2.3 describes the method used to model net panels as porous surfaces. Section 2.4 describes two cases to verify and assess the proposed method. The first test case is a flat square net panel used to compare numerical results with experimental data. The second case is

a complex net geometry used to compare the performance of the proposed porous surface method with the porous solid method. Results for the two test cases are presented and discussed. Finally, Section 2.5 presents the conclusions.

2.2 Numerical model

In the present study, the flow is assumed to be incompressible and steady. The Navier-Stokes equations used for representing the flow are the continuity equation:

$$\nabla \cdot \mathbf{u} = 0 \tag{2.1}$$

and the momentum equation:

$$\nabla \cdot (\mathbf{u} \otimes \mathbf{u}) - \nabla \cdot \mathbf{R} = -\nabla p + \mathbf{S}_i \tag{2.2}$$

where $\mathbf{u}$ is the velocity, p is the kinematic pressure and $\mathbf{S}_i$ is the source term where resistance from the netting will be introduced.

The stress tensor $\mathbf{R}$ is calculated by

$$\mathbf{R} = \nu_{eff} \nabla \mathbf{u} \tag{2.3}$$

where ν_{eff} is the effective kinematic viscosity calculated using Newtonian transport model and the turbulence model. The Finite Volume Method is used to discretize the fluid domain for solving the governing equations.

2.2.1 Porous media model

The porous media model proposed by [36] for low Reynolds numbers and revised by [37] for higher Reynolds numbers is the representation of pressure drop induced by the presence of porous media in a fluid flow. The source term $\mathbf{S}_i$ in the momentum equation is calculated using the Darcy-Forchheimer equation:

$$\mathbf{S}_i = -\left(\mathbf{D}_{ij}\mu\mathbf{u} + \mathbf{C}_{ij}\frac{1}{2}\rho|\mathbf{u}|\mathbf{u}\right) \tag{2.4}$$

where ρ is the density, μ is the dynamic viscosity of the fluid and $\mathbf{D}_{ij}$, $\mathbf{C}_{ij}$ are the material matrices containing porous media resistance coefficients in the principle axes of the porous media (x_1, x_2, x_3), where x_1 is normal to the net panel and x_2, x_3 are tangent to the net panel.

$$\mathbf{D}_{ij} = \begin{pmatrix} D_{\mathrm{n}} & 0 & 0 \\ 0 & D_{\mathrm{t}} & 0 \\ 0 & 0 & D_{\mathrm{t}} \end{pmatrix}, \mathbf{C}_{ij} = \begin{pmatrix} C_n & 0 & 0 \\ 0 & C_t & 0 \\ 0 & 0 & C_t \end{pmatrix} \tag{2.5}$$

Here D_{ij} is a material matrix which contains normal (D_n) and tangential (D_t) viscous resistance coefficients and C_{ij} is a material matrix contains normal (C_n) and tangential (C_t) inertial resistance coefficients. The normal coefficients are along the local x_1 direction of the porous media while the tangential coefficients, which are the ones in the perpendicular axes (x_2, x_3) were considered identical. This

porous media resistance coefficients (D_n, D_t, C_n, C_t) represents the effect of porosity and the physical features of porous media like the thickness. Magnitude of these coefficients are inversely proportional to the thickness t of the porous media. In the researches of [1, 3] the porous media coefficients were calculated by minimizing the error between a simplified analytical porous media model and the hydrodynamic force measurements from the experiments.

2.2.2 Turbulence models

There are different techniques to represent turbulence in the flow which are Reynolds Averaged Navier Stokes Equations (RANS),Large Eddy Simulation (LES) or by Direct Numerical Simulation (DNS). RANS, which are the decomposed forms of Navier stokes equation into time averaged quantities and fluctuating quantities is used in the current works for modelling the turbulence. In RANS Equations, turbulence can be modelled in many different ways and depending on the physics of the problem, some turbulence models are more suitable than others. In this work, RANS is used with different 2 equation turbulence models and compared their results for finding the one which gives more stable and accurate results. In two equation turbulence models, the turbulence is modelled using two transport equations.

2.2.2.1 Standard $k-\epsilon$ model and realizable $k-\epsilon$ model

In the equation 2.3, the effective kinematic viscosity is given by,

$$\nu_{eff} = \frac{\mu + \mu_t}{\rho} \tag{2.6}$$

where the turbulent viscosity (μ_t) is modelled as :

$$\mu_t = \rho C_\mu \frac{k^2}{\epsilon} \tag{2.7}$$

These models use transport equations for turbulent kinetic energy and dissipation.

$$\frac{\partial}{\partial x_i}(\rho k u_i) = \frac{\partial}{\partial x_j}\left[\left(\mu + \frac{\mu_t}{\sigma_k}\right)\frac{\partial k}{\partial x_j}\right] + P_k + P_b - \rho\epsilon - Y_M + S_k \tag{2.8}$$

$$\frac{\partial}{\partial x_i}(\rho \epsilon u_i) = \frac{\partial}{\partial x_j}\left[\left(\mu + \frac{\mu_t}{\sigma_\epsilon}\right)\frac{\partial \epsilon}{\partial x_j}\right] + C_{1\epsilon}\frac{\epsilon}{k}(P_k + C_{3\epsilon}P_b) - C_{2\epsilon}\rho\frac{\epsilon^2}{k} + S_\epsilon \tag{2.9}$$

Model coefficients used are [50]

Table 2.1: Model coefficients for standard $k-\epsilon$ turbulence model.

C_μ	C_1	C_2	σ_k	σ_ϵ
0.09	1.44	1.92	1	1.3

The difference between the standard $k-\epsilon$ model and realizable $k-\epsilon$ model is the definition of C_μ. In standard $k-\epsilon$ model it is a constant equals to 0.09 but in

realizable $k-\epsilon$ model it is a variable calculated by

$$C_\mu = \frac{1}{A_0 + A_s \frac{kU^*}{\epsilon}} \tag{2.10}$$

The realizable model also has a slightly different transport equation for ϵ.

$$\frac{\partial}{\partial t}(\rho\epsilon) + \frac{\partial}{\partial x_i}(\rho\epsilon u_i) = \frac{\partial}{\partial x_i}\left[\left(\mu + \frac{\mu_t}{\sigma_\epsilon}\right)\frac{\partial \epsilon}{\partial x_i}\right] + \rho C_1 S\epsilon - \rho C_2 \frac{\epsilon^2}{k+\sqrt{\nu\epsilon}} + C_{1\epsilon}\frac{\epsilon}{k}C_{3\epsilon}P_b + S_\epsilon \tag{2.11}$$

2.2.2.2 SST k-omega model

The shear stress transport formulation of $k-\omega$ turbulence model is a two equation eddy-viscosity model which is famous for providing good results for separation flows and flows with adverse pressure conditions.

Kinematic eddy viscosity

$$\nu_t = \frac{a_1 k}{\max(a_1\omega, SF_2)} \tag{2.12}$$

Turbulent kinetic energy

$$\frac{\partial k}{\partial t} + U_j\frac{\partial k}{\partial x_j} = P_k - \beta^* k\omega + \frac{\partial}{\partial x_j}\left[(\nu + \sigma_k\nu_T)\frac{\partial k}{\partial x_j}\right] \tag{2.13}$$

Specific dissipation rate

$$\frac{\partial \omega}{\partial t} + U_j\frac{\partial \omega}{\partial x_j} = \alpha S^2 - \beta\omega^2 + \frac{\partial}{\partial x_j}\left[(\nu + \sigma_\omega\nu_T)\frac{\partial \omega}{\partial x_j}\right] + 2(1-F_1)\sigma_{\omega 2}\frac{1}{\omega}\frac{\partial k}{\partial x_i}\frac{\partial \omega}{\partial x_i} \tag{2.14}$$

The initialisation of these coefficients are done by the following equations,

$$k = \frac{3}{2}(I|U_{ref}|)^2 \tag{2.15}$$

$$\epsilon = \frac{C_\mu^{0.75}k^{1.5}}{L} \tag{2.16}$$

$$\omega = \frac{k^{0.5}}{C_\mu L} \tag{2.17}$$

Table 2.2: Parameters used to find initial turbulence coefficients.

I (Turbulent Intensity)	U_{ref}	C_μ	L (Reference Length)
1 %	Reference Velocity	0.09	0.15m

2.2.3 CFD simulation

A steady-state, incompressible solver for turbulent flows with implicit or explicit porous media implementation were used for solving the numerical model described in section2. Opensource CFD toolkit [51] was used with *porousSimpleFoam* solver for an implicit treatment for porous medium. This solver uses a SIMPLE (Semi-Implicit Method for Pressure Linked Equations) algorithm as the solution strategy. The turbulence part of the numerical model is modelled using Reynolds Average Navier Stokes (RANS) equations. They are the decomposed forms of Navier stokes equation into time averaged quantities and fluctuating quantities. In RANS, turbulence can be modelled in many different ways and depending on the physics of the problem, some turbulence models are more suitable than others. After comparing different turbulence models, for the particular test cases described in 2.4, realizable k-epsilon turbulence model was used for the simulations. The initial turbulence kinetic energy (k) and turbulence dissipation (ϵ) was found for the particular flow speed using the turbulence length scale (T_l) of 0.15 m and intensity (T_u) of 1%. The slip velocity boundary condition is applied to all walls while no-slip condition on the frame. A fixed inlet velocity and a zero gradient pressure condition at the inlet was given and a uniform zero pressure field and inletOutlet generic outflow boundary condition for the velocity at outlet in order to obtain a velocity induced flow. The simulations were assumed to be converged when the final residuals are of the order 10^{-4}.

2.3 Modelling net panels as porous surfaces

The fishing net is easy to compare to a surface than a volume due to its low thickness compared to the higher surface area and the complexity of the shape formed by the net in a fishing gear. Fishing nets can be represented as surfaces and this surfaces are triangulated in order to use them in the fluid domain for dealing with the mesh. Modelling the nets as surfaces are also proven to be an efficient way to simulate the structural solvers for finding the shapes of the fishing net. Each net panel is described by a triangle mesh that represents its mid-surface. Such triangle mesh is easily generated from Computer Aided Design (CAD) models by exporting the surface to a tessellated format composed by triangles, such as the STL file format.

2.3.1 Meshing near the surface

The cells in the fluid domain, which are close to and cut by the surface are refined to smaller cells and snapped to the surface for a better shape of the final porous media model. According to the distance of the cell centres from the surfaces, cells can be classified for applying the porous coefficients. The approach will also work without having to refine the cells, even though this step is done for representing complex shaped netting without needing to have smaller cells through out the domain.

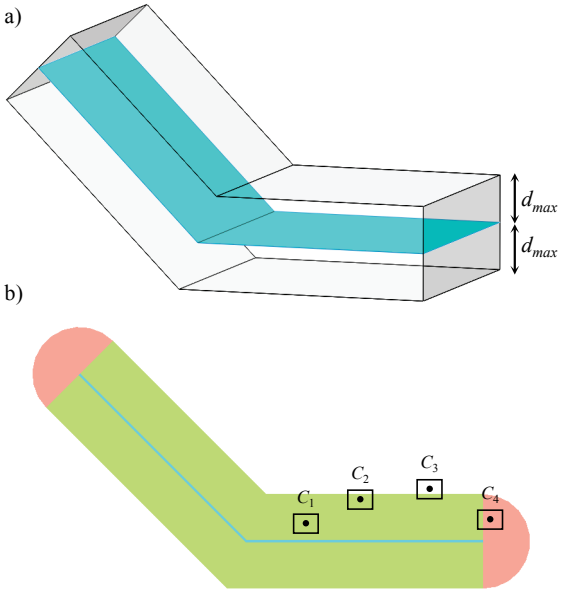

Figure 2.1: Body of influence of a surface for selecting cells near it: a) 3D view; b) 2D view, cells with center inside the green area are selected, cells with center in the the red areas are not selected.

2.3.2 Selecting cells near the surface

A cell C_i in the mesh is included in the group of cells near surface S^i if $d_i < d_{max}$, where d_i is the distance from the cell centre to the triangulated surface, $d_{max} = t/2$ and t is the desired thickness of the porous media. Cells that fulfil this condition but are outside the external edge of the surface are not included in the group. For example, as seen in the Figure 2.1 (b), cells C_1, C_2 are included in the group; cell C_3 is excluded because $d_3 > d_{max}$, and cell C_4 is excluded because it is outside the external edge of the surface. Another example with a real mesh is shown in Figure 2.2.

2.3.3 Dealing with multiple surfaces

Some kinds of fishing gears consist of many net panels of different netting materials. These net panels might vary in properties like mesh size, twine diameter, twine type or other properties like mesh opening which makes them to have different porous resistance coefficients. Each net panel is described as independent triangulated surface and is treated individually yet its body of influence can overlap with bodies of influence from other net panels as seen in Figure 2.3. In such cases, cells inside the overlap volume between two bodies (orange area in Figure 2.3) will initially belong to multiple surfaces. To assign each cell to only one surface, the distance d_i^j from cell C_i to surface S^j is calculated for each cell inside the overlap volume, and the cell is assigned to the surface which is closer to it. In Figure 2.3, cell C_1 is assigned to surface S^1 since $d_1^1 < d_1^2$, and cell C_2 is assigned to surface S^2 since $d_2^2 < d_2^1$. Note that algorithm does not select cell C_3 for the body of influence of neither surfaces. However, in real applications the volume of cells like C_3 is very small compared with the volume of cells assigned to porous surfaces, and this only happens in seams

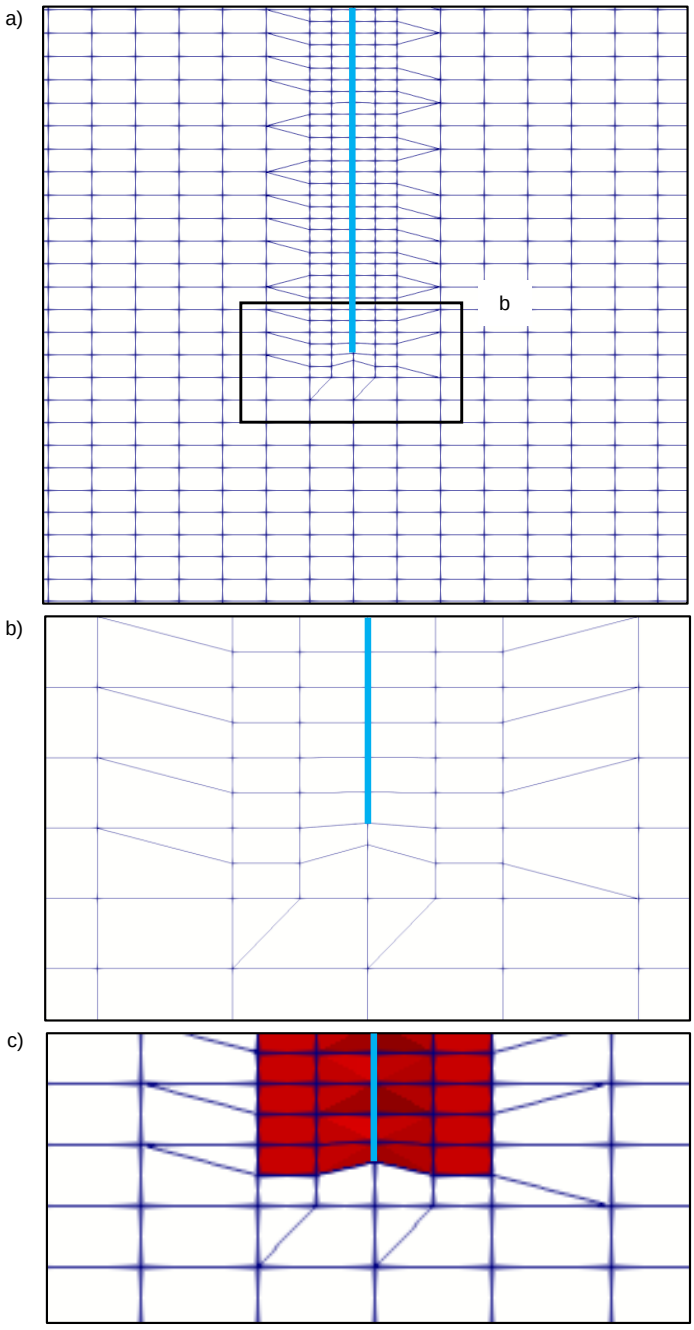

Figure 2.2: Selecting cells near a surface: (a) 2D view of the mesh near the surface, represented in blue color; (b) detail of the mesh near the edge of the surface; (c) cells selected in red.

between net panels which form angles not close to 180°.

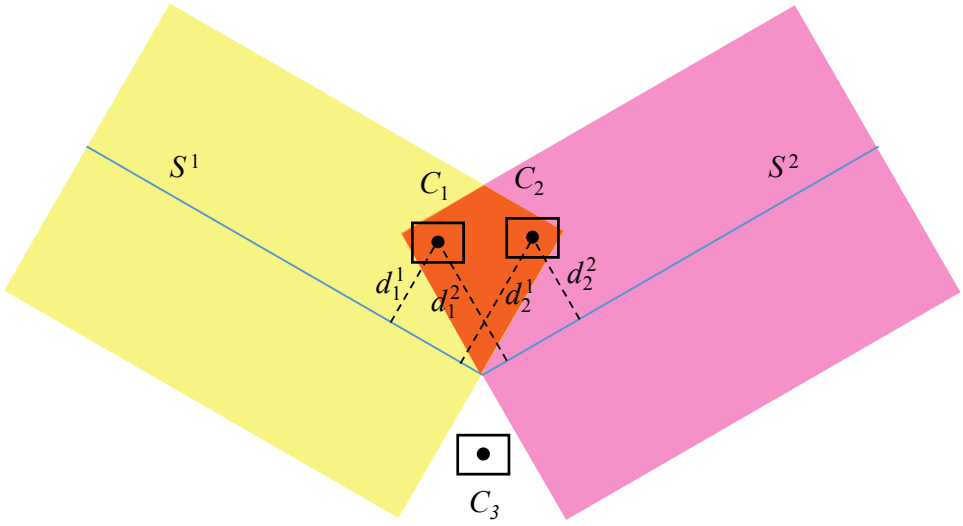

Figure 2.3: 2D view describing selection of cells for multiple surfaces: surfaces S^1 and S^2 in blue and the body of influences in yellow and pink respectively.

2.3.4 Grouping triangles with similar orientation

Porous properties will be applied to cells selected near a porous surface. But surfaces are often curved, and therefore the porous resistance coefficients, expressed in the global coordinate system of the model, are not constant, and a unique porous zone with constant properties will not represent the porosity of the curved net panel. Therefore, multiple porous zones need to be created to model a curved porous surface. On the other hand, a very large number of porous media zones may cause performance problems in some CFD softwares.

To solve this, triangles with similar orientation in each surface are grouped to create a single porous zone with the cells close to each triangle group. This is done with an heuristic algorithm that creates groups of triangles where the angle between the normal of each triangle and the average normal of the group is smaller than a user-defined threshold angle. Smaller threshold angles will create more triangle groups (and porous zones), capturing better the shape of a curved surface. An example is shown in Figure 2.4. For best accuracy, it is also possible to create one group per triangle, so the number of generated porous zones will be equal to the number of triangles.

2.3.5 Generating porous zones

A porous zone will be generated for each triangle group in each surface. For each cell C_i in surface S^j, the closest triangle in the surface is found, and the cell is assigned to its triangle group. The porous resistance coefficients for the surface were provided by the user in the principal axis as normal and tangential components: D_n, D_t, C_n, C_t. They need to be adjusted in two ways before applying them to the porous zone:

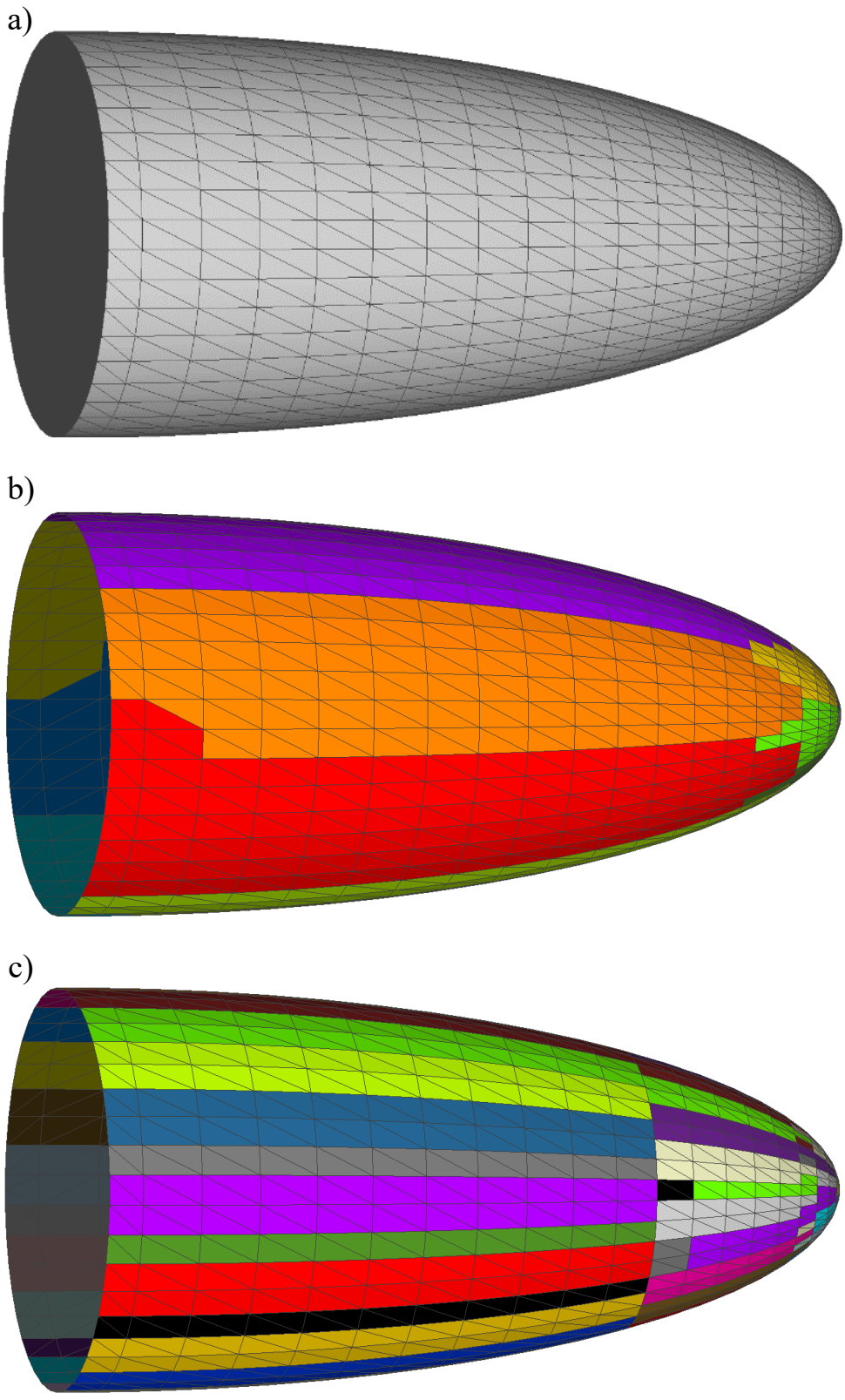

Figure 2.4: Grouping triangles with similar orientation: (a) triangle mesh of a quadric surface with 1723 triangles; (b) 23 groups of triangles with threshold angle of 25°; (b) 95 groups of triangles with threshold angle of 10°.

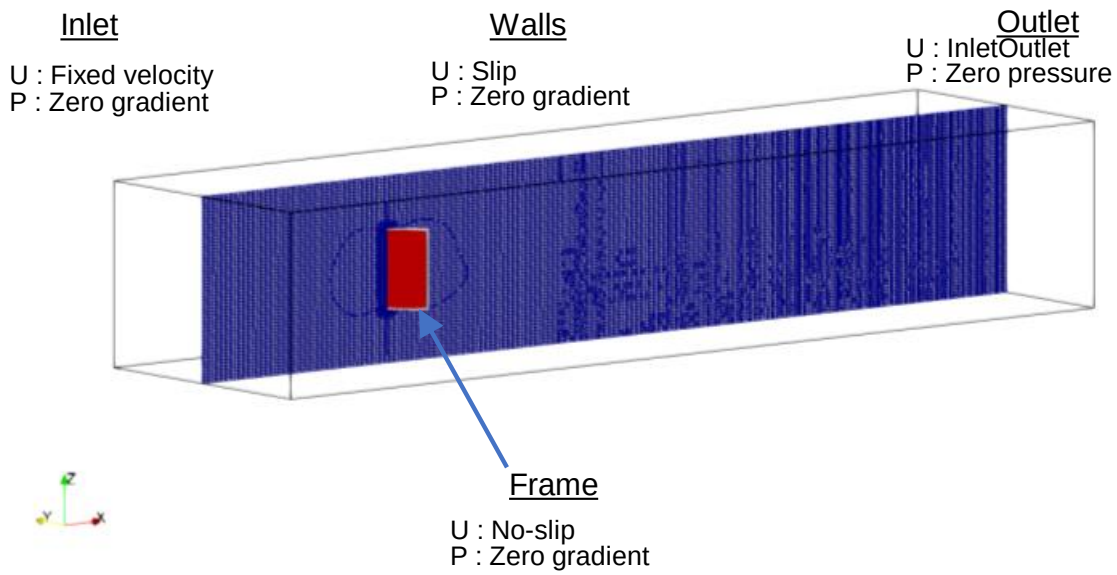

Figure 2.5: Computational domain used to simulate the example 1, including the net (in red), frame, mesh and the boundary conditions

1. The user-provided resistance coefficients were calculated for a particular reference thickness t_{ref} of the porous media, which may be different from the thickness t used to select cells near each porous surface. In addition, the groups of cells assigned to each triangle group may have a slightly different average thickness t_{avg}, which needs to be calculated. Then, the user-provided resistance coefficients are scaled by the ratio t_{ref}/t_{avg}.

2. The resistance coefficient matrices $\mathbf{D}_{ij}$, $\mathbf{C}_{ij}$ in equation 2.5 need to be rotated to match the average normal of each triangle group.

2.4 Results and discussion

Two test cases have been used to verify and assess the proposed method. The first test case is a flat square net panel used to compare the numerical results with experimental data. The second case is a complex net geometry used to compare the performance of the proposed porous surface method with the porous solid method.

2.4.1 Example 1: flat net panel

The first example is used to validate the proposed porous surface method with the experiment done by [1] on a flat net panel towed at different angles and velocities. A square net panel of 1 x 1 m was attached to a rigid frame and towed in a towing tank at different velocities (0.25, 0.5, 0.75 m/s) and angles of attack (0, 15, 30, 45, 60 75, 90 degrees) and the drag and lift forces on the net were measured.

The experiment [1] was carried out in a towing tank of 37 m long, 3.66 m wide and 2.44 m depth. Full details about the measurement setup can be found in the original reference. The dimensions of the experimental setup were used to define the control volume of the CFD model, that is, width and depth are the same while restricting the horizontal length to 13 meters for capturing the wake without disturbances Figure 2.5 shows the control volume, boundary conditions and mesh in the CFD model. The net panel was modeled as a square flat surface attached to the frame.

The domain was discretized with a structured base mesh and an unstructured mesh snapped to the surface of the net with an total number of 1.8 million cells. For this example, the porous resistance coefficients given by [1] using LANE error minimization method for a knotless net of solidity 0.184 were used: $D_n = 51370$, $D_t = 26379$, $C_n = 5.0980$ and $C_t = 1.6984$.

Since the surface is flat, only one porous zone is created. Figure 2.6 shows the mesh and the porous cell zone generated when using two different porous media thickness of 20 mm and 60 mm, including the solid frame which can be seen in grey in the zoomed views. The coloured cells are those which are selected for the porous zone. This figure shows that the method works well with irregular shaped unstructured meshes.

As noted in [1], the choice of thickness of the porous media has no significant effect on the final results of the simulation if it is comparable to or larger than the thickness of the net. This is because the magnitude of the porous media resistance coefficients were estimated taken into account the thickness of the porous media. A thickness $t = 50$ mm was chosen for the porous media generated from the net panel. Simulations were carried out to find the independence of the thickness of the porous media, which will be explained later. The drag and lift coefficients were calculated by the following equations :

$$\begin{aligned} C_D &= \frac{2F_{\text{Drag}}}{\rho A u_\infty^2} \\ C_L &= \frac{2F_{\text{Lift}}}{\rho A u_\infty^2}. \end{aligned} \tag{2.18}$$

where F_{Drag} is the force component in the direction of the freestream velocity, F_{lift} is the force component normal to F_{Drag}, A is the total area of the net panel and u_∞ is the freestream velocity.

Figure 2.7 shows the flow field obtained from the simulations using the porous surface method method, which is very similar to that obtained by [1, 43], showing similar velocity fields upstream and at the wake of the netting panel. Figure 2.8 compares the drag and lift coefficients from the simulations with experimental measurements in [1] for a freestream velocity of 0.5 m/s. Results from the CFD model have very good agreement with experimental data.

A parametric study was conducted to assess the impact of the thickness t of the porous medium by running simulations with t ranging from 0.02 m to 0.06 m and keeping the mesh constant. Details of the porous zones for $t = 0.02$ and $t = 0.06$ m are shown in Figure 2.6. Figure 2.9 shows the drag and lift coefficients obtained for a for a freestream velocity of 0.5 m/s at an angle of attack of 45°. Results are practically constant and independent of t, and this is also the case for other velocities and angles of attack. Note that, since the same mesh was used for all the thicknesses,

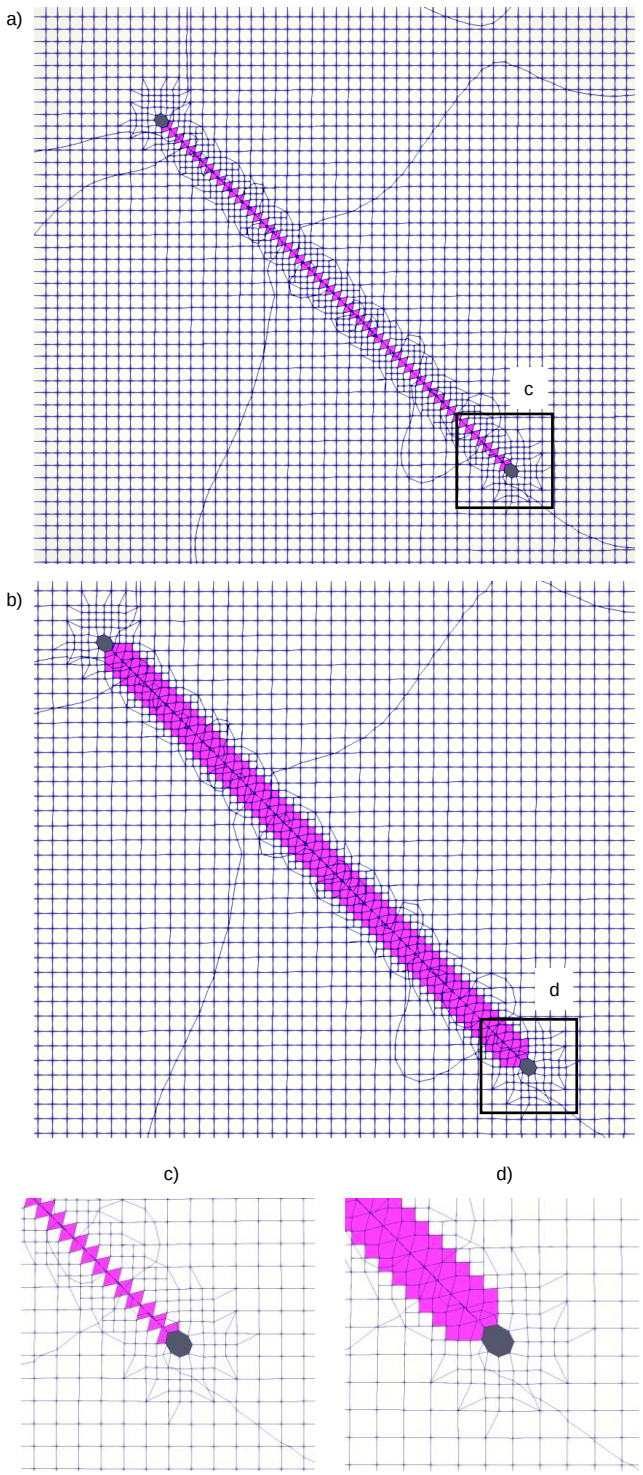

Figure 2.6: Porous media zones generated in example 1 for a thickness of 20 mm (a) and 60 mm (b). (c) and (d) are closer views of the edge of the surface. Grey areas represent the solid frame attached to the net panel.

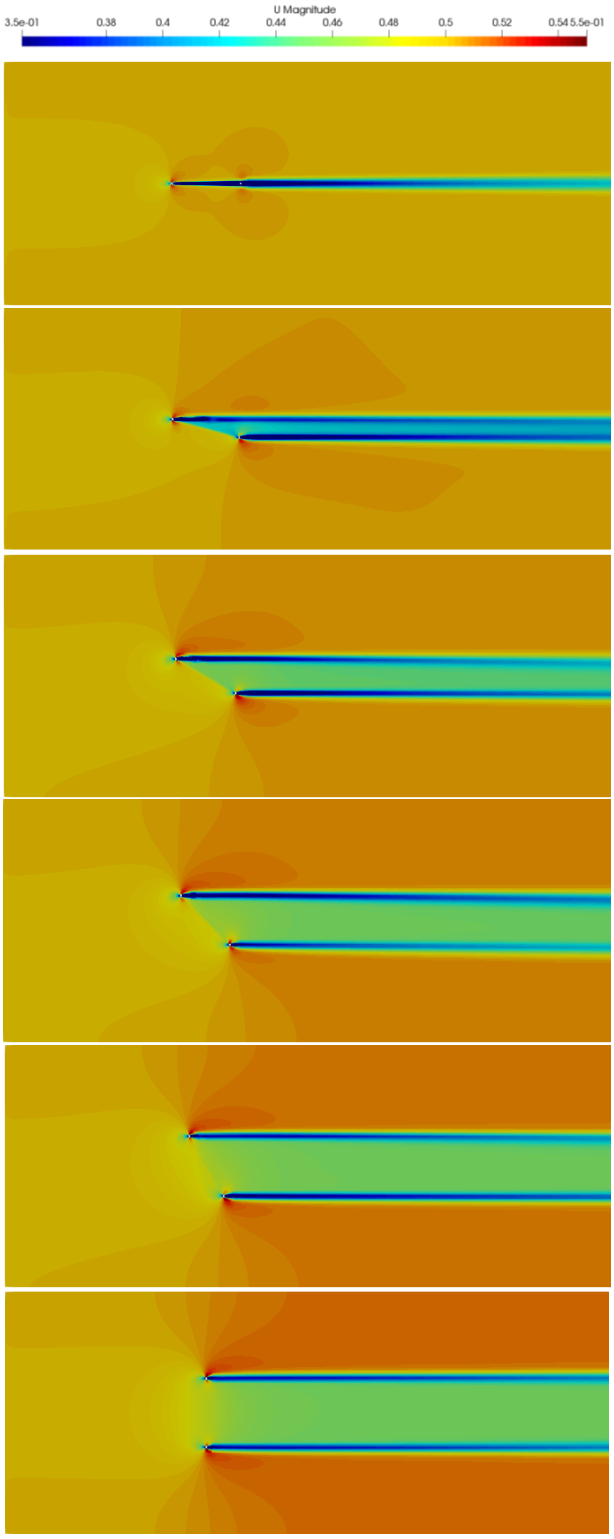

Figure 2.7: Example 1: velocity field from CFD simulations for a flow speed of 0.5 m/s at different angles of attack. From top to bottom: 0°, 15°, 30°, 45°, 60°, 90°.

different but close values of t may generate identical porous zones with the same average thickness t_{avg}, hence producing exactly the same results. This explains

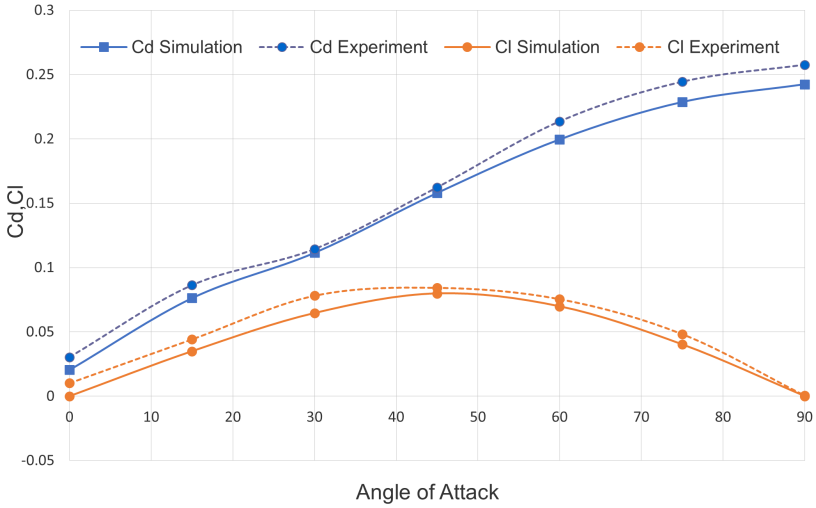

Figure 2.8: Example 1: comparison of hydrodynamic coefficients over angles of attack ranging from 0°to 90°with experimental results from [1] for a flow velocity of 0.5 m/s.

why different values of t produce identical results (e.g. $t = 0.035$, 0.04 and 0.045 m). It is also worth noting that when small values of t (e.g. 20 mm) are combined with an angle of attack of 45°, cells in the porous zone form an very odd-shaped volume as shown in Figure 2.6c, with an average of just one cell throughout the thickness of the porous zone. Nonetheless, the simulations produce correct results. Therefore, the porous surface method produces correct results even if a coarse mesh is used to represent the porous media, thus reducing the computational cost of the simulations. This contrasts with the findings in [43] for the same example modelled with a solid porous medium: they recommended using at least 3 layers of cells across the thickness of the porous zone, because using just one layer results in errors in drag force about 40% compared to using 4 layers.

2.4.2 Example 2: complex net geometry

Fishing gears, and specially trawls with selective devices, are made up by multiple curved net panels with complex intersections. Modeling them with the porous solid method is cumbersome due to the amonth of pre-processing required to build the CFD model. This example is introduced to demonstrate such situations. It is an simplified academic example easy to replicate by other researchers and it does not represent the actual shape and structure of a fishing gear.

The net configuration shown in Figure 2.10 is made up of three net panels represented by their mid-surfaces: a revolute surface similar to a paraboloid (red), a flat horizontal surface (blue) inside the previous one and a flat inclined surface (gree) that intersects the blue surface. Each net panel has different values for the porous resistance coefficients: the red one has the same values as the example 1 described in Section 2.4.1, the blue one half and the green one double.

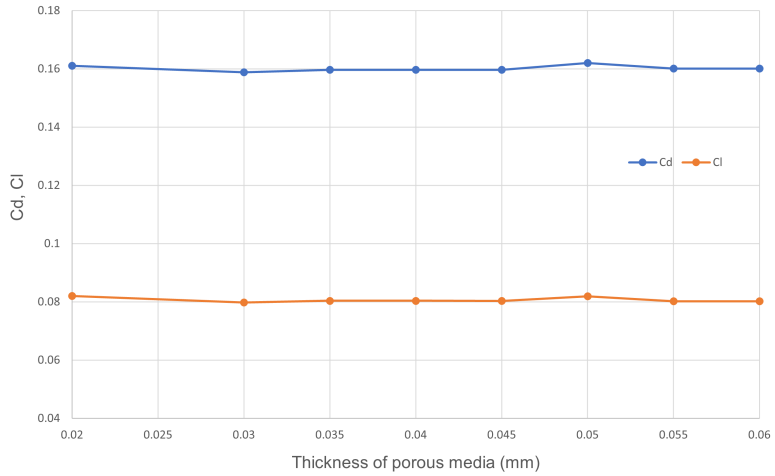

Figure 2.9: Example 1: hydrodynamic coefficients for different thicknesses of the porous media for a freestream velocity of 0.5 m/s and an angle of attack of 45°.

The nets are submerged in water and the incoming fluid velocity is 0.5 m/s along the x direction. The computational domain used to simulate this example (Figure 2.11) has a length of 13 m, width of 3.6 m and height of 2.4 m. The boundary conditions and turbulence coefficients are the same as in example 1 described in Section 2.2.3. A velocity induced flow is attained using a fixed velocity condition along with zero gradient pressure at inlet and an zero pressure condition with an inletOutlet velocity boundary condition at outlet. A slip boundary condition was given to the walls of the domain. The problem was solved using the porous solid method and the porous surface method.

2.4.2.1 Porous solid method

In the porous solid method (Figure 2.12), the three net panels were modeled in a CAD software as thin solids with a thickness of 20 mm. Special care was needed to avoid overlapping between solids, and the green net was divided in two solids. Then, since the outer solid corresponding to the red net is not flat, it had to be divided into smaller, roughly flat solids. In this case, it was divided into 33 solids, resulting in a total of $33 + 1 + 2 = 36$ solids which were exported as separate triangle meshes in STL format to prepare the CFD numerical model.

Each solid was modelled as a porous medium with constant resistance coefficients. For each solid, the principal directions of the resistance coefficients (normal and tangent vectors) were approximated by the principal axes of inertia of the solid, which were calculated in the CAD software and manually introduced the input files for the CFD software.

The computational domain was discretized into structured and unstructured cell mesh, including the inner volume of thin solids. A mesh convergence analysis was carried out to select an adequate mesh for the simulation. Table 2.3 shows the total drag force on the nets for different mesh refinement levels.

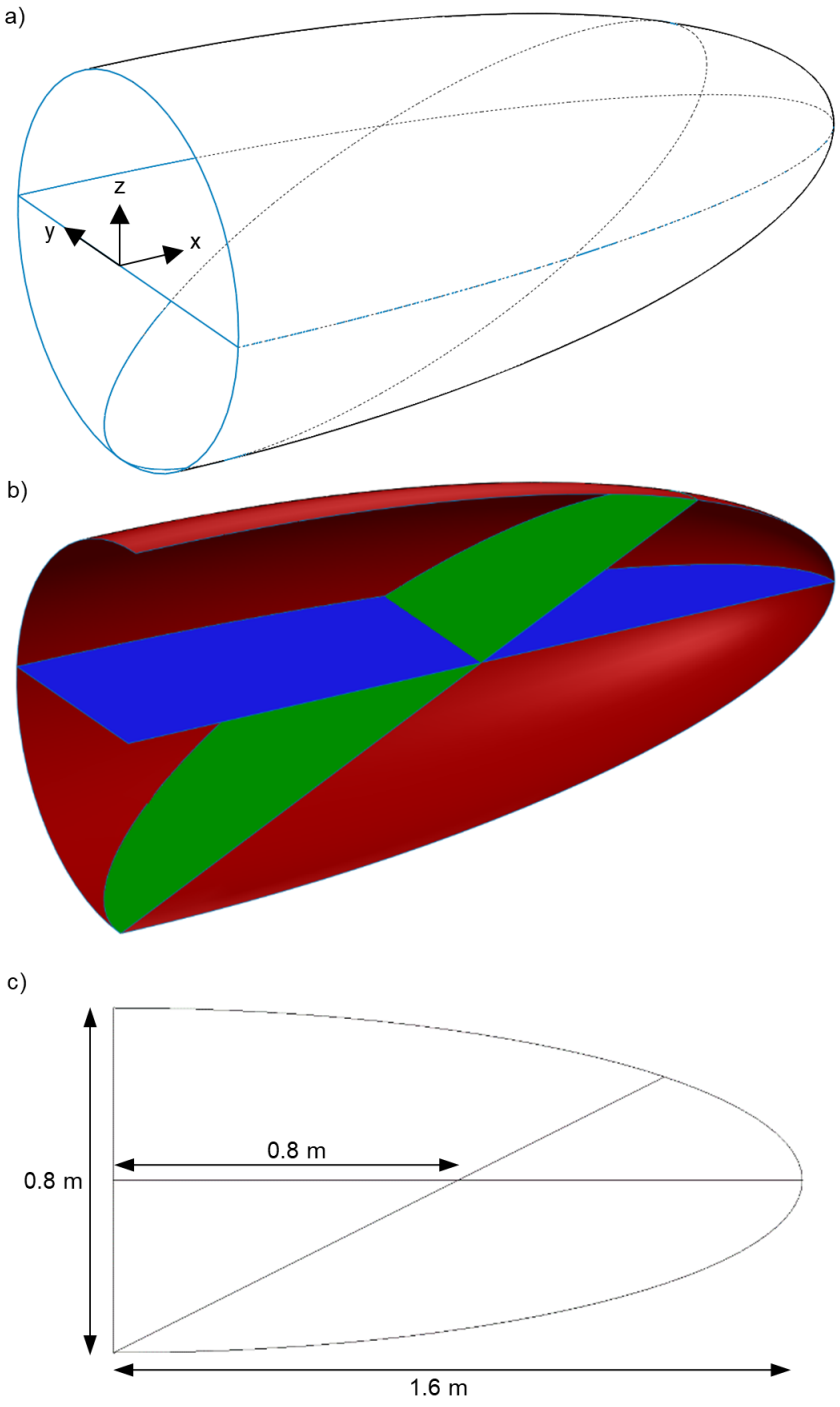

Figure 2.10: Example 2: complex net geometry. (a) 3D wireframe view of the 3 surfaces and coordinate system; (b) 3D section view at $y = 0$ with different colors for each surface; (c) dimensions of the nets.

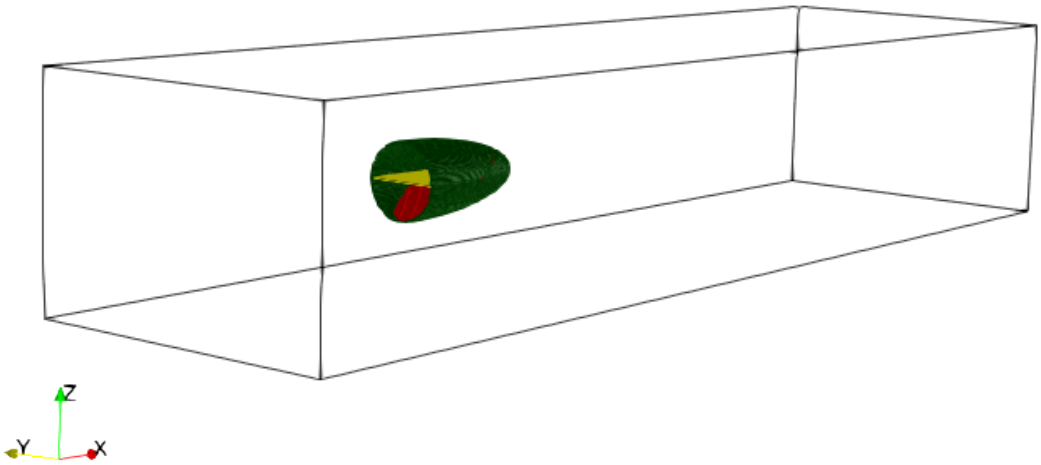

Figure 2.11: Example 2: domain used to simulate the example.

Table 2.3: Example 2 - porous solid method: results from the mesh convergence analysis.

Number of cells (Million)	Drag force (N)
1.5	70.86
3	70.88
12	73.85
13.8	76.42
25.18	76.46

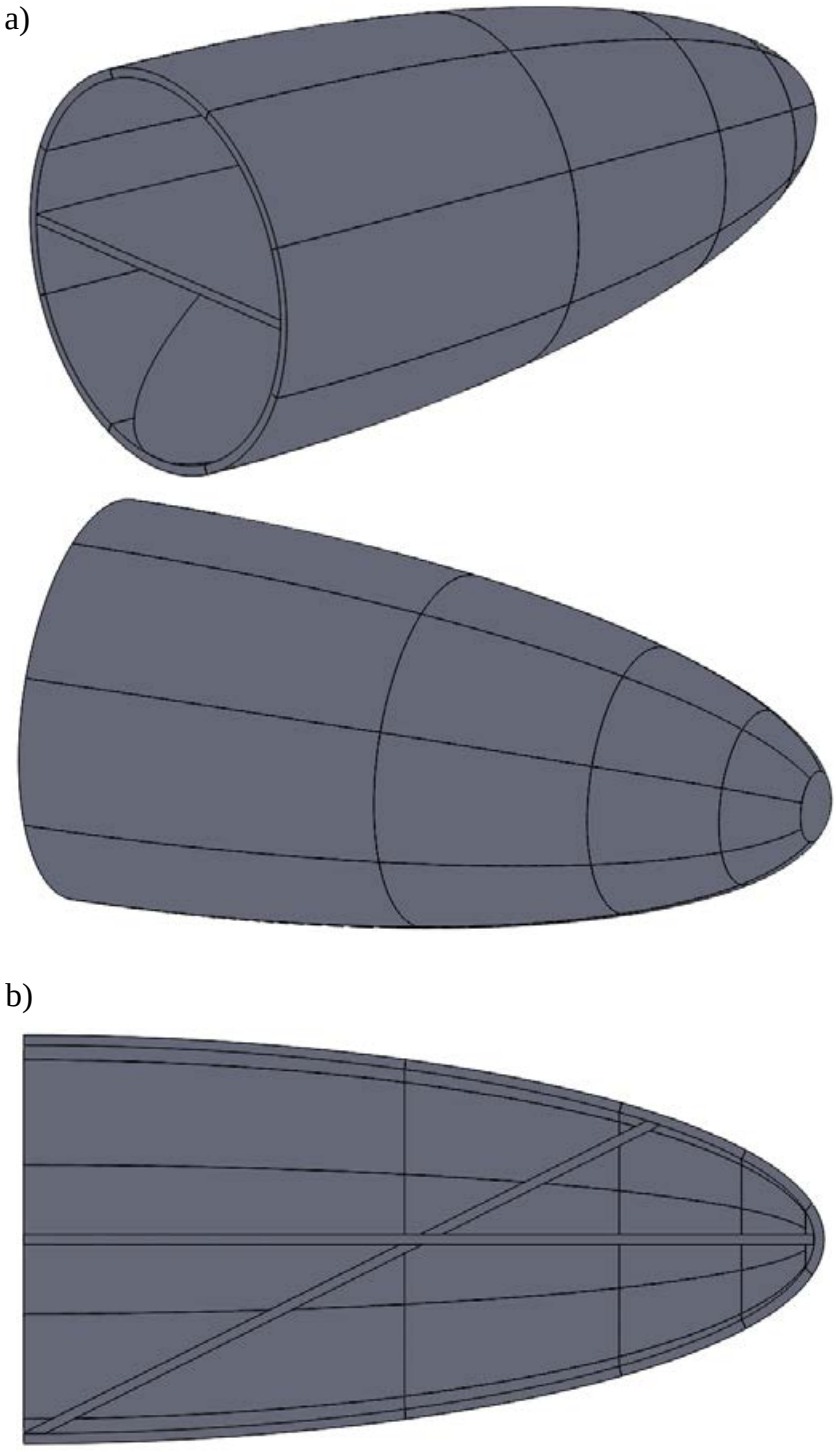

Figure 2.12: Example 2 - porous solid method: complex net geometry approximated by 36 non-overlapping, roughly flat solids with a thickness of 20 mm: a) 3D views; b) section view at $y = 0$.

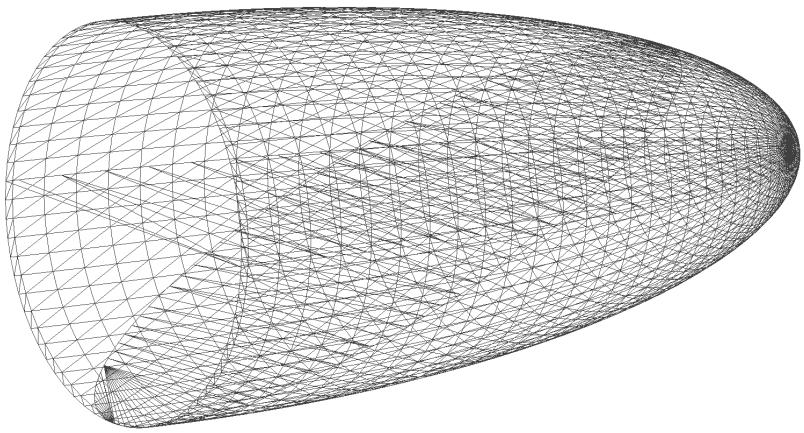

Figure 2.13: Example 2 - porous surface method: triangle meshes used to describe the shape of the net panels.

2.4.2.2 Porous surface method

With the porous surface method described in this work, the three net panels were modelled in as surfaces in a CAD software and exported as triangle meshes in STL format, as shown in Figure 2.13. In this case, the red net was discretized with 4490 triangles, the blue net with 51 triangles and the green net with 121 triangles. There is no need to divide curved surfaces (red net) into roughly flat patches or to deal with intersections between surfaces. For example, in the actual netting structure, the green or the blue panel would have to be divided into 2 sub-panels to be able to sew the nets. But since both sub-panels are made from the same material, they can be modelled as a single surface with this method.

The computational domain was discretized using a structured base mesh with cell size of 0.1 m and an unstructured mesh near the net surfaces refined up to 3 levels to achieve a good fitting to the surfaces. Details about the mesh convergence analysis will be provided later.

The method described in Section 2.3 was applied to the input surfaces with a porous media thickness of 20 mm and a threshold angle of 15° for grouping triangles. Figure 2.14 shows the cells assigned to each net and the generated porous zones. Since the blue and green nets are flat, only one porous zone is generated for each. The curved red net generates 50 porous zones.

Figure 2.15 shows a section view of the generated porous zones for each net and demonstrates the robustness and effectiveness of the method when dealing with multiple curved surfaces with intersections. Since the thickness t is about the same order of magnitude of the average cell size near the surfaces, some porous zones have a sawtooth shape, but example 1 proved that this does not affect the results of the simulation.

As in the porous solid method, a mesh convergence analysis was carried out: Table 2.4 shows the total drag force on the nets for different mesh refinement levels.

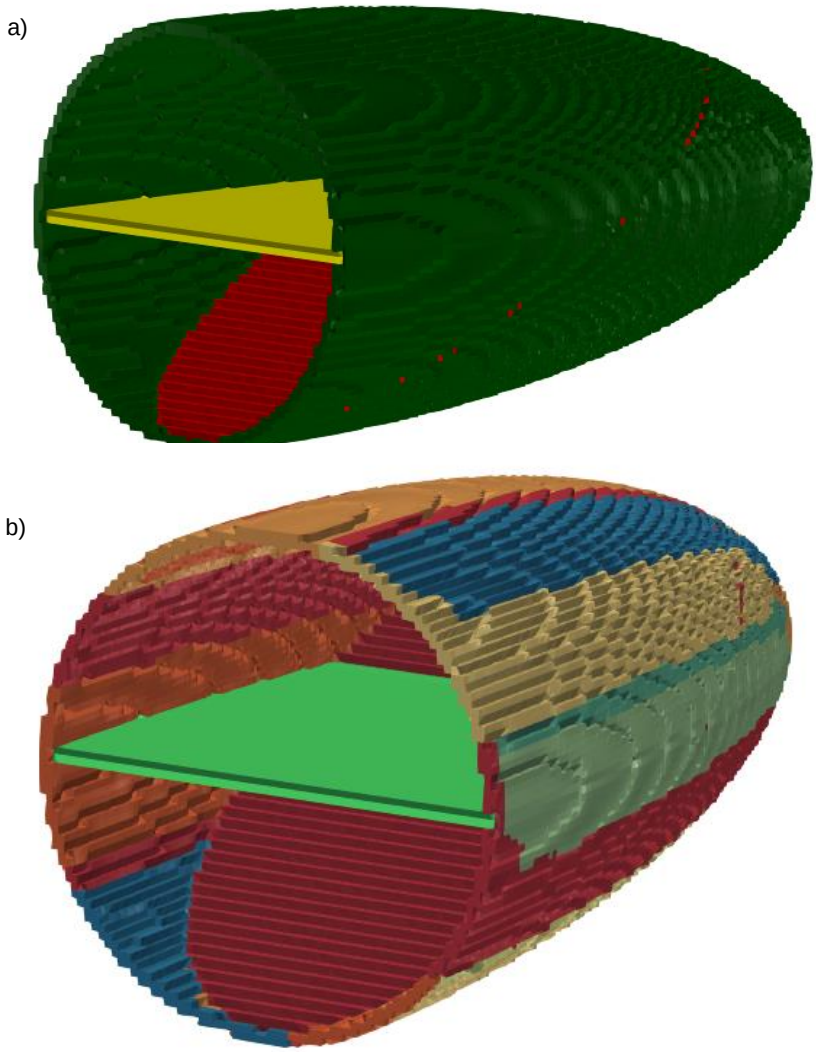

Figure 2.14: Example 2 - porous surface method: a) 3D view of the body of influence of each surface. b) 52 porous zones generated for the nets with a threshold angle of 15°.

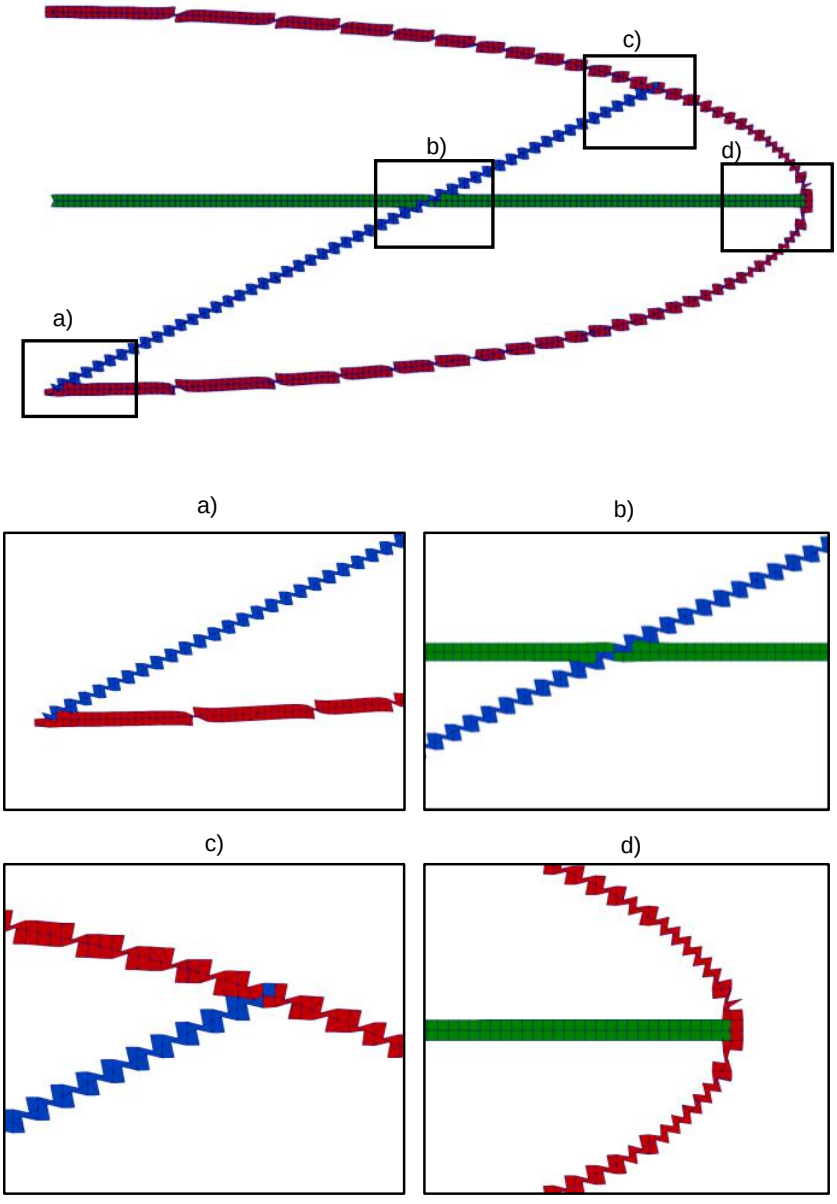

Figure 2.15: Example 2 - porous surface method: 2D section view at $y = 0$ of the generated porous zones with a thickness of 20 mm. Zoomed views a,b,c,d show the intersection between different surfaces and with created porous zones according to the grouping angle 15°on a coarse mesh.

Table 2.4: Example 2 - porous surface method: results from the mesh convergence analysis.

Number of cells (Million)	Drag force (N)
3	60.55
3.2	76.41
24	76.65
29	77.63

Table 2.5: Example 2 - porous surface method: effect of threshold angle on drag force

Threshold angle (°)	No. of porous zones	Drag force (N)
25	34	77.64
20	42	77.10
15	52	77.91
10	94	78.49
5	392	78.93

The two methods converge to a very similar value.

The effect of the threshold angle on the results was also investigated. The lower the threshold angle, the higher the number of generated cell zones for the curved red net, and therefore the numerical model approximates better the actual net. Table 2.5 shows total drag force on the nets for different threshold angles and number of porous zones.

2.4.2.3 Comparison of results from both methods

Figures 2.16 and 2.17 show top sections views of the flow field from the CFD simulations. The results from the simulations with the porous surface method correspond to threshold angle of 25°, which generates a similar number of porous zones as in the porous solid method. Both methods produce similar pressure and velocity fields, although small differences can be seen.

Despite the problem is symmetric across $y = 0$, the zoomed view of the velocity field in the porous surface method (Figure 2.16b) shows small asymmetries which are caused by the asymmetry of the generated porous zones (Figure 2.14b), since the heuristic algorithm for grouping triangles did not generate symmetric groups (Figure 2.4). The pressure fields demonstrates a higher pressure at the entrance of the net configuration and a notable pressure drop across the netting surfaces, especially the middle part where two plane nets intersect.

Figures 2.18 and 2.19 plots the pressure and the velocity along the x axis. Results from both methods are nearly identical, with minor differences in the region inside the nets.

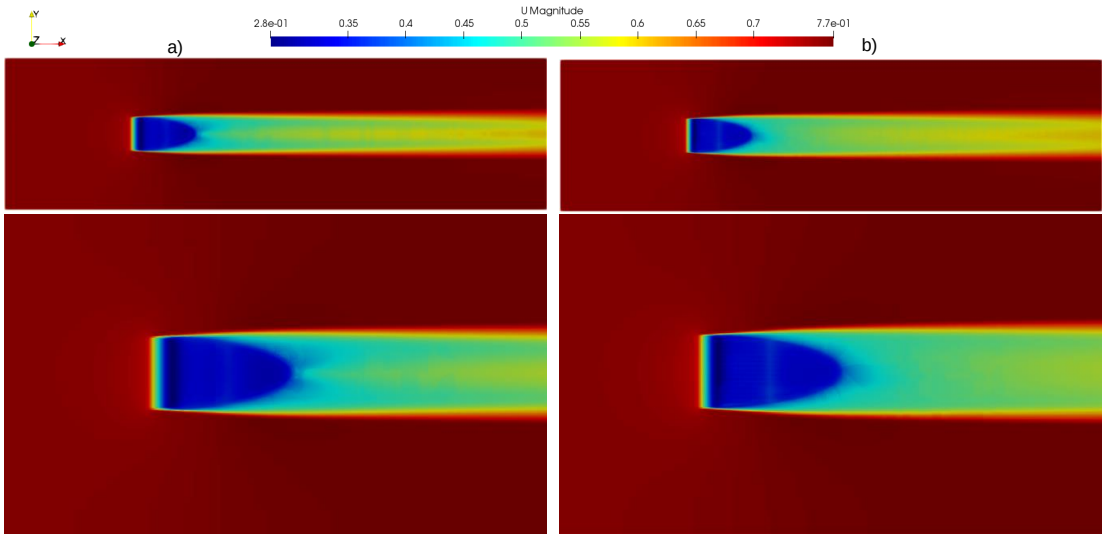

Figure 2.16: Example 2: top section views at $z = 0$ of the velocity field of the porous solid method (a) and the porous surface method (b) along with zoomed views.

2.5 Conclusions

Computational simulation of fishing nets is being demanded to provide understanding of the hydrodynamics of fishing gears and aquaculture cages. A porous media approach has been recently proposed to represent the net panels as thin porous solids in CFD simulations, which proved to be an efficient alternative to detailed models of knots and twines with traditional no-slip boundary conditions. In this study, a new method is proposed to model net panels as porous surfaces instead of thin porous solids, aiming at simplifying the modelling of net configurations with complex shapes, as seen in the real life fishing gears.

In example 1 (Section 2.4.1), the proposed method was validated against experimental results from [1]. The results from CFD simulations show very good agreement with experimental measurements, and the obtained flow fields are also very similar to those obtained with the porous solid method. We have also found that the results are independent of the thickness of the generated porous zones, allowing to use even just one or two layers of cells without causing significant errors. In example 2 (Section 2.4.2), the proposed method was used to simulate a complex net geometry with curved nets and intersections. It demonstrated that the porous surface method is able to deal with such complex net geometries and generate results very similar to the porous solid method. The improvements achieved with the porous surface method are:

1. Modelling curved nets. The porous solid method requires the user to approximate them by a collection of non-overlapping, roughly flat thin solids, and to calculate the principal directions of the porous resistance coefficients for each solid, which is time consuming and prone to errors. With the porous surface method, curved nets are described by a single triangle mesh, which is easily

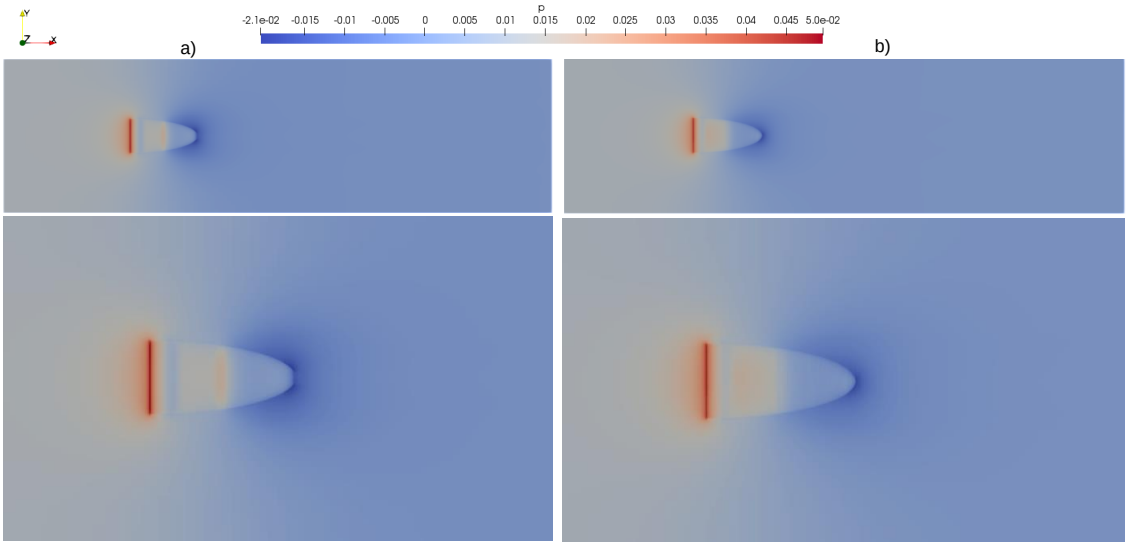

Figure 2.17: Example 2: top section views at $z = 0$ of the pressure field of the porous solid method (a) and the porous surface method (b) along with zoomed views.

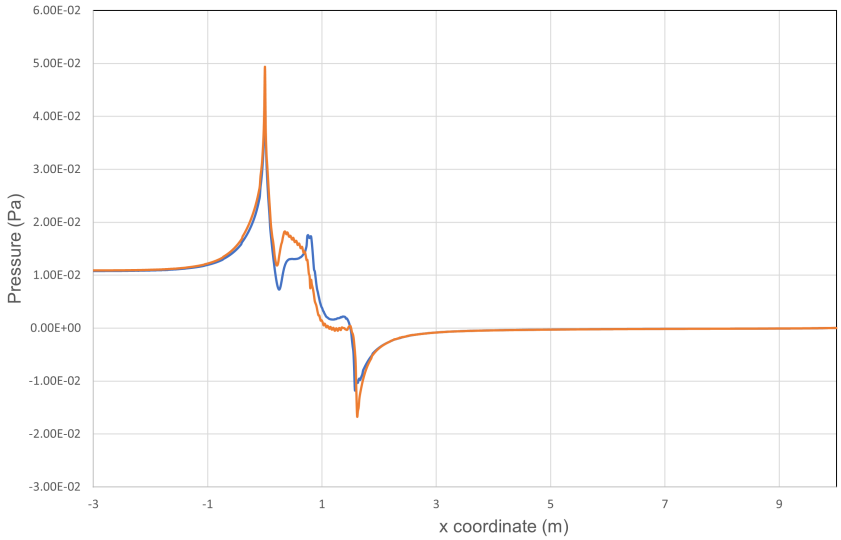

Figure 2.18: Example 2: pressure along the x axis for the porous solid method (blue) and the porous surface method (orange).

generated from CAD models, and the process of generating porous zones is fully automated, and hence it is faster and free from human errors.

2. Modelling multiple nets with intersections. The porous solid method requires the user to be careful to avoid interference between the thin solids that model each net panel. The porous surface method automatically deals with intersections and generates non-overlapping porous zones in that regions.

3. Easier control over the thickness of the porous zones. In the porous solid method, the thickness is implicitly defined by the size and shape of the thin solids used

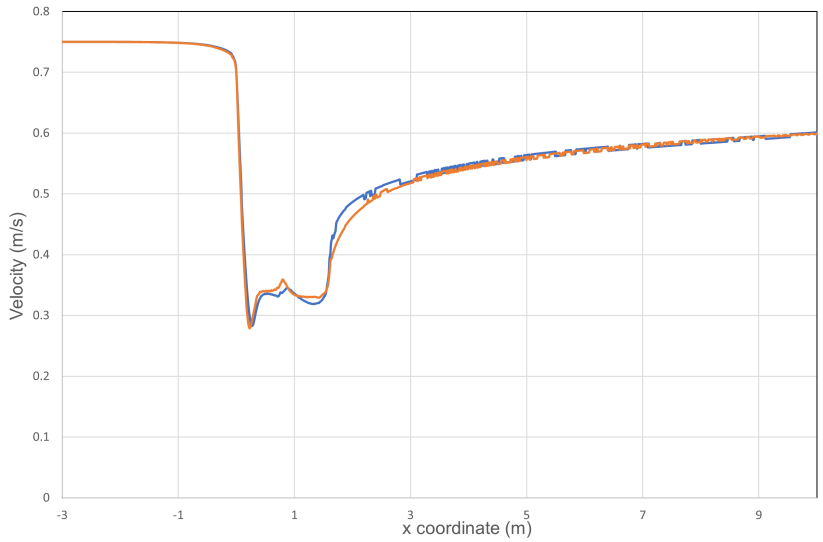

Figure 2.19: Example 2: magnitude of velocity along the x axis for the porous solid method (blue) and the porous surface method (orange).

to represent the net panels: changing the thickness requires modifying the CAD model, and probably meshing again to achieve a good quality mesh around the solids. In the porous surface method, the thickness is a parameter of the algorithm: it can be easily modified without changing the input triangle meshes used to describe the net panels or the computational mesh.

4. Easier control over the size and number of porous zones. In the porous solid method, the size and number depend on how curved nets are approximated by a collection of roughly flat thin solids. Increasing the number solids allows to capture better the curvature of the net and generating a more accurate CFD model, but it requires a lot of pre-processing work, as explained in the previous items. In the porous surface method, the size and number of porous zones is easily controlled with the threshold angle used to group triangles with similar orientation in the triangle mesh describing the net. Again, it can be easily modified without changing the input triangle meshes or the computational mesh.

5. The ability to deal with larger deflections. As mentioned in previous researches [40, 48], modelling nets as thin porous media solids can create complications and missing cells while simulating large deflections. With the porous surface method, continuous porous zones are created around the surfaces representing the nets, without missing cells despite the level of deflection on the net. Missing cells can only happen in seams between net panels which form angles far from 180°.

Furthermore, the porous surface method may facilitate the communication with a structural solver in fluid-structure interaction problems, since some structural models for nets are based on a triangle mesh [14].

Chapter 3

Estimation of resistance coefficients of porous media

Modelling net panels as thin porous media is a very effective approach to carry out computational fluid dynamics (CFD) simulations of full-scale fishing nets and aquaculture cages. This technique requires to estimate from experimental data the resistance coefficients of the D'arcy-Forchheimer equation for porous media. Two methods exist for this, both of them based on simplified analytical models that relate the drag and lift coefficients of the net panel to its resistance coefficients, and use regression analysis to estimate such coefficients. Instead of that, we propose a new method that uses a full CFD model of the flow through a layer of porous media, the same type of model used to simulate full-scale net panels in fishing and aquaculture applications. To increase the computational performance of the regression analysis, the model response is precalculated by a parametric study and interpolated to build an efficient regression model. The proposed method is applied to different net panels and results are compared with existing methods. We also investigate: (i) the difference between estimating both the inertial and the viscous resistance coefficients or estimating just the inertial ones, as proposed by some authors; (ii) the effect of using different error functions in the regression analysis. Results show that the proposed method achieves similar or better results than previous methods. In addition, it is easier to implement and it can be used to estimate the resistance coefficients of materials other than net panels. Estimating both the inertial and the viscous resistance coefficients always provides better results than estimating just the inertial coefficients and it does not complicate the regression analysis too much with the proposed method. It is not clear which error function provides better results, hence we recommend doing the regression analysis with different error functions and selecting the one that works better for a particular experimental data set.

3.1 Introduction

Computational simulation of fishing gears and aquaculture cages is getting more attention from researchers and industry, since it allows to improve and optimize their performance. Net panels are an important part of such underwater structures. They are very flexible, hence the simulation of flow through them is a fluid-structure

interaction (FSI) problem. The fluid part of this problem is very difficult to solve using computational fluid dynamics (CFD) if the exact geometry of netting is considered: net panels of large size made up of many twines and knots of small size. It would need large fluid domains with very fine computational meshes, making it computationally unachievable for real-scale problems. To overcome this limitation, researchers either use techniques like super-positioning the effect of individual components to calculate the flow field of 3-dimensional structures [52] or representing the permeability of the netting by introducing a source term in the Navier-Stokes equations [20, 53]. This later one is similar to considering the net panel as a porous medium and adding the porous media resistance as the source term to the Navier-Stokes equations. This approach has been proposed by different authors [1, 21] and it have been successfully used to simulate the dynamics of aquaculture cages with a FSI solver [22,31,42,46,48].

This porous media approach, which will be described in detail in section 3.2, models a net panel as a thin volume of porous media with a thickness of a few centimeters. The porous media model is characterized by a set of viscous resistance coefficients D_i and inertial resistance coefficients C_i, which must be calibrated from tow tank measurements of drag and lift forces on a net panel at different angles of attack and flow velocities. To avoid using a very time-consuming full CFD model to estimate the resistance coefficients from experimental data, researchers have proposed two methods based on analytical models:

[1] proposed to use regression analysis to estimate the resistance coefficients that best fit experimental data. Such experimental data consist in towing tank measurements of drag and lift forces on a net panel at different incoming fluid velocities and angles of attack. To avoid using a very time-consuming full CFD model in the regression analysis, a simplified analytical model for calculating hydrodynamic forces on a net panel is proposed, where drag and lift forces were linearly related to the porous resistance coefficients. The resistance coefficients in the two directions tangent to the net panel were assumed to be identical, estimating only 4 parameters: normal (D_n) and tangential (D_t) viscous resistance coefficients and normal (C_n) and tangential (C_t) inertial resistance coefficients. Results of CFD simulations using the estimates of the resistance coefficients show good agreement with experimental measurements. However, this analytical model depends on a parameter r_n which is estimated from CFD simulations of flow through the porous media, making the approach iterative and difficult to use.

[43] proposed a different approach that does not need experimental data. Due to the characteristics of the flow regimes through fishing and aquaculture nets, viscous resistance coefficients were neglected and inertial resistance coefficients were calculated with analytical expressions based on the transformation of Morison type load model. In addition, two new coefficients were introduced to account for the interaction effects in-between the twines, which were estimated from existing experimental data. The method often showed good agreement with experimental data, but in some cases the drag force was underestimated with errors about 20%-30%. The disadvantage of this method is that the calculated resistance coefficients are not constant, but depend on the incoming fluid velocity. This makes them quite more difficult to introduce in CFD software.

In this work we make two original contributions to the problem of estimating the

resistance coefficients of a net panel modeled with the porous media approach:

1. We use regression analysis with experimental data to estimate the resistance coefficients, as in [1], but instead of using a simplified analytical model, we use a full CFD model that simulates the flow through a thin layer of porous media, the same kind of model used to simulate full-scale net panels in fishing and aquaculture applications. To avoid a time-consuming estimation process, a parametric study is carried out to pre-calculate the response of the CFD model for a range of values of the resistance coefficients, and then it is interpolated to build the regression model used to estimate the coefficients that best fit experimental data.

2. We investigate the difference between estimating both the inertial and the viscous resistance coefficients, as in [1], or neglecting the viscous resistance coefficients, as in [43], to find which approach is more convenient.

This chapter is organized as follows. Section 3.2 describes the CFD model used to relate the drag and lift on the porous media to its resistance coefficients. Section 3.3 describes the CFD parametric study and how the regression model is built using interpolation techniques. Section 3.4 describes the method used to estimate the resistance coefficients from experimental data. Section 3.5 applies the proposed method to different net panels. Section 3.6 discusses the results and compares them with previous researches. Finally, Section 3.7 presents the conclusions.

3.2 CFD model

In order to estimate the resistance coefficients of a porous medium from experimental data, a model that relates the hydrodynamic drag and lift forces on the porous medium to its resistance coefficients is required. Instead of using a simplified analytical model, we use a full CFD model that simulates the flow through a layer of porous medium, as shown in Figure 3.1.

The model is based on the experimental setup described in [1]. Figure 3.1a shows a flat net panel in a water current flow with an incoming velocity U and an angle of attack α. The net panel is modelled as a thin layer of porous media of constant thickness e. Figure 3.1b shows the computational domain of the 2D CFD model used to simulate the flow through the porous medium.

3.2.1 Numerical Model

The flow in the computation domain is described by the Reynolds Averaged Navier Stokes (RANS) equations for the incompressible and steady state flow, the continuity equation and the momentum equation:

$$\frac{\partial u_i}{\partial x_i} = 0 \tag{3.1}$$

$$\frac{\partial \left(\rho u_i u_j\right)}{\partial x_j} = -\frac{\partial P}{\partial x_i} + \rho g_i + \frac{\partial}{\partial x_j}\left(\mu + \mu_t\right)\left(\frac{\partial u_i}{\partial x_j} + \frac{\partial u_j}{\partial x_i}\right) + S_i \tag{3.2}$$

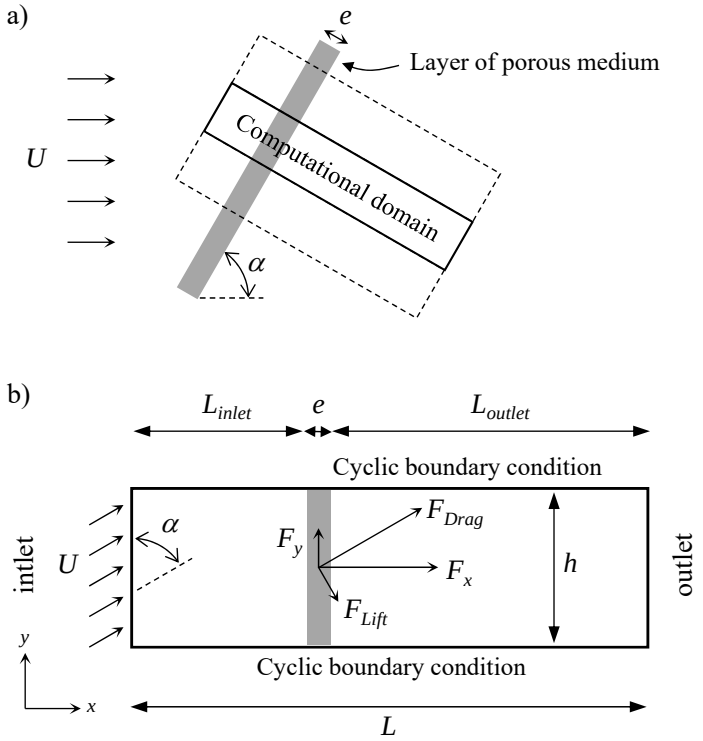

Figure 3.1: (a) Layer of porous medium of constant thickness e in a current flow with an incoming velocity U and an angle of attack α. (b) Computational domain of the 2D CFD model.

where ρ is the fluid density, u is the velocity, $x_i = (x, y, z)$ is the global Cartesian coordinate system, P is the pressure, g_i is the acceleration due to gravity, μ is the dynamic viscosity, μ_t is the turbulent viscosity calculated using the realizable K-Epsilon turbulence model, and S_i is the source term that describes the resistance inside the porous medium ($S_i = 0$ outside the porous medium).

3.2.1.1 Porous media model

The source term S_i that describes the resistance inside the porous medium in equation 3.2 is usually modelled by the D'arcy-Forchheimer equation [36, 37]:

$$\mathbf{S}_i = -\left(\mathbf{D}_{ij}\mu\mathbf{u} + \mathbf{C}_{ij}\frac{1}{2}\rho|\mathbf{u}|\mathbf{u}\right) \tag{3.3}$$

where $\mathbf{D}_{ij}$ and $\mathbf{C}_{ij}$ are coefficient matrices that describe the viscous resistance and the inertial resistance through the porous media.

In the principal axes of the porous medium, where x_1 is normal to the net panel and x_2 and x_3 are tangent to the net panel and normal to each other, $\mathbf{D}_{ij}$ and $\mathbf{C}_{ij}$ can be expressed as:

$$\mathbf{D}_{ij} = \begin{pmatrix} D_1 & 0 & 0 \\ 0 & D_2 & 0 \\ 0 & 0 & D_3 \end{pmatrix}, \mathbf{C}_{ij} = \begin{pmatrix} C_1 & 0 & 0 \\ 0 & C_2 & 0 \\ 0 & 0 & C_3 \end{pmatrix} \tag{3.4}$$

[43] neglected the effect of the viscous resistance coefficients $\mathbf{D}_{ij}$ due to the characteristics of the flow regimes through fishing and aquaculture nets: they assumed that for Reynolds numbers about $Re \sim O(10^2 \sim 10^3)$ the quadratic term dominates over the linear term in equation 3.3. Hence, only the three resistance coefficients C_1, C_2 and C_3 were estimated. The estimates of C_2 and C_3 were almost identical for all the studied net panels, with differences about 1%.

[1] did not neglect the viscous resistance coefficients, but assumed that the coefficients in the two directions tangent to the net panel were identical, thus simplifying the coefficient matrices to

$$\mathbf{D}_{ij} = \begin{pmatrix} D_n & 0 & 0 \\ 0 & D_t & 0 \\ 0 & 0 & D_t \end{pmatrix}, \mathbf{C}_{ij} = \begin{pmatrix} C_n & 0 & 0 \\ 0 & C_t & 0 \\ 0 & 0 & C_t \end{pmatrix} \tag{3.5}$$

and four coefficients D_n, D_t, C_n and C_t were estimated, with $D_n = D_1$, $D_t = D_2 = D_3$, $C_n = C_1$ and $C_t = C_2 = C_3$.

In this work we also assume that the coefficients in the two directions tangent to the net panel are identical, hence we use the coefficient matrices in equation 3.5.

3.2.2 Geometry and boundary conditions

The RANS equations described in section 3.2.1 were solved on the 2D computational domain shown in figure 3.1b using a finite volume discretization method.

A thickness of the porous medium $e = 0.05$ m was chosen, the same as in [1] and [43]. The resistance coefficients are inversely proportional to the thickness, therefore the simulation results will not be affected by this parameter. The incoming fluid velocity U, the angle of attack α and the resistance coefficients were included as parameters in the parametric study that will be described in section 3.3. The height of the domain h was arbitrary chosen to 1 m. Inlet and outlet boundaries were placed far enough from the porous medium to avoid significant influences on the results for any of the conditions simulated in the parametric study: after some preliminary tests, the inlet boundary was placed at a distance $L_{inlet} = 2$ m and the outlet boundary at a distance $L_{outlet} = 6$ m, so the total length of the domain was $L = e + L_{inlet} + L_{outlet} = 8.05$ m. It was checked that increasing these distances by a factor of 1.5 produced very similar results.

A fixed velocity defined flow is introduced by applying fixed velocity and the gradient of pressure to be zero at the inlet. The flow happens due to the zero pressure at the outlet and for the velocity boundary condition at outlet, an *inletOutlet* condition is applied, which is similar to assigning gradient of velocity to be zero with an additional option of controlling the possible backward flow. Cyclic conditions were applied on the top and bottom walls to approximate the infinite height domain shown in figure 3.1a to the computational domain shown in figure 3.1b.

3.2.3 CFD Simulation

[51], an opensource CFD toolkit, was used to set up and solve the numerical model. To solve the RANS equations with the porous media resistance, the *porousSimpleFoam*

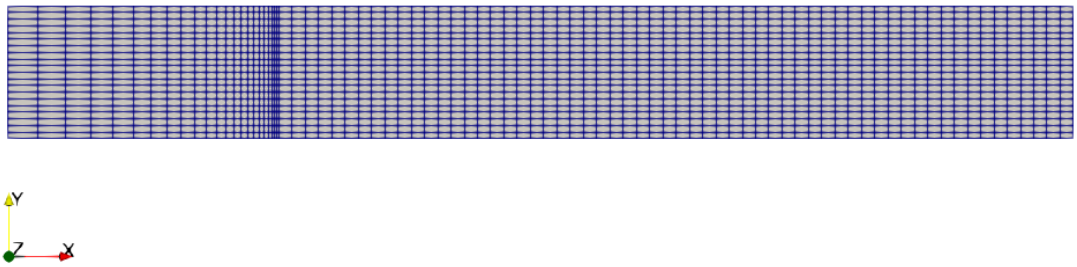

Figure 3.2: Structured mesh used to discretize the computational domain.

solver was used. It employs a SIMPLE (Semi-Implicit Method for Pressure Linked Equations) algorithm solution method and it works for turbulent flows with implicit or explicit porous media implementations. In this research, the implicit porous media implementation was used, which can have an under relaxation factor bigger than it will be with an explicit implementation [54].

The realizable K-Epsilon turbulence model was used for modelling the non linear Reynolds Stress term of the RANS equation. Initial conditions of the turbulence coefficients were calculated for a turbulence intensity of 1% and a turbulence length scale of 0.15 m.

A structured mesh was used for the discretization of the fluid domain using a finite volume approach, as shown in figure 3.2. A mesh independence study was conducted to ensure that the results are independent of the underlying mesh. In the final mesh, the domain was discretized with 20 cells along the vertical direction and 83 cells along the horizontal direction, which was divided into 3 blocks: 20 cells in the upstream region, 3 cells in the porous medium and 60 cells in the downstream region. The mesh has 1660 cells with an average cell size of 0.07 m.

Figure 3.3 shows the velocity profile of a simulation carried out with U = 2.5 m/s, α=15°and the porous media resistance coefficients of a net with a solidity of 0.184 given by [1]. The figure shows the increase in the magnitude of velocity close to the porous medium due to the pressure drop and a reduction in the velocity at the wake near to the porous media. The characteristics of the flow field are similar to those shown in [1, 43].

Among the results of the CFD simulation are the horizontal and vertical hydrodynamic forces on the porous medium, F_x and F_y, which are used to calculate the drag and lift forces according to figure 3.1:

$$\begin{aligned} F_{Drag} &= F_x \sin\alpha + F_y \cos\alpha \\ F_{Lift} &= F_x \cos\alpha - F_y \sin\alpha \end{aligned} \tag{3.6}$$

and the drag and lift coefficients of the porous medium:

$$\begin{aligned} C_D &= \frac{2F_{Drag}}{\rho A U^2} \\ C_L &= \frac{2F_{Lift}}{\rho A U^2} \end{aligned} \tag{3.7}$$

The proposed approach relates the drag and lift coefficients of the porous medium

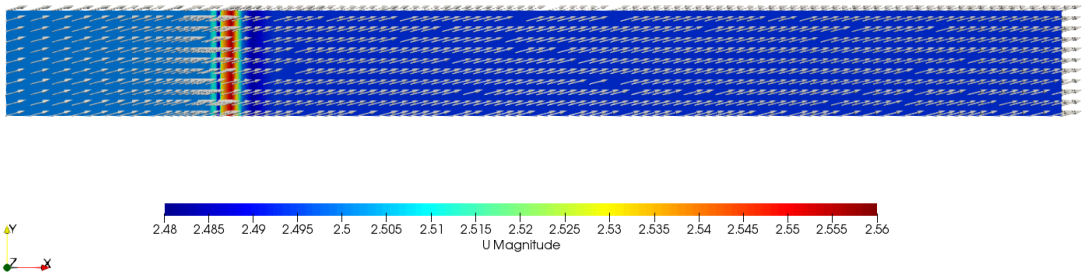

Figure 3.3: Velocity profile of the 2D simulation for the flow through porous media with a velocity U of 2.5 m/s, angle of attack α of 75 °and resistance coefficients of a net with a solidity of 0.184 given by [1].

to its resistance coefficients though a CFD-based numerical model, in contrast to the analytical models proposed by [1] and [43].

3.3 Parametric study and regression model

The 2D CFD model described in section 3.2 is not computationally expensive and it can be solved in a few seconds in a personal computer. However, using it directly to estimate the resistance coefficients from experimental data would be time-consuming, because this process needs hundreds of evaluations of the model.

To reduce the computational cost of the regression analysis, we carried out a parametric study to pre-calculate C_D and C_L for a range of values of the physical parameters of the model. Then, the results of the parametric study are interpolated to build an computationally efficient regression model, thus avoiding to evaluate the CFD model during the estimation process.

3.3.1 Parametric study

The parameters included in the parametric study were the incoming fluid velocity U, the angle of attack α and the resistance coefficients C_n, C_t, D_n and D_t. Table 3.1 summarizes the parameter values used in the study, which will be justified in the next paragraphs. A parameter grid with uniform spacing in each dimension was chosen to facilitate the interpolation of results that will be described in Section 3.3.3.

Regarding the incoming fluid velocity U, model tests usually achieve up to 1 m/s [1, 3, 34]. This is a physical maximum for aquaculture applications, were water currents rarely exceed this value. However, fishing towed gears usually achieve higher velocities: about 1 m/s in pair trawling, 1.5-2 m/s in classical bottom trawls and up to 2.5-3 m/s in beam trawls [55]. The velocity in model tests is also limited by the experimental facility: flume tanks can achieve speeds up to 1 m/s while calm water towing tanks can achieve up to 10 m/s. Therefore, in this study we considered incoming fluid velocities between 0.25 and 2.5 m/s. This parameter has a small effect on the drag and lift coefficients, hence only three equally spaced values were

Table 3.1: Parameter values used in the CFD parametric study.

Parameter	Values	
U (m/s))	0.25, 1.375, 2.5	
α (°)	15, 30, 45, 60, 75, 90	
C_n (m^{-1})	0.30, 15.15, 30.00	
C_t (m^{-1})	0.10, 5.05, 10.00	
	Sub-study 1	Sub-study 2
D_n (m^{-2})	0	1.0×10^4, 5.05×10^5, 1.0×10^6
D_t (m^{-2})	0	2.5×10^3, 1.2625×10^5, 2.5×10^5
Size	162	1458

simulated: $U = (0.25, 1.375, 2.5)$ m/s.

The angle of attack α can take physical values between 0° and 90°. When the net panel is almost parallel to the water flow, the shadow effect occurs: the interaction between netting and flow becomes more complex and special methods are required to study the hydrodynamics of the netting [30, 56]. To avoid this effect, angles lower than 15° were not considered in this study, and α was varied between 15° and 90°. In order to capture the nonlinear relationship of the angle of attack with the lift coefficient, 6 equally spaced values were simulated: $\alpha = (15, 30, 45, 60, 75, 90)°$.

Regarding the resistance coefficients C_n, C_t, D_n and D_t, [1] estimated the four coefficients, while [43] only estimated the inertial coefficients C_n and C_t and assumed the viscous coefficients $D_t = D_n = 0$ as explained before in section 3.2.1.1. To compare both approaches, we carried out two parametric sub-studies: the first one includes only C_n and C_t as parameters ($D_t = D_n = 0$), and the second one includes the four resistance coefficients as parameters.

The maximum values of C_n and C_t in the parametric study were calculated as follows: we considered a incoming fluid velocity $U = 2.5$ m/s and a netting with a solidity ratio $S = 0.5$, which is a 10% higher than the highest values of S found in fishing or aquaculture applications [57]. Then we used the analytical expressions proposed by [34] to predict the drag and lift coefficients of the netting for angles of attack of 90°, 60°and 45°. Finally, the values of C_n and C_t were adjusted in the 2D CFD model (with $D_t = D_n = 0$) to achieve similar values of drag and lift coefficients, taking into account that C_n is usually about 3 times higher than C_t in net panels [43]. The obtained maximum values were $C_n = 30$ and $C_t = 10$, and minimum values were taken as 1% of the maximum values. Preliminary parametric studies shown that the drag and lift coefficients are almost linear with respect to C_n and C_t. Hence, three equally spaced values were considered in the parametric study: $C_n = (0.30, 15.15, 30.00)$ m^{-1} and $C_t = (0.10, 5.05, 10.00)$ m^{-1}.

A similar procedure was followed to calculate the maximum values of D_n and D_t, resulting in $D_n = 1.0 \times 10^6$ m^{-2} and $D_t = 2.5 \times 10^5$ m^{-2}. Again, the minimum values were taken as 1% of the maximum values, and three equally spaced values were considered in the parametric study: $D_n = (1.0 \times 10^4, 5.05 \times 10^5, 1.0 \times 10^6)$ m^{-2} and $D_t = (2.5 \times 10^3, 1.2625 \times 10^5, 2.5 \times 10^5)$ m^{-2}.

Typical values of resistance coefficients reported by other authors (table 3.2)

Table 3.2: Typical values of resistance coefficients of net panels reported in the literature, as a function of the solidity ratio S.

S	C_n (m^{-1})	C_t (m^{-1})	D_n (cm^{-2})	D_t (cm^{-2})
		[1]		
0.184	4.8 - 5.1	1.1 - 1.7	5.2 - 7.6	2.6 - 8.5
0.130	3.3	2.0	11.2	3.4
0.243	6.1	2.8	15.3	3.7
0.317	12.4	6.6	84.5	10.6
		[43]		
0.128	3.7 - 5.2	1.3 - 1.9	0	0
0.215	7.1 - 9.9	2.2 - 3.0	0	0
0.223	6.5 - 8.7	2.0 - 2.7	0	0

are within the selected ranges for the parametric study. Note that these values of resistance coefficients can be directly compared because the thickness of the porous media layer was the same in all cases ($e = 0.05$ m).

The parametric sub-study 1 has $3x6x3x3 = 162$ parameter combinations, while sub-study 2, which includes D_t and D_n as parameters, has $162x3x3 = 1458$ parameter combinations.

3.3.2 Results of the parametric study

Figure 3.4 shows the drag and lift coefficients (C_D and C_L) from the parametric sub-study 1, as a function of the angle of attack, for different values of the incoming velocity U and the resistance coefficients C_n and C_t. The data sets for different velocities are overlapped, since the obtained C_D and C_L are independent of U: The maximum differences in C_D and C_L for $U = 0.25$ and $U = 2.5$ m/s are 2.0×10^{-5} and 1.6×10^{-5} respectively. The curves have the usual shapes of measured drag and lift: the drag increases with the angle of attack, while the lift has its maximum for an angle of attack of 45°. It can be observed that shapes of the curves are different when small values of C_n are combined with high values of C_t: these are combinations of edge values in the parametric study grid are not physically meaningful, since C_n is always higher than C_t in net panels.

Figure 3.5 shows the results of parametric sub-study 2 in the same format as figure 3.4, for different values of the resistance coefficients D_n and D_t. For the sake of brevity, only plots for the middle values of (C_n, C_t) in the parametric grid are shown: $C_n = 15.15$ and $C_t = 5.05$. Plots for other combinations of (C_n, C_t) are similar. The curves also have the usual shapes of measured drag and lift. In this sub-study, C_D and C_L for $U = 1.375$ and $U = 2.5$ are very similar, but they are higher for the smallest velocity $U = 0.25$, specially when D_n gets higher. As expected, sub-study 2 converges to sub-study 1 when D_n and D_t get close to zero: it can be observed that results for small values of D_n and D_t, shown in the upper-left sub-plots, are very similar to those obtained from the parametric sub-study 1.

Figure 3.6 shows C_D and C_L from the parametric sub-study 1, as a function of

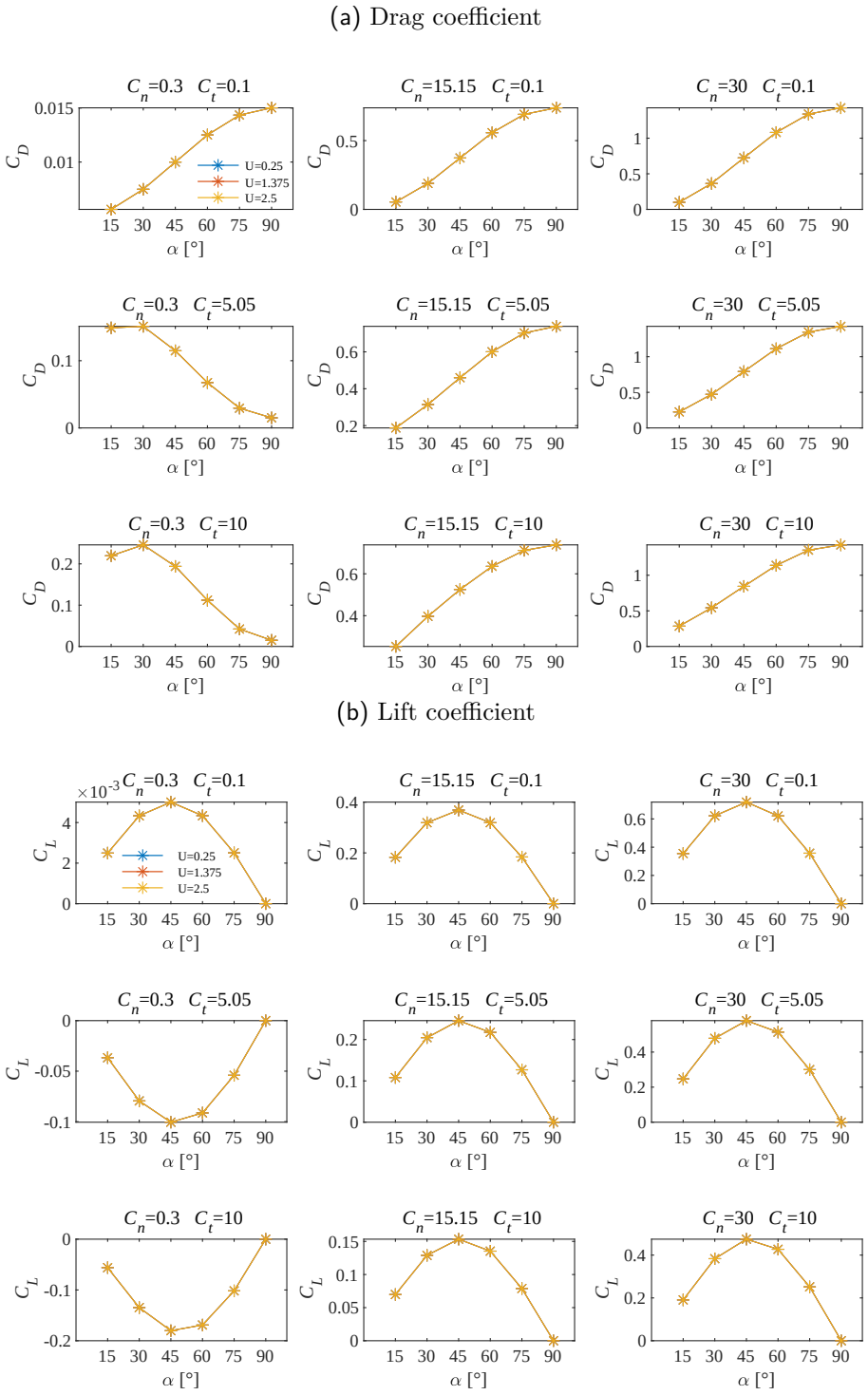

Figure 3.4: Drag and lift coefficients C_D and C_L from the CFD parametric sub-study 1 ($D_n = D_t = 0$), as a function of the angle of attack α. The data sets for different velocities are overlapped. All magnitudes are in SI units except α.

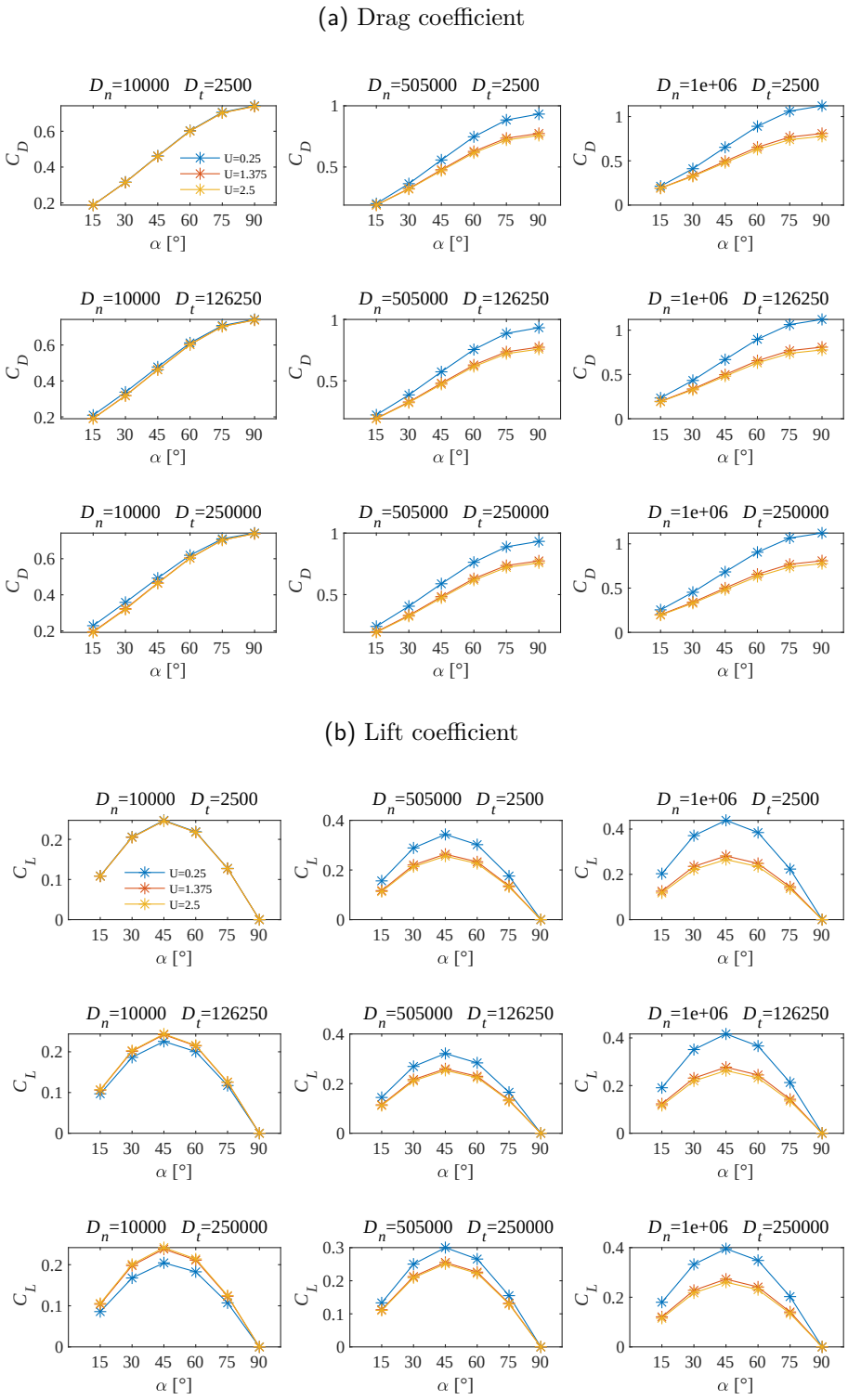

Figure 3.5: Drag and lift coefficients C_D and C_L from the CFD parametric sub-study 2, as a function of the angle of attack α, particularized for $C_n = 15.15$ and $C_t = 5.05$. All magnitudes are in SI units except α.

the resistance coefficients C_n and C_t, for different velocities and angles of attack. Again, the data sets for different velocities are overlapped. It can be observed that C_D and C_L have a linear dependence with C_n and a slightly non-linear dependence with C_t, specially for angles of attack smaller than 45°. This fact justifies the decision of considering just three values of the resistance coefficients in the parametric study, since they are enough to capture their effect on drag and lift.

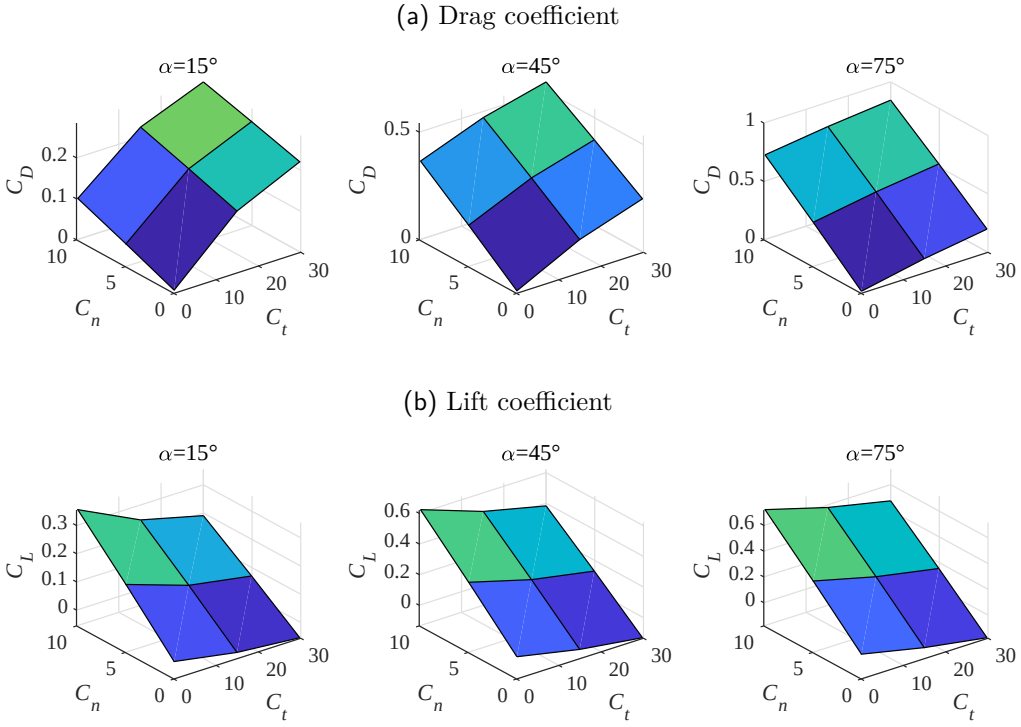

Figure 3.6: Drag and lift coefficients C_D and C_L from CFD parametric sub-study 1 as a function of the resistance coefficients C_n and C_t. Only three angles of attack α are shown. All magnitudes are in SI units except α.

Figure 3.7 shows the results of parametric sub-study 2 in the same format as figure 3.6, for different values of the resistance coefficients D_n and D_t. Again, only plots for $C_n = 15.15$, $C_t = 5.05$ and $U = 0.25$ are shown, since plots for other values are similar. It can be observed that C_D and C_L have a linear dependence with D_n and D_t, as expected from equation 3.3.

Finally, drag and lift coefficients C_D and C_L obtained from parametric sub-study 1 are listed in table 3.3. The incoming fluid velocity U is not included in the table because it does not affect results. Results from parametric sub-study 2 are not listed for the sake of brevity.

3.3.3 Regression model

The results of the CFD parametric study are used to interpolate the drag and lift coefficients of the net panel, C_D and C_L, as a function of the angle of attack α, the incoming fluid velocity U and the resistance coefficients of the porous medium.

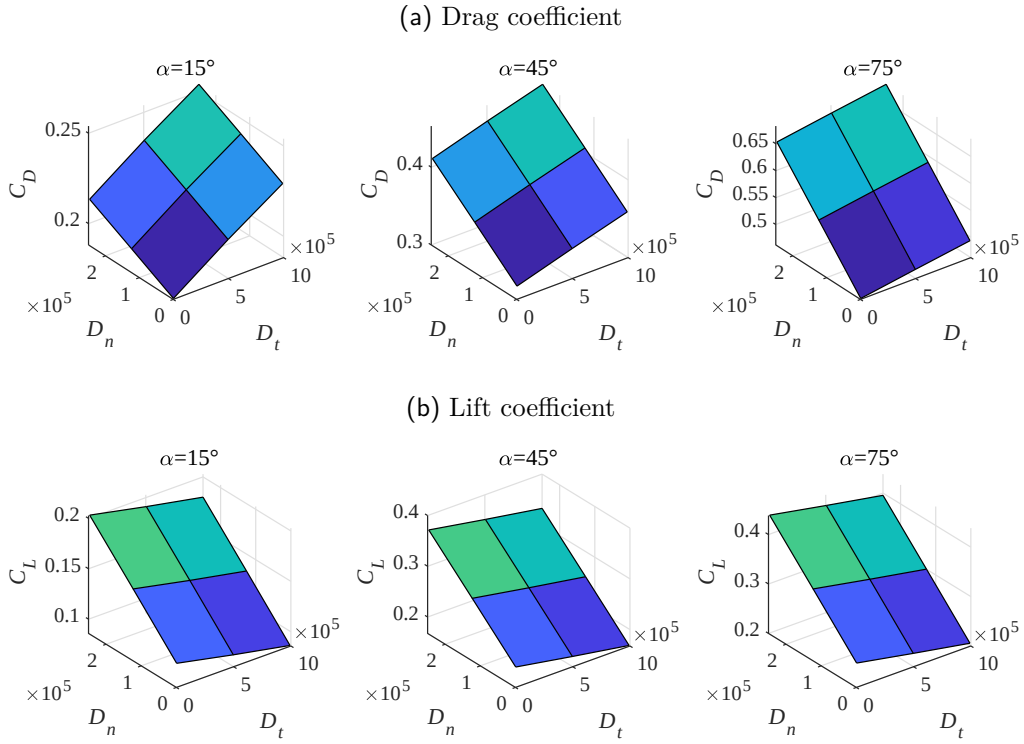

Figure 3.7: Drag and lift coefficients C_D and C_L from CFD parametric sub-study 2 as a function of the resistance coefficients D_n and D_t, for $C_n = 15.15$, $C_t = 5.05$ and $U = 0.25$. Only three angles of attack α are shown. All magnitudes are in SI units except α.

Table 3.3: Drag and lift coefficients C_D and C_L obtained in the parametric sub-study 1.

$\alpha(°)$	C_n	C_t	C_D	C_L
15	0.3	0.1	0.00561	0.00249
15	0.3	5.05	0.14892	-0.03669
15	0.3	10	0.21960	-0.05605
15	15.15	0.1	0.05388	0.18266
15	15.15	5.05	0.18750	0.10812
15	15.15	10	0.25302	0.06980
15	30	0.1	0.10002	0.35487
15	30	5.05	0.22450	0.24694
15	30	10	0.28512	0.19064
30	0.3	0.1	0.00747	0.00433
30	0.3	5.05	0.15112	-0.07944
30	0.3	10	0.24595	-0.13476
30	15.15	0.1	0.18908	0.31890
30	15.15	5.05	0.31442	0.20469
30	15.15	10	0.39703	0.12894
30	30	0.1	0.36392	0.62177
30	30	5.05	0.47183	0.47848
30	30	10	0.54274	0.38315
45	0.3	0.1	0.00999	0.00500
45	0.3	5.05	0.11480	-0.10054
45	0.3	10	0.19388	-0.18016
45	15.15	0.1	0.37369	0.36873
45	15.15	5.05	0.45981	0.24583
45	15.15	10	0.52516	0.15338
45	30	0.1	0.72378	0.71886
45	30	5.05	0.79199	0.57926
45	30	10	0.84412	0.47439
⋮	⋮	⋮	⋮	⋮
⋮	⋮	⋮	⋮	⋮
60	0.3	0.1	0.01250	0.00433
60	0.3	5.05	0.06745	-0.09136
60	0.3	10	0.11204	-0.16903
60	15.15	0.1	0.55759	0.31906
60	15.15	5.05	0.60050	0.21753
60	15.15	10	0.63585	0.13531
60	30	0.1	1.08082	0.62118
60	30	5.05	1.11214	0.51397
60	30	10	1.13846	0.42725
75	0.3	0.1	0.01434	0.00250
75	0.3	5.05	0.02942	-0.05406
75	0.3	10	0.04215	-0.10176
75	15.15	0.1	0.69113	0.18386
75	15.15	5.05	0.70240	0.12692
75	15.15	10	0.71211	0.07888
75	30	0.1	1.33823	0.35726
75	30	5.05	1.34575	0.29991
75	30	10	1.35243	0.25149
90	0.3	0.1	0.01502	0
90	0.3	5.05	0.01502	0
90	0.3	10	0.01502	0
90	15.15	0.1	0.73831	0
90	15.15	5.05	0.73831	0
90	15.15	10	0.73831	0
90	30	0.1	1.42645	0
90	30	5.05	1.42645	0
90	30	10	1.42645	0

If the viscous resistance coefficients are neglected as in [43], the incoming flow velocity does not affect C_D and C_L, and the interpolation of results from parametric sub-study 1 provides

$$\begin{aligned} C_D &= C_D\left(\alpha, C_n, C_t\right) \\ C_L &= C_L\left(\alpha, C_n, C_t\right) \end{aligned} \tag{3.8}$$

If the viscous resistance coefficients are considered as in [1], the interpolation of results from parametric sub-study 2 provides

$$\begin{aligned} C_D &= C_D\left(\alpha, U, C_n, C_t, D_n, D_t\right) \\ C_L &= C_L\left(\alpha, U, C_n, C_t, D_n, D_t\right) \end{aligned} \tag{3.9}$$

Such N-D gridded data interpolation was implemented with the function *interpn* from the Matlab software [58], using the *spline* interpolation method, which also

allows to extrapolate values outside of the domain of the data grid. A alternative implementation could be achieved with the functions *scipy.interpolate.interpn* or *scipy.interpolate.RegularGridInterpolator* from the open source ScyPy Python library [59].

3.4 Estimation of resistance coefficients

Equations 3.8 and 3.9 describe a regression model with two dependent variables (the drag and lift coefficients, C_D and C_L), two independent variables (the angle of attack α and the incoming fluid velocity U) and two or four unknown model parameters (the resistance coefficients C_n, C_t, D_n and D_t). The estimation of the resistance coefficients from experimental data is a model fitting problem, where model parameters are optimized to minimize the difference between measured experimental data and values calculated by the model. As explained in section 3.3.2, the dependent variables are slightly nonlinear in terms of one of the model parameters. Therefore, this is a non-linear multivariate regression problem which can be formulated as an optimization problem that minimizes an error function.

3.4.1 Error functions

[1] proposed different statistical metrics or error functions to evaluate the difference between measured data and values predicted by the model. The authors recommended LANE (least square absolute normalized error)

$$\begin{aligned} LANE = \frac{1}{N}\sum^{N}\left|\frac{C_D - C_D^{measured}}{C_D}\right| \\ +\frac{1}{M}\sum^{M}\left|\frac{C_L - C_L^{measured}}{C_L}\right| \end{aligned} \tag{3.10}$$

over LSNE (least square normalized error)

$$\begin{aligned} LSNE = \frac{1}{N}\sum^{N}\left(\frac{C_D - C_D^{measured}}{C_D}\right)^2 \\ +\frac{1}{M}\sum^{M}\left(\frac{C_L - C_L^{measured}}{C_L}\right)^2 \end{aligned} \tag{3.11}$$

where N and M and the number of observations in drag and lift, arguing that LSNE has a higher response to outlier points than LANE due to its dependency on the squared residuals. They did not recommend using the least absolute error (LAE) error function similar to that used by [3].

We also used LANE and LNSE in this work, and we compared them to a not normalized error metric, the sum of squares of the mean absolute error (MAE) in each coefficient

$$\begin{aligned} MAE = \left(\frac{1}{N}\sum^{N}\left|C_D - C_D^{measured}\right|\right)^2 \\ +\left(\frac{1}{M}\sum^{M}\left|C_L - C_L^{measured}\right|\right)^2 \end{aligned} \tag{3.12}$$

The optimization problem was solved with the Matlab software. Several non-linear unconstrained multivariable minimization methods were tested, and finally the Nelder-Mead Simplex Method [60] implemented in the function *fminsearch* was selected, since it provides the best convergence properties. The optimization is solved in less than one second in a personal computer. An alternative implementation could be achieved with the function *scipy.optimize.minimize* from the ScyPy software.

3.4.2 Goodness of fitting

Previous authors [1, 43] did not provide any quantitative measure of the goodness of fitting of the proposed models, which were evaluated in a qualitative way from plots of the fitted models against the measurements. In this work we propose to use the coefficient of determination R^2 as an intuitive measure of the goodness of fit of a model. It should be applied with caution in non-linear models, but the model proposed in this work is only slightly non-linear in one of the coefficients, so it can be used in its most general definition:

$$R^2 = 1 - \frac{SS_{res}}{SS_{tot}} \tag{3.13}$$

where SS_{res} is the residual sum of squares and SS_{tot} is the total sum of squares.

In multivariate regression, R^2 increases when additional parameters are added to the model (e.g. sub-study 1 has 2 parameters and sub-study 2 has 4 parameters). To avoid this effect, the adjusted coefficient of determination $\bar{R}^2$ is used instead:

$$\bar{R}^2 = 1 - (1 - R^2)\frac{n-1}{n-p} \tag{3.14}$$

where n is the sample size (M and N in equations 3.10 to 3.12) and p is number of explanatory variables (2 in the parametric sub-study 1 and 4 in the sub-study 2). For each estimation of the resistance coefficients, $\bar{R}^2$ was calculated for the drag and lift coefficients.

3.5 Results

In this section, method described in section 3.4 is used to estimate the resistance coefficients of net panels based on experimental data published by other authors.

3.5.1 Example 1

The first example uses the experimental data presented in [1]. The experimental setup used a flat net panel of 1 m by 1 m knotless nylon with twine diameter $d = 2.8$ mm and mesh bar length $\lambda = 29$ mm, with an estimated solidity $S = 0.184$. Measurements were carried out in a towing tank at towing speeds of 0.125, 0.25, 0.50, 0.75 m/s and angles of attack of 0, 15, 30, 45, 60 and 90 degrees. Drag and lift forces on the net panel were measured and used to calculate C_D and C_L.

Table 3.4 shows the estimates of resistance coefficients using the parametric sub-studies 1 and 2 and different error functions, and the resulting adjusted coefficients

of determination for drag and lift. Estimates obtained by other authors are also listed, since they can be directly compared because the thickness of the porous media layer was the same in all cases; they were used to evaluate our CFD-based model and obtain the corresponding $\bar{R}^2$ values. Note that [43] calculated a set of resistance coefficients for each incoming fluid velocity, and the table only lists the estimates for $U = 0.5$ and $U = 0.75$ m/s, which are equal. Figure 3.8 plots a selection of fitted models against measurements for different velocities.

Table 3.4: Resistance coefficients for the experimental data in [1]. All magnitudes in SI units.

Method	C_n	C_t	D_n	D_t	$\bar{R}^2_D$	$\bar{R}^2_L$
Sub-study 1						
LSNE	5.527	1.908	0	0	0.948	0.925
LANE	5.412	1.828	0	0	0.956	0.924
MAE	5.268	1.761	0	0	0.953	0.919
[43]						
Chen	5.32	1.71	0	0	0.955	0.924
Sub-study 2						
LSNE	4.085	0.917	195032	124953	0.975	0.935
LANE	4.645	1.088	100121	89213	0.980	0.921
MAE	4.470	1.084	121763	91414	0.981	0.926
Patursson [1]						
LSNE	4.842	1.444	75854	35409	0.971	0.928
LAE	5.073	1.130	76486	84741	0.963	0.901
LANE	5.098	1.698	51730	26379	0.964	0.925

3.5.2 Example 2

The second example used the experimental data presented in [2]. It used three different net panels with solidity ratios S of 0.130, 0.243 and 0.317. Measurements were carried out at towing speeds of 0.159, 0.316, 0.966 m/s and angles of attack of 10, 30, 45, 60 and 90 degrees. Note that an angle of attack of 10° is outside the range of α used in the CFD parametric study, so the regression models in equations 3.8 and 3.9 need to extrapolate data during the regression analysis.

Tables 3.5, 3.6 and 3.7 show the estimates of resistance coefficients for each net panel. Figures 3.9, 3.10 and 3.11 plot a selection of fitted models against measurements for each net panel.

3.5.3 Example 3

The third example used the experimental data presented in [3]. They used three different flat net panels with solidity ratios S of 0.128, 0.215 and 0.223. Measurements

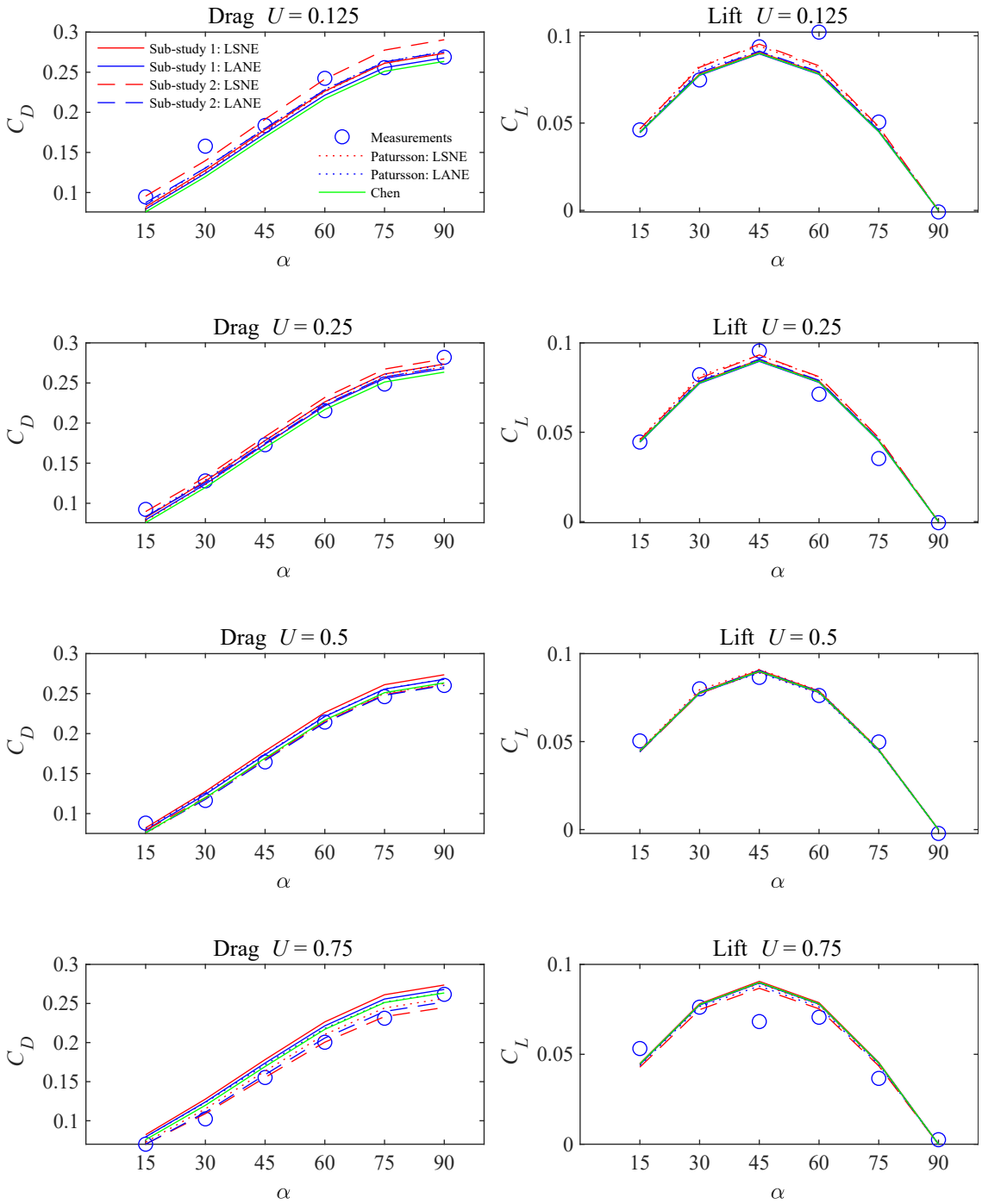

Figure 3.8: Fitted models for the experimental data in [1].

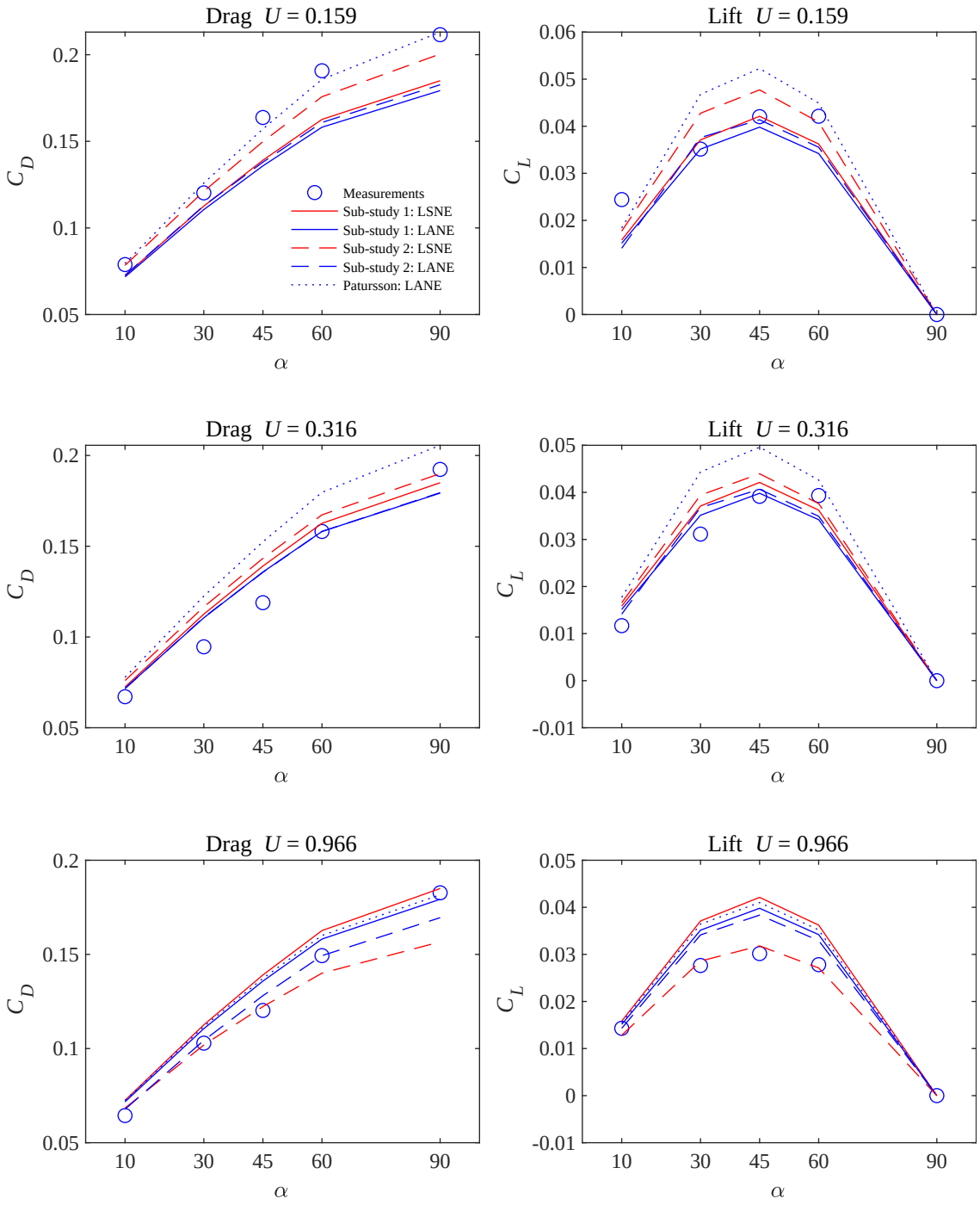

Figure 3.9: Fitted models for the experimental data in [2] with solidity $S = 0.13$.

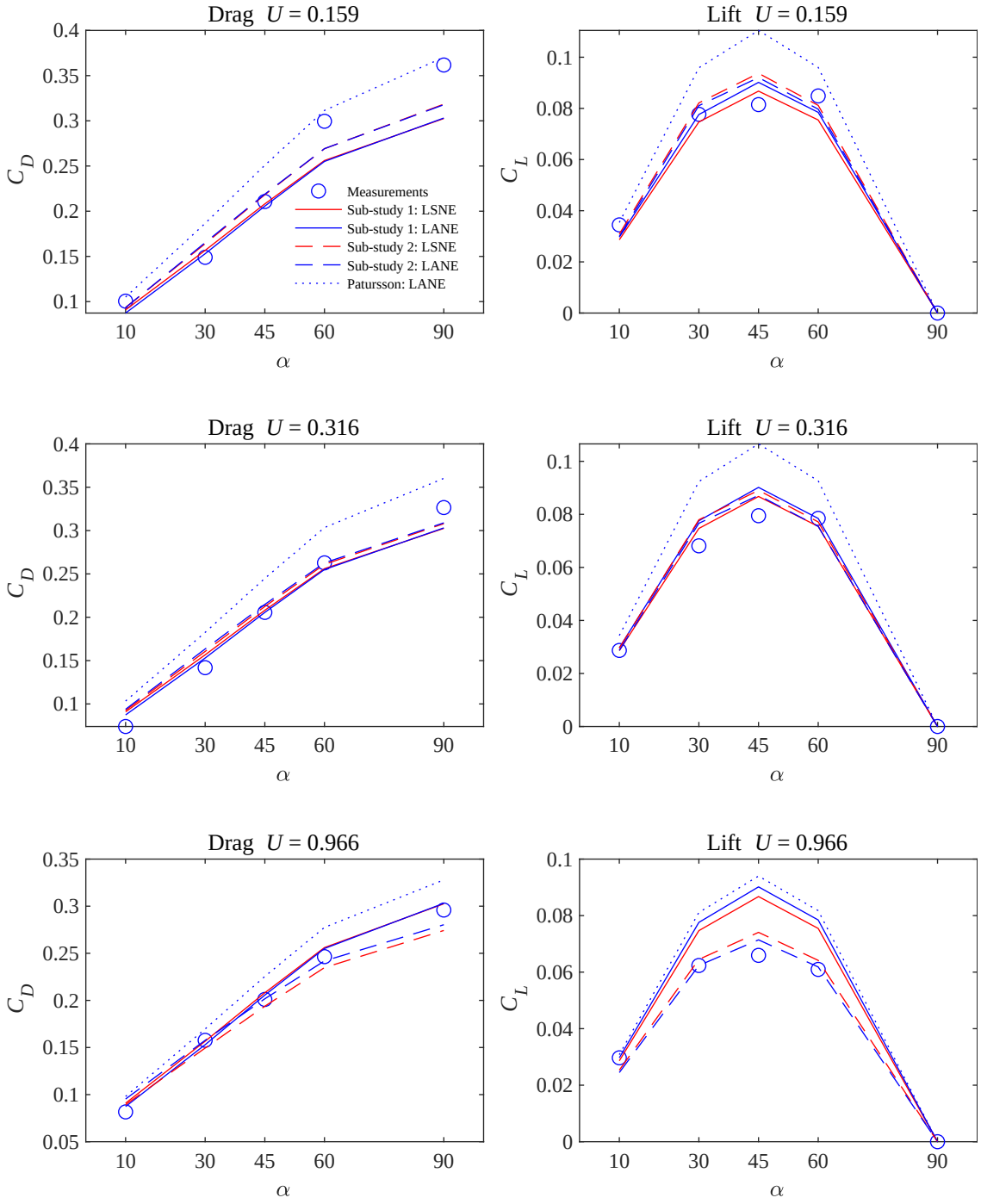

Figure 3.10: Fitted models for the experimental data in [2] with solidity $S = 0.243$.

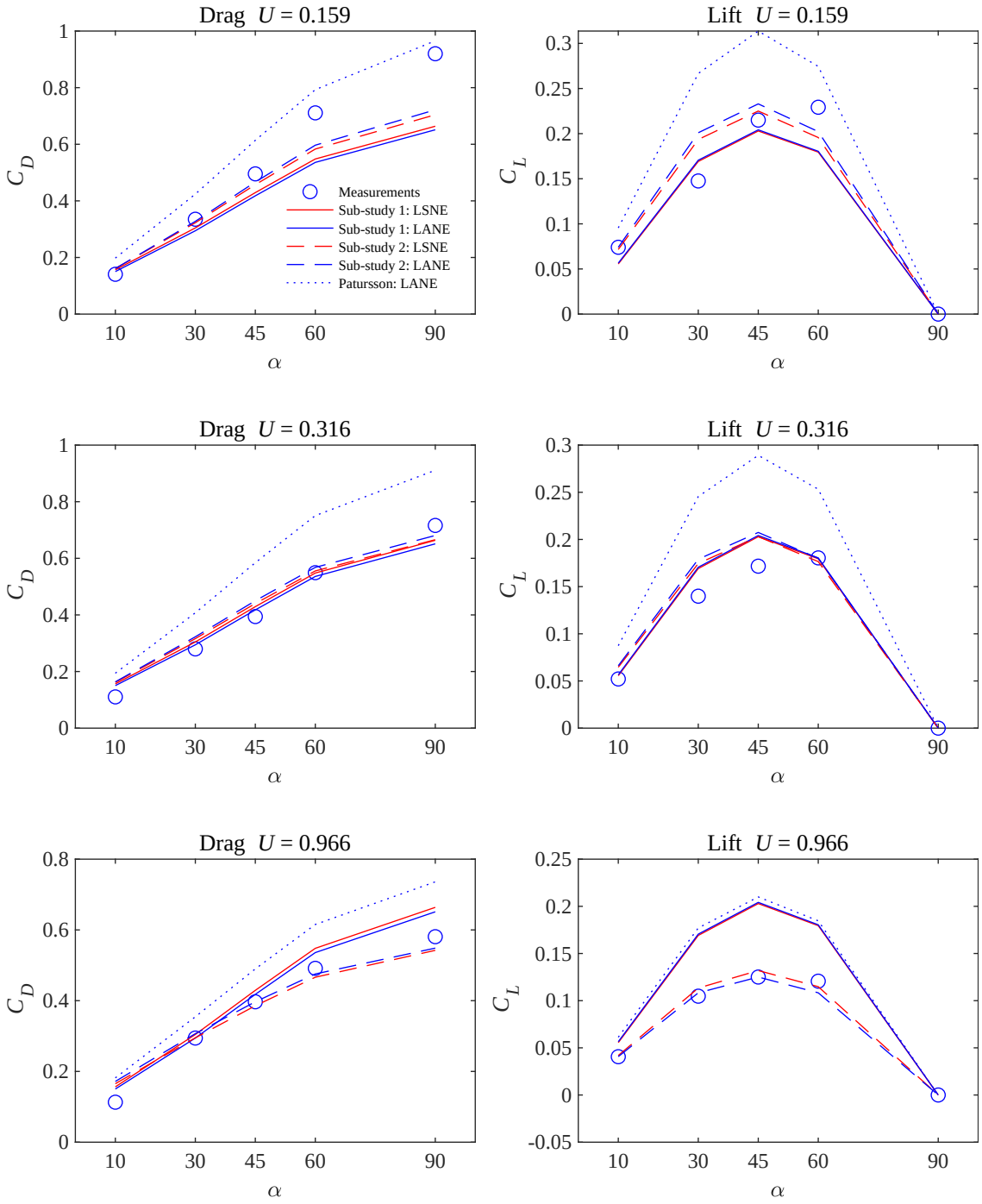

Figure 3.11: Fitted models for the experimental data in [2] with solidity $S = 0.317$.

Table 3.5: Resistance coefficients for the experimental data in [2] with solidity $S = 0.13$. All magnitudes in SI units.

Method	C_n	C_t	D_n	D_t	$\bar{R}_D^2$	$\bar{R}_L^2$
Sub-study 1						
LSNE	3.726	2.121	0	0	0.826	0.864
LANE	3.610	2.099	0	0	0.787	0.873
MAE	3.679	1.928	0	0	0.834	0.826
Sub-study 2						
LSNE	2.656	1.822	156123	45927	0.861	0.918
LANE	3.263	1.866	46912	27049	0.793	0.875
MAE	3.339	1.629	71009	65443	0.891	0.802
Patursson [1]						
LANE	3.302	1.993	112250	34352	0.862	0.802

Table 3.6: Resistance coefficients for the experimental data in [2] with solidity $S = 0.243$. All magnitudes in SI units.

Method	C_n	C_t	D_n	D_t	$\bar{R}_D^2$	$\bar{R}_L^2$
Sub-study 1						
LSNE	6.117	2.694	0	0	0.910	0.932
LANE	6.128	2.554	0	0	0.916	0.913
MAE	6.130	2.552	0	0	0.916	0.913
Sub-study 2						
LSNE	5.035	2.592	158745	19542	0.923	0.963
LANE	5.236	2.952	134645	-14120	0.922	0.971
MAE	5.420	3.067	120872	-66758	0.946	0.919
Patursson [1]						
LANE	6.149	2.815	152760	37283	0.870	0.790

were carried out at towing speeds of 0.25, 0.5, 0.75 and 1 m/s and angles of attack of 30, 60 and 90 degrees. Only the drag forces were measured.

Tables 3.8, 3.9 and 3.10 show the estimates of resistance coefficients for each net panel. Figure 3.12 plot a selection of fitted models against measurements for each net panel. Results are compared with those in [43].

When the resistance coefficients calculated in [43] are used to evaluate the proposed 2D CFD model, the obtained drag and lift coefficients are slightly different that those published by the same authors, which were obtained using a 3D CFD model that replicated the conditions of the experimental setup. As a consequence, the fitting with experimental data is also slightly worse. The goodness of fitting of the proposed method is similar to that of [43] when only C_n and C_t are estimated. When D_n and D_t are also estimated, the fittings are clearly better. Again, the estimates of D_t were negative in some cases. Note that [43] calculates one set of resistance coefficients per velocity, while we estimated just one set for all the velocities. None of

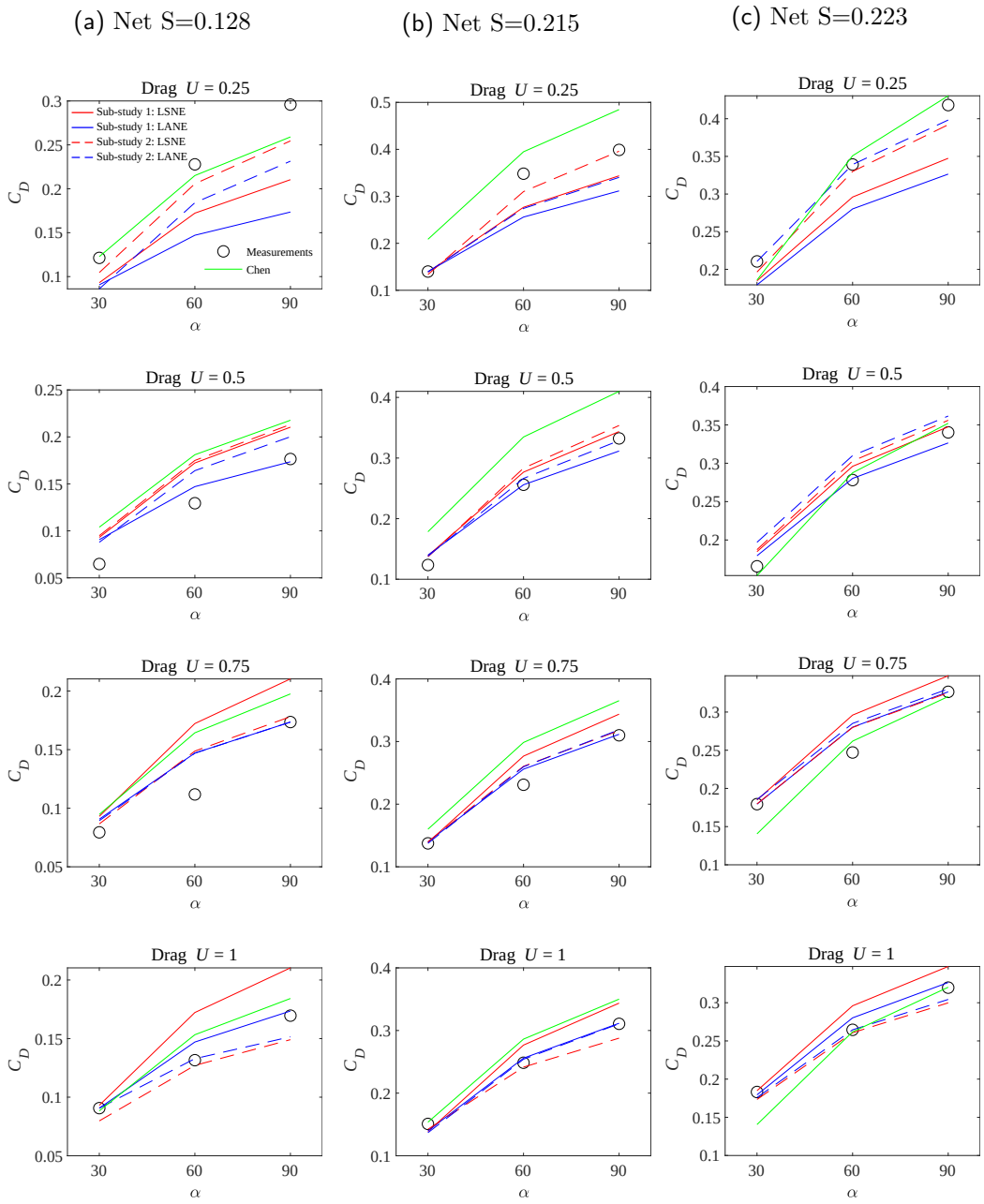

Figure 3.12: Fitted models for the experimental data in [3]. All magnitudes are in SI units except α.

Table 3.7: Resistance coefficients for the experimental data in [2] with solidity $S = 0.317$. All magnitudes in SI units.

Method	C_n	C_t	D_n	D_t	$\bar{R}_D^2$	$\bar{R}_L^2$
Sub-study 1						
LSNE	13.585	5.380	0	0	0.736	0.788
LANE	13.322	5.036	0	0	0.714	0.784
MAE	13.641	4.875	0	0	0.754	0.759
Sub-study 2						
LSNE	9.174	6.481	590140	-102079	0.776	0.917
LANE	9.175	7.303	630939	-187126	0.813	0.906
MAE	9.676	7.378	662756	-208439	0.879	0.853
Patursson [1]						
LANE	12.401	6.574	845370	105900	0.736	0.584

the methods can provide a good fitting for the first net panel ($S = 0.128$), with values of $\bar{R}^2$ below 0.51 and even negative in some cases. Regarding the error functions, LSNE provides better fittings in terms $\bar{R}^2$ although the in the plots LANE looks better for some velocities.

3.6 Discussion

The estimates of resistance coefficients obtained with the proposed method are within the same order of magnitude of those obtained by other authors, but differences exist even if the same error function is used: differences in inertial and viscous resistance coefficients can reach up to 70% and 250% respectively. The goodness of fitting of the proposed method is similar or better than that of methods proposed by other authors, both quantitatively (adjusted coefficient of determination $\bar{R}^2$) and qualitatively (plots of fitted models against measured data). The values of $\bar{R}^2$ were above 0.80 in 6 of the 7 net panels. The main disadvantage of the method is that, contrary to the method in [43], it needs experimental measurements of the net panel.

In example 2, the fitting of the drag coefficients with experimental data is not very good at velocity $U = 0.159$ even if the four resistance coefficients are calculated. This could be explained because that velocity is outside the range of incoming fluid velocity U used in the parametric study, which started at $U = 0.25$ m/s, and therefore extrapolation of the 2D CFD model is required in the regression analysis. According to figure 3.5, extrapolation for $U < 0.25$ m/s is not accurate because the sampled points cannot capture the non-linear relation between drag and U at very small velocities. This could be resolved using more sample points in U in the parametric study, but we consider that is not worth it: real fishing and aquaculture applications focus on estimating the maximum hydrodynamic forces on the structures, which occur at velocities higher than 0.25 m/s.

The estimates of D_t were negative for some cases in examples 2 and 3. This is not

Table 3.8: Resistance coefficients for the experimental data in [3] with solidity $S = 0.128$. All magnitudes in SI units.

Method	C_n	C_t	D_n	D_t	$\bar{R}_D^2$	$\bar{R}_L^2$
Sub-study 1						
LSNE	4.240	1.260	0	0	0.140	-
LANE	3.493	1.475	0	0	-0.756	-
MAE	3.493	1.109	0	0	-0.314	-
[43]						
$U = 0.25$	5.230	1.86	0	0	0.140	-
$U = 0.5$	4.390	1.56	0	0	0.070	-
$U = 0.75$	3.980	1.415	0	0	-0.105	-
$U = 1$	3.710	1.315	0	0	-0.289	-
Sub-study 2						
LSNE	1.733	1.329	422167	-9152	0.645	-
LANE	2.088	2.121	320032	-152500	0.411	-
MAE	1.829	0.938	379093	110987	0.510	-

Table 3.9: Resistance coefficients for the experimental data in [3] with solidity $S = 0.215$. All magnitudes in SI units.

Method	C_n	C_t	D_n	D_t	$\bar{R}_D^2$	$\bar{R}_L^2$
Sub-study 1						
LSNE	6.959	1.709	0	0	0.821	-
LANE	6.301	2.016	0	0	0.694	-
MAE	6.329	1.919	0	0	0.712	-
[43]						
$U = 0.25$	9.860	3.030	0	0	0.364	-
$U = 0.5$	8.320	2.555	0	0	0.587	-
$U = 0.75$	7.400	2.275	0	0	0.748	-
$U = 1$	7.090	2.175	0	0	0.781	-
Sub-study 2						
LSNE	4.504	3.026	436981	-236726	0.934	-
LANE	5.922	2.036	120184	-42391	0.807	-
MAE	5.100	1.358	370128	80155	0.906	-

Table 3.10: Resistance coefficients for the experimental data in [3] with solidity $S = 0.223$. All magnitudes in SI units.

Method	C_n	C_t	D_n	D_t	$\bar{R}^2_D$	$\bar{R}^2_L$
Sub-study 1						
LSNE	7.036	3.355	0	0	0.744	-
LANE	6.606	3.336	0	0	0.655	-
MAE	6.606	3.336	0	0	0.655	-
[43]						
$U = 0.25$	8.740	2.650	0	0	0.600	-
$U = 0.5$	7.130	2.160	0	0	0.787	-
$U = 0.75$	6.480	1.965	0	0	0.649	-
$U = 1$	6.480	1.965	0	0	0.649	-
Sub-study 2						
LSNE	4.944	3.308	372330	-271	0.912	-
LANE	5.014	3.112	379492	80202	0.895	-
MAE	5.733	2.252	198619	229788	0.826	-

a fault in the proposed regression model and estimation method, but a consequence of using an unconstrained optimization method for the non-linear regression analysis described in section 3.4. A constrained optimization method would avoid this by setting lower bound constraints on the resistance coefficients, but its goodness of fitting would be worse due to the active constraint on D_t. Therefore, we prefer using an unconstrained method, because a negative value of D_t does not cause any practical problem in CFD models of porous media and provides better agreement with experimental data.

Estimating just the inertial resistance coefficients (C_n,C_t) gives good fittings, but estimating both the inertial and viscous resistance coefficients always gives better fittings, as expected: $\bar{R}^2$ increases up to 3% in example 1, up to 16% in example 2 and up to 36% in example 3. The main advantage of including the four resistance coefficients in the regression analysis is that the regression model in equation 3.9 also depends on the incoming fluid velocity, and hence the model fits better the data set for each measured velocity. Regarding the error functions, it is not clear which one provides better results: results vary depending on the netting solidity, the measured velocity and and the force component (drag or lift). Therefore, we recommend doing the regression analysis with different error functions and selecting the one that best fits a particular netting material.

Compared with the method in [1], we have found that our 2D CFD model provides different drag and lift coefficients for the resistance coefficients calculated in that work, and the resulting fitting with experimental data is worse, specially for the lift coefficient and in example 2. This suggests that estimates of coefficients obtained by regression analysis with a simplified analytical model not always deliver good agreement with measured data when used in a full CFD model. Our 2D CFD model also provides drag and lift coefficients different from those calculated with a 3D model in [43]. The reason could be in the differences between models: the 2D CFD

model assumes a porous media with infinite area, while the 3D CFD model replicates the experimental setup in a towing tank, with a finite porous media and boundary conditions on the walls.

We estimated a set of resistance coefficients for all measured velocities, as in [1]. In case that better agreement with experimental data is required, the method could be used to calculate a different set of coefficients per measured velocity, as in [43], and interpolate them for other velocities. However, introducing velocity-dependent resistance coefficients in a CFD model is quite more complex than using constant coefficients, and hence we consider that it is more convenient to estimate a set of constant coefficients.

The proposed method is quite easy to use compared with that in [1], since its implementation only requires the interpolation of results of the CFD parametric study, as described in Section 3.3.3, and coding the selected error function for the regression analysis. In addition, estimating 4 resistance coefficients instead of 2 does not appreciably increase the complexity of the implementation. The obtained regression model has a high computational performance, allowing to carry out a regression analysis within seconds despite being based on a full CFD model.

The method proposed in [43] has the advantage of not relying on experimental data. But it is based on expressions to calculate hydrodynamic forces on a idealized knotless net panel with small single twines, the typical netting used in aquaculture applications. Due to this assumption, it may predict wrong values for netting used in fishing applications, with often has big knots and thick or double twines. In comparison, method presented in this work is based on a CFD model of porous media without any assumption about the geometric characteristics of the actual material. The range of values of resistance coefficients used in the CFD parametric study was quite wide, and the regression model can be safely extrapolated outside the data grid because it is linear with respect C_n, D_n and D_t and only slightly non-linear with respect C_t for the range of sampled velocities. Therefore, the method could be used to estimate the resistance coefficients of materials other than knotless, single-twine net panels. This includes knotted and double twine netting, but also materials other than netting that may be modelled as porous media. Future research should include validating the approach for such materials.

3.7 Conclusions

Modelling net panels as porous media is a practical approach to carry out CFD simulations of aquaculture cages and fishing gears. This work presents a method to estimate the resistance coefficients of such porous media, based on regression analysis with experimental data. The main contribution is a new regression model based on a full CFD model of the flow through a layer of porous media, the same type of CFD model used to simulate net panels in fishing and aquaculture applications. To increase the computational performance of the regression analysis, the CFD model response is pre-calculated by a parametric study and interpolated to build an efficient regression model. The methods allows to estimate both the viscous and the inertial resistance coefficients or just the inertial ones, as proposed by some authors. It was applied to different net panels and results were compared with existing methods.

The new method provides similar or better goodness of fitting than existing methods, depending on the analyzed net panel. Values of the adjusted coefficient of determination $\bar{R}^2$ were close or above 0.9 for most of the net panels. In addition, it is easier to use than the method in [1] because the regression model is explicit and easy to implement. The computational performance is very good, allowing to estimate the resistance coefficients within one second. Estimating both the inertial and the viscous resistance coefficients always provides better results than estimating just the inertial coefficients and it does not complicate the implementation too much with the proposed method. It is not clear which error function provides better results, hence we recommend doing the regression analysis with different error functions and selecting the one that works better for a particular experimental data set.

Another advantage of the method is that, being based on a CFD model of porous media without any assumption about the geometric characteristics of the actual material, it may be applied to estimate the resistance coefficients of a wide range of netting (knotless or knotted, single or double twine, thin or thick twines ...) or other materials that may be modelled as porous media. Future research should include validating the methods for such materials.

Chapter 4

Application: Understanding effect of bottom trawling on sediment transport

Demersal fishing and its impact on seabed alteration is an area which needs urgent attention. Trawl gears and their impact on sediment mobilization are studied extensively in the recent years, even though the contribution of fishing nets on sediment mobilization is yet to be investigated. In this research we conduct numerical simulations of netting panel close to the seabed to understand the impact of fishing net on sediment entrainment while trawling. An comprehensive study has been carried out for understanding the importance of different parameters which are usual variables in demersal trawling including the velocity of trawling, angles of attack net makes with the seabed, distance from the seabed, type of fishing net, length of the fishing net among some of them. Results shows the dependence of these parameters on sediment transport and also hydrodynamic forces which contributes to the efficiency of towing and will permit a better assessment of environmental impact of towed fishing gears.

4.1 Introduction

Demersal fishing gears are responsible for about 25 per cent of global catches of wild fish. These gears, when towed across the seabed can have a physical impact. Their seabed contacting components can penetrate into the substrate, laterally displace sediment and cause compaction, shearing and increased pressure in the sediment. The hydrodynamic turbulence that is formed in their wake can mobilise sediment into the water column, increasing turbidity, and if transported away, cause a winnowing of the seabed [61]. These processes can lead to increased mortality and alter the benthic environment, which may reduce productivity and threaten the biological and economic sustainability of a fishery.

There have been many studies of the sediment mobilisation of the towed demersal gears. These have ranged from measurements taken during experimental trials with particular gears, to monitoring and modelling studies ([62–66]). It is evident that the physical impact of a gear is not uniform across its swept width, and that a

full understanding will only be achieved if the impacts are considered at the level of each of the gear components ([66–68]). [69] demonstrate that the quantity of sediment mobilised by individual trawl components that are towed across the seabed is directly related to the turbulence they generate and the sediment type. Their studies, however, only investigate gear components that contact the sea floor and do not examine the effect of the turbulence generated by the trawl netting.

This is a significant gap in our understanding of the seabed impacts of towed fishing gears, as in general, the trawl netting is the largest part of a trawl gear. Demersal trawl gears are designed so that the netting panels are towed close to, but do not come into contact with, the sea floor. Nevertheless, their passage through the water causes turbulence, which has the capacity to mobilise sediment into the water column.

The study of towed fishing gears and aquaculture cages in a current are fluid-structure interaction problems, where the fluid flow deforms the netting structure, which in turn, will modify the flow. A number of numerical netting deformation models have been developed, which either consider the twine bars and knots to be mass elements in large dynamical systems, or the netting surface to be a thin membrane [11, 13, 14, 70–73].

When it comes to the hydrodynamics of fishing nets, fluid simulations are more challenging and to make them computationally affordable, methods using the porous media model have been considered ([1, 21, 46]). In this approach, the netting surface is considered in terms of the porous resistance it offers and is introduced into the Navier - Stokes equations as a source term. Most of these studies model the netting as porous solids, which tend to have difficulties while simulating fishing nets with large deflections ([43, 48, 49]). In order to deal with the complex shapes of trawl gears and facilitate easy coupling with structural solvers [74] have developed a porous media approach which considers netting as a surface. This approach is applied here to get a better understanding of the flow through and around netting panels that are towed close to the seabed.

In particular, numerical simulations are carried out to better understand the importance of the following parameters in relation to sediment mobilisation while demersal trawling:

- Distance of the netting from the seabed.
- Angle of the netting with respect to the seabed.
- Solidity of the fishing net.
- Length of the netting.
- Trawling velocity.

4.2 Numerical approach

4.2.1 Governing Equations

The numerical approach used in this study solves the Reynolds Averaged Navier Stokes equations (RANS) with an additional source term to account for the porous resistance offered by the fishing net. A steady state solution for a netting panel in an incompressible, uniform flow is found for the following equations :

the continuity equation,

$$\nabla \cdot \mathbf{u} = 0 \tag{4.1}$$

and the momentum equation,

$$\nabla \cdot (\mathbf{u} \otimes \mathbf{u}) - \nabla \cdot \mathbf{R} = -\nabla p + \mathbf{S}. \tag{4.2}$$

where $\mathbf{u}$ is the velocity of the fluid, p is the kinematic pressure, and the source term $\mathbf{S}$ is the resistance offered by the fishing net in the fluid flow which is calculated by the porous media model. $\mathbf{R}$ is the Reynolds stress tensor,

$$\mathbf{R} = \nu_{eff} \nabla \mathbf{u}. \tag{4.3}$$

where ν_{eff} is the effective kinematic viscosity calculated using the transport models and turbulence models. The hydrodynamic force coefficients are defined as:

$$\begin{aligned} C_D &= \frac{2F_{\text{Drag}}}{\rho A u_\infty^2} \\ C_L &= \frac{2F_{\text{Lift}}}{\rho A u_\infty^2}. \end{aligned} \tag{4.4}$$

where F_{Drag} is the force in the x direction and F_{lift} is the force in the y direction, A is the total area of the netting panel and u_∞ is the free-stream velocity. The wall shear stress vector, τ_w, is given by:

$$\tau_w = (\mu + \mu_t) \left(\frac{\partial u_i}{\partial x_j} \right)_{x_j = 0}. \tag{4.5}$$

where μ, μ_t is the dynamic and turbulent viscosity, u_i is the flow velocity parallel to the wall and x_j is the distance to the wall. i and j are along the x and y axes which are along the length and depth of the domain respectively.

4.2.2 Porous media model

The D'arcy-Forchheimer porous media model ([36, 37]) was used to calculate the source term for equations (4.2).This is a second degree polynomial equation in terms of $\mathbf{u}$ that quantifies the pressure drop caused by the netting

$$\mathbf{S} = -\left(\mu \mathbf{D} + \frac{1}{2} \rho |\mathbf{u}| \mathbf{C} \right) \mathbf{u} \tag{4.6}$$

where $\mathbf{D}$ and $\mathbf{C}$ are the matrices of the viscous and inertial porous media coefficients:

$$\mathbf{D} = \begin{pmatrix} D_1 & 0 & 0 \\ 0 & D_2 & 0 \\ 0 & 0 & D_3 \end{pmatrix}, \mathbf{C} = \begin{pmatrix} C_1 & 0 & 0 \\ 0 & C_1 & 0 \\ 0 & 0 & C_3 \end{pmatrix} \tag{4.7}$$

and D_1,D_2,D_3 are the viscous porous media resistance coefficients and C_1,C_2,C_3 are the inertial resistance coefficients, along the principle axes of the porous media x_1,x_2,x_3. [1, 21] find the porous media coefficients by conducting experiments in a towing tank with a stiff net frame and fitting the hydrodynamic forces with an analytical model. [43], on the other hand, compare the Morison type load model with the porous media forces and use error minimization to deduce the coefficients for their porous media model.

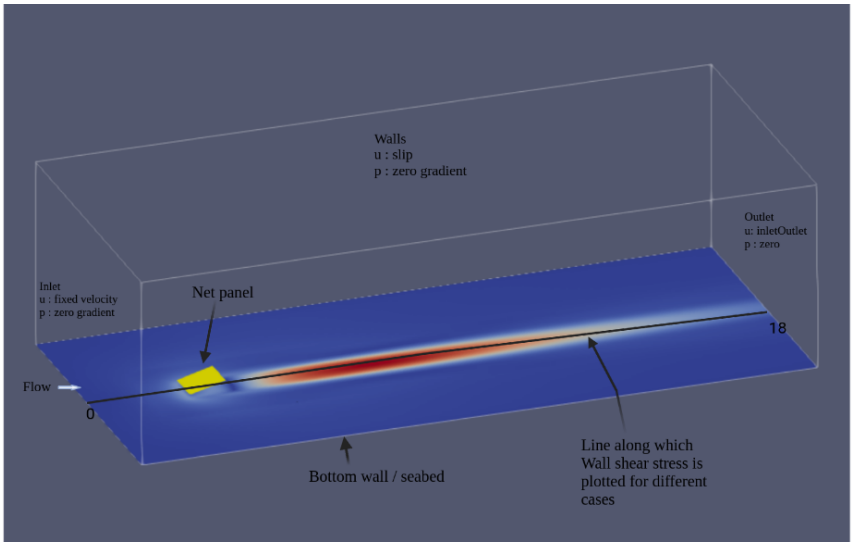

Figure 4.1: Domain used to simulate the net panel trawling.

4.3 CFD simulations

CFD simulations were carried out using the OpenFOAM, open source CFD toolkit. A steady-state, incompressible solver for turbulent flows with explicit porous media implementation was used. The solver uses a SIMPLE (Semi-Implicit Method for Pressure Linked Equations) algorithm and a finite volume discretization strategy.

The netting is represented by triangular numerical meshes (determined from CAD models), which has been shown to accurately capture the three dimensional complexity of the netting of a real fishing gear [14]. The base netting used in this study is a knotless nylon netting that has been extensively investigated, both numerically and experimentally. It has a twine diameter of 2.8mm, and a mesh bar length of 29mm, yielding a solidity ratio of 0.184, where the solidity ratio is the ratio of the projected area of the netting to the total area enclosed by the net

$$Sn = \frac{2d}{\lambda} - \left(\frac{d}{\lambda}\right)^2 \tag{4.8}$$

where d is the diameter of the netting twine and λ is half the mesh length (length of the mesh bar between twine intersections) ([52]).

The simulations use stiff rectangular netting panels in a fluid domain that is 18 meters long, 8 meters wide, and 5 meters deep, with the leading edge of the net at 2.5 meters from the inlet. Fixed velocity and zero pressure gradient conditions are applied to the lower wall, which represents the seabed. On the other walls, the velocity has a slip condition and the pressure has a zero gradient. The flow is achieved by supplying zero pressure at the outlet, which is regulated by a fixed velocity at the inlet. The two equation shear stress model, K-Omega SST is used to model the turbulence in the flow. The computational domain was discretized using structured and unstructured meshes with a more refined meshing close to the bottomwall(seabed), around the netting panel and the wake. A mesh independence study was carried out to finally choose the most adapt mesh containing 12-14 Million

Table 4.1: Values of critical bed shear stress for various sand types.

grain type	Diameter (μm)	CSS_{Motion} (N/m^2)	$CSS_{Suspension}$ (N/m^2)
Fine Silt	20	0.075	0.075
Fine sand	300	0.2	0.3
Coarse sand	1000	0.5	1.5

cells of cell types hexahedra and polyhedra.

Simulations were carried out to understand the effect of a range of different parameters on the seabed shear stress caused by the flow through and around netting panels. The shear stress along the center line of the seabed (Figure 4.1), and the drag and lift coefficients of the netting panel are calculated for each of the simulations. Negative lift coefficient values indicate that the netting panel experiences a downwards force towards the seabed. The shear stress values are compared with values that initiate the motion of fine silt and fine and coarse sand. The mobilisation and transport of sediment particles has been extensively studied in river erosion and coastal engineering problems. Sediment transport occurs when the induced bed shear stress exceeds the critical shear stress needed for initiating the motion of the grains in the bed. The critical shear stress varies according to the sediment size and is represented by the Shields diagram, which relates the dimensionless critical shear stress as a function of the particle Reynolds number [75]. Table 4.1 shows the critical bed shear stress for 3 different soil types calculated from the Shields curve.

4.4 Results and discussion

4.4.1 Height above the seabed

In bottom trawl fisheries, the lower netting panels of a fishing gear generally have a low angle of attack and can be at different heights from the seabed. In order to understand the effect of this latter aspect of gear design, simulations were carried out on a 1m x 1m netting panel with a solidity of 0.184, a 10°angle of attack and a 2 m/s towing speed, where the height of the leading edge ranges from 0.1 to 1.0 m. The results show that there is a notable decrease in the wall shear stress as the height of the panel increases. When its leading edge is 0.1 m from the seabed, it will mobilise fine sand particles, but when placed at 0.4 m from the seabed, the shear bed stress is not sufficiently large enough to mobilise fine silt, and when the leading edge is greater than 0.6 m, there is little interaction between the netting panel and the bottom boundary (Figure 4.2). Furthermore, there is little change of the magnitude of the drag and lift coefficients over the range of heights examined here.

4.4.2 Angle of attack

The wall shear stress, where the leading edge is kept constant at 0.1 m, are higher at smaller angles and decrease as the angle of attack increases (Figure 4.4).

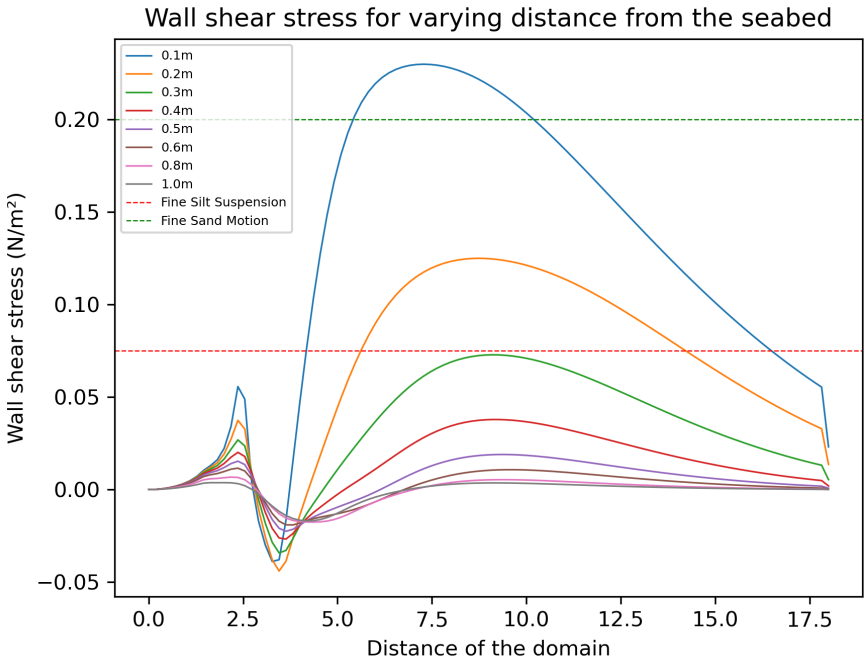

Figure 4.2: 1 x 1 m flat netting panel, with a solidity of 0.184, making 10°with seabed trawled at velocity 2 m/s with varying distance from the seabed.

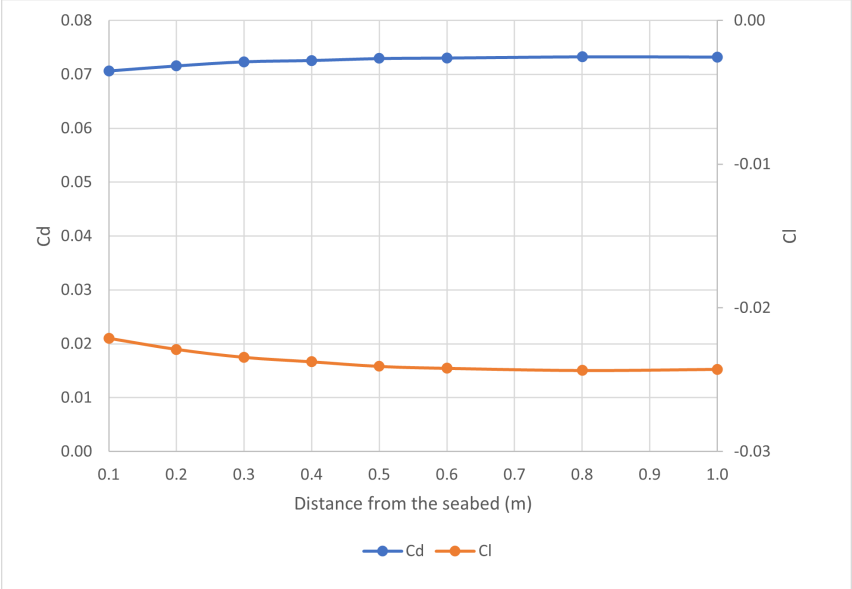

Figure 4.3: Hydrodynamic coefficients of a 1 m x 1 m flat netting panel, with a solidity of 0.184, at 10°angle of attack at 2 m/s flow speed for varying distance from the seabed.

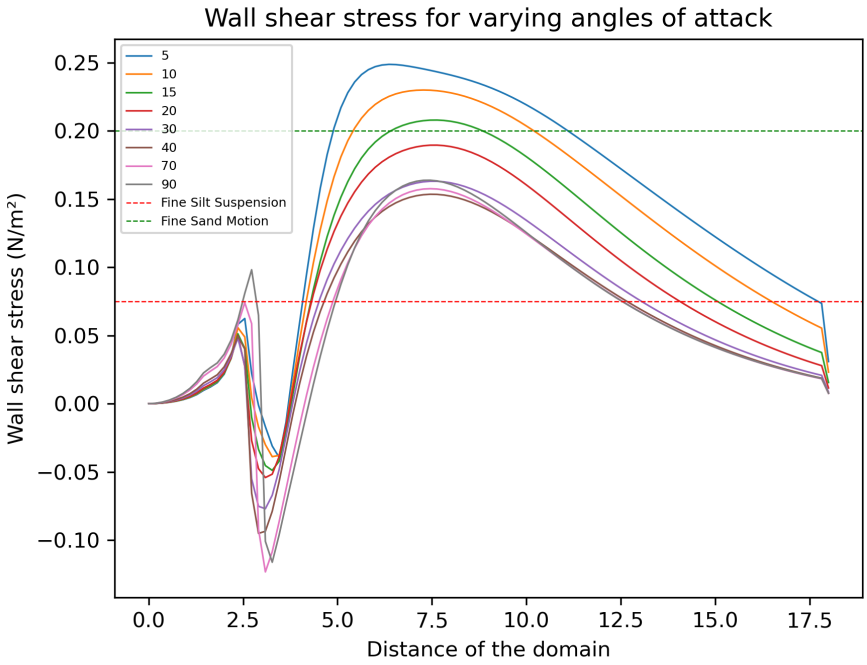

Figure 4.4: 1 m x 1 m flat netting panel, with a solidity of 0.184, making different angles from the seabed at a distance of 0.1 m velocity 2 m/s.

After about 45°, however, there is very little change, which reflects the fact that at larger angles, more of the netting panel is distant from the seabed and has less of an influence on it. The drag coefficient on the netting panel increases as the angle of attack increases from 0°to 90°whereas the lift coefficient increases to a maximum at 45°before decreasing again.

4.4.3 Netting solidity

The solidity of the netting used in the many types of fishing nets worldwide varies considerably, and indeed can differ in different parts of a single gear. Hence, we need to investigate the effect of different solidities on the wall shear stress and the hydrodynamic force coefficients. Here, we examine three different nets in the solidity range from 0.13 to 0.314, using the porous media coefficients determined by [1] from the experiments of [2]. Figure 4.6 shows that the wall shear stress increases as the solidity increases and that the peak of the 0.31 solidity net is about twice that of the 0.13 one and hence will cause more sediment entrainment. Similarly the magnitude of hydrodynamic coefficients increases with increasing solidity, indicating higher forces for high solidity nets (Figure 4.7).

4.4.4 Netting panel length

The effect of panel length was investigated in two ways. In the first case, the height of the leading edge and the angle of attack of the panel were kept constant (0.1 m and 10°). In the second case the height of the leading and trailing edges were

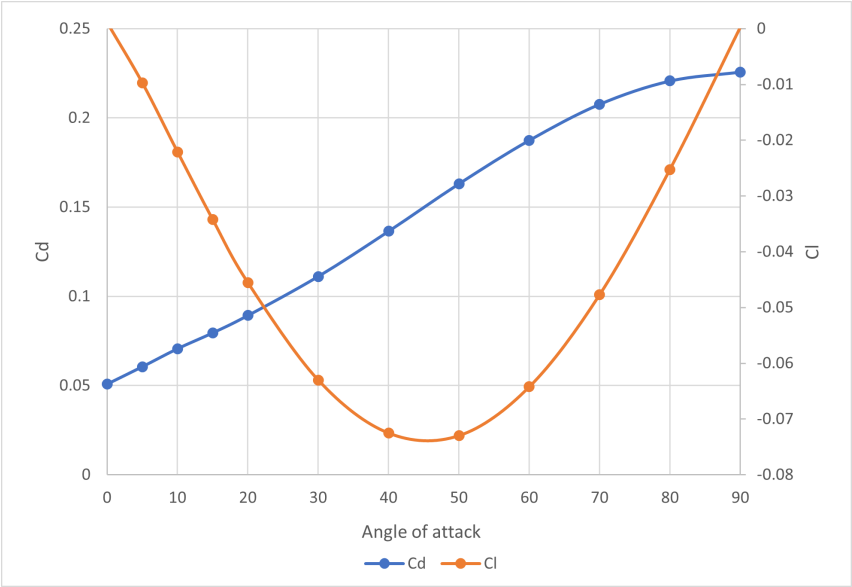

Figure 4.5: Hydrodynamic coefficients for a netting panel, with a solidity of 0.184, making different angles from the seabed at a distance 0.1 m from the seabed and velocity 2 m/s.

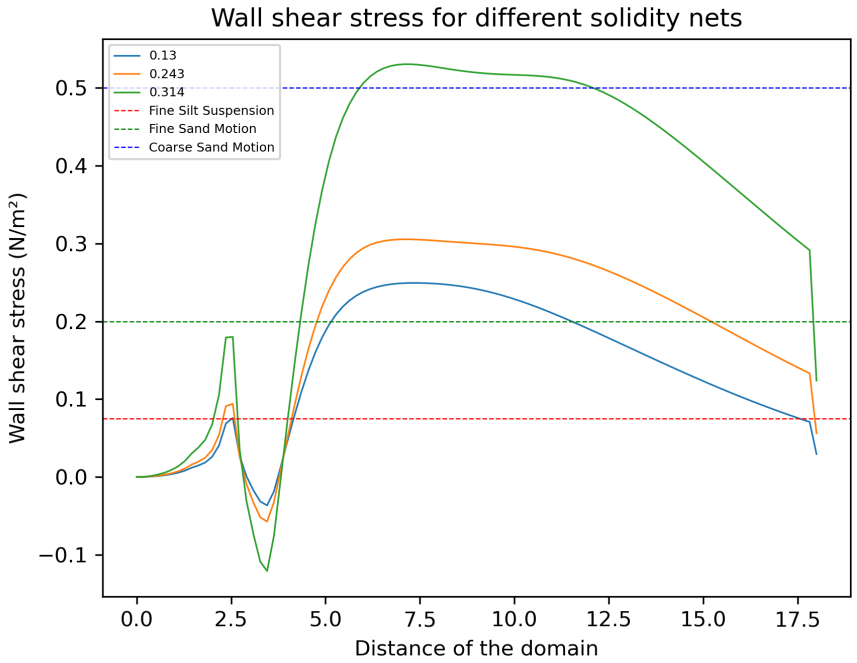

Figure 4.6: 1 x 1 m flat netting panel, with different solidity nets for angle of attack 10°and velocity 2 m/s.

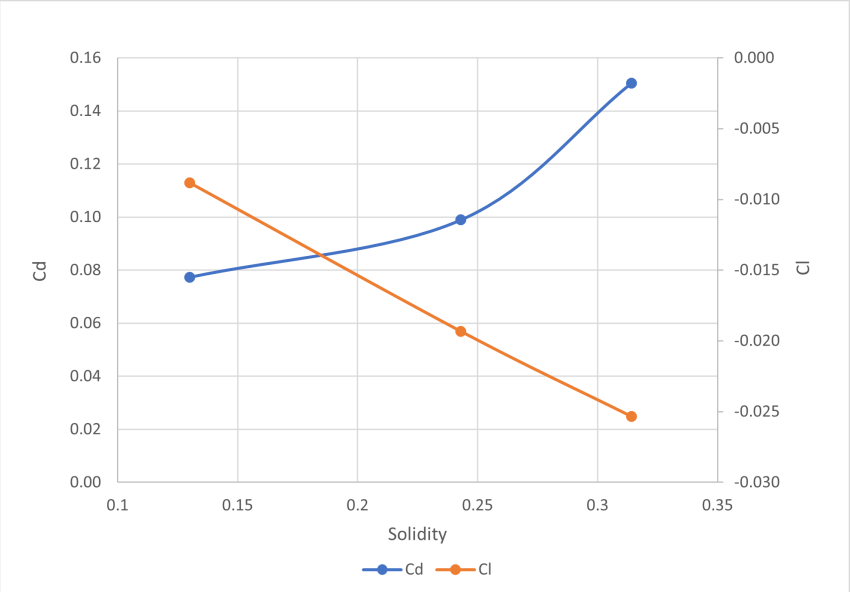

Figure 4.7: Hydrodynamic coefficients for 1 x 1 m flat net with different solidity nets for angle of attack 10°and velocity 2 m/s.

kept constant (0.1 and 0.28 m). In both cases the panel length was varied between 0.5 and 3.5m.

For the case where the angle of attack is kept constant, the wall shear stress increases as the panel length increases from 1 to about 2 m (Figure 4.8). As the length further extends the increase is relatively small, which is due to the fact that the additional panel netting is increasingly distant from the seabed. In this case, there is very little change to the drag and lift coefficients as the length increases (Figure 4.9).

The situation is very different for the case where the height of the leading and trailing edges of the netting panel are kept constant. Here, as the panel length is increased, the wall shear stress increases as more netting material is brought closer to the seabed, and accordingly more and increasingly coarser sediment is likely to be mobilised (Figure 4.10). Furthermore, the magnitudes of both drag and lift coefficient decrease reflecting the associated decrease of the angle of attack from 21 to 3° as the length increases (Figure 4.11).

4.4.5 Velocity of trawling

The speed at which fisheries operate varies considerably. It can range from speeds as low as 1.5 knots up to 7 knots and is dependent on the size and power of the fishing vessel but also on the swimming ability and behaviour of the target species [67,76,77].

As expected the wall shear stress increases as the trawling speed increases, which will lead to larger quantities and coarser sediment sizes being mobilised (Figure 4.12). The fact that the hydrodynamic coefficients are almost constant, reflects the fact that the magnitude of lift and drag forces increase with the square of the velocity (Figure 4.13). Hence, by towing more slowly, there will be a reduction in the physical impact to the seabed and a better fuel efficiency.

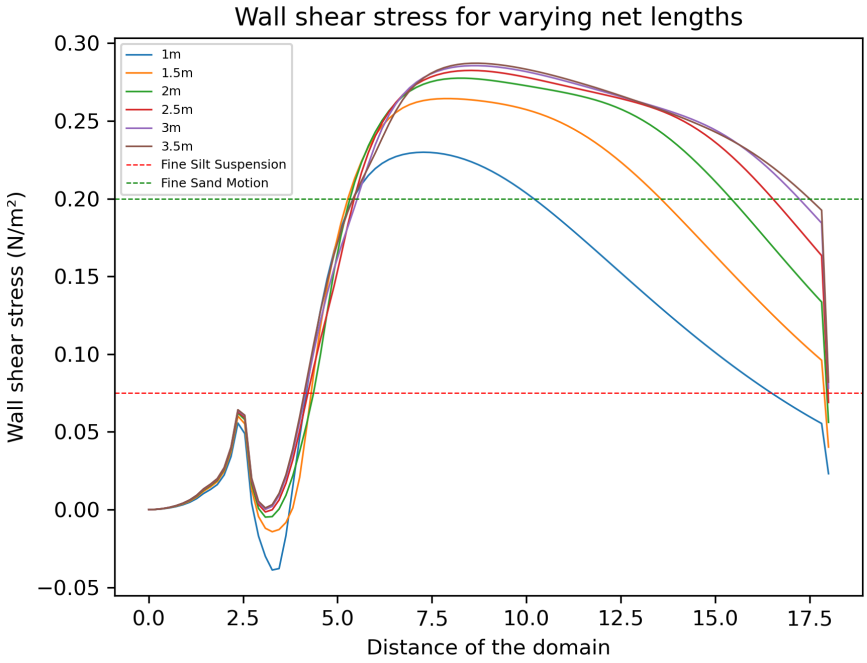

Figure 4.8: Wall shear stress along the center line of the bottom wall for varying net lengths making 10 degree from the seabed.

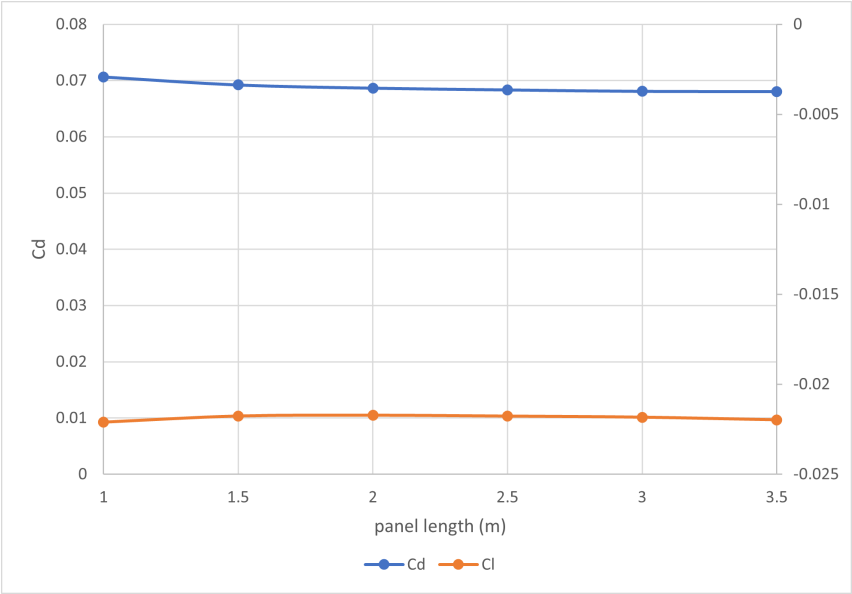

Figure 4.9: Hydrodynamic coefficients for varying net lengths making 10°from the seabed.

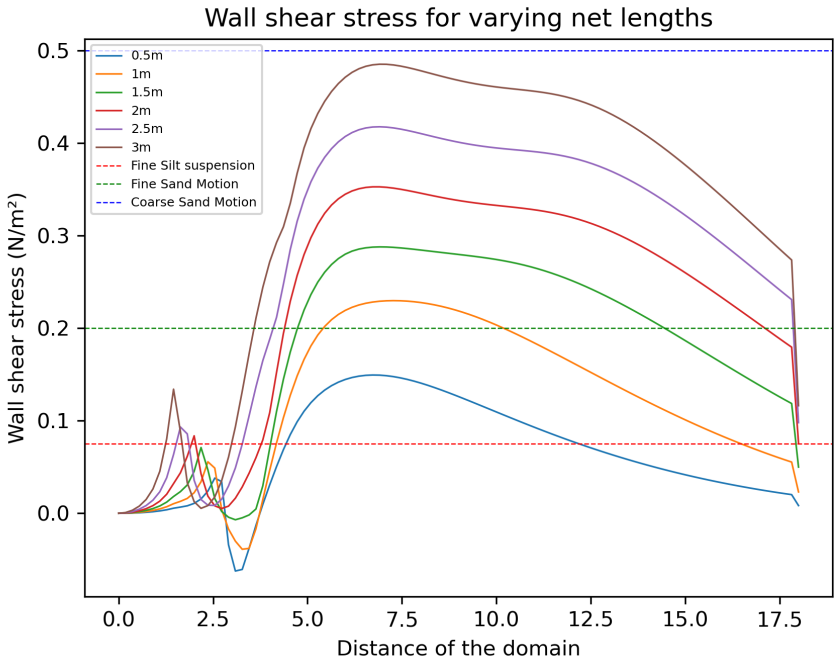

Figure 4.10: Wall shear stress along the center line of the bottom wall for varying net lengths making same distance front and back from the seabed.

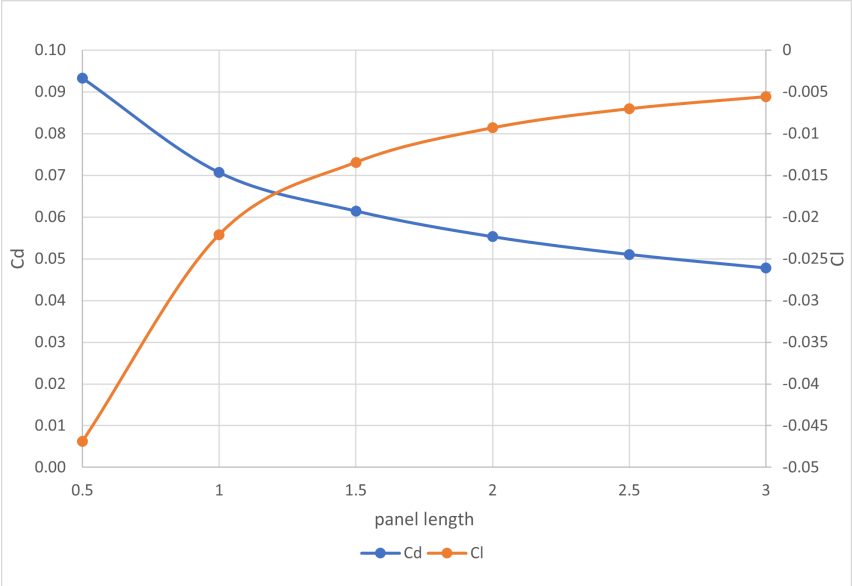

Figure 4.11: Hydrodynamic coefficients for varying net lengths making same height front and back from the seabed.

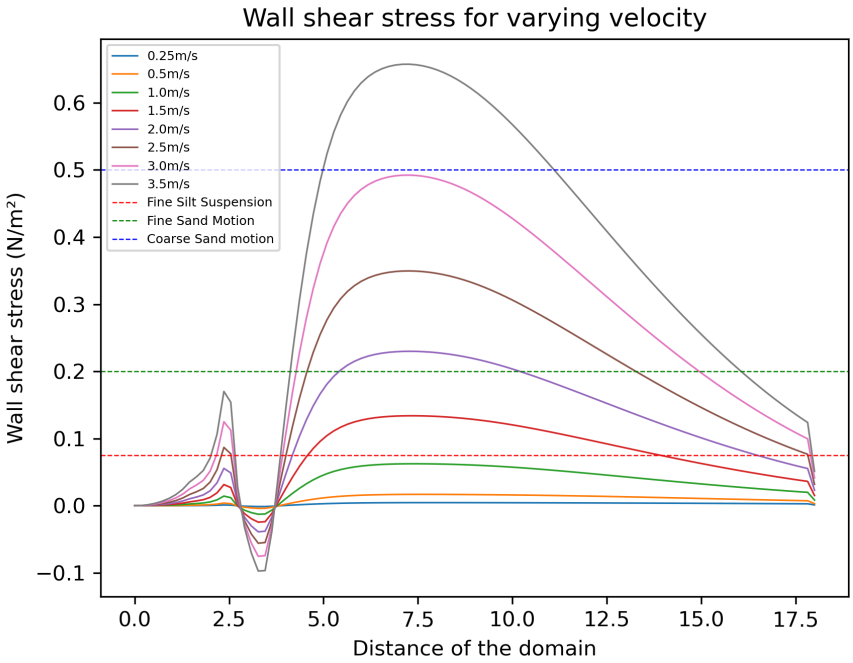

Figure 4.12: Wall shear stress along the center line of the bottom wall for a Net making 10 cm and 10 degree from the seabed for varying velocity

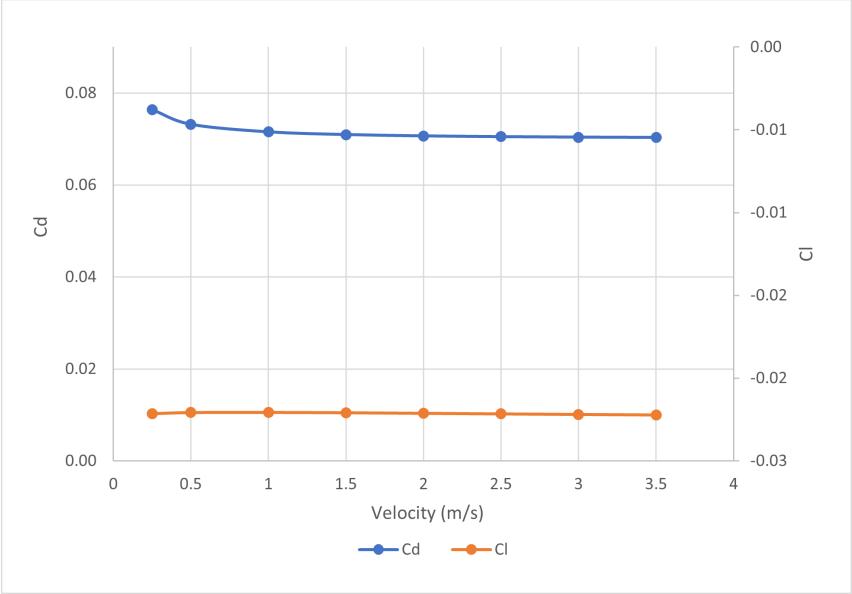

Figure 4.13: Hydrodynamic forces for varying trawl speed for a 1 X 1 m net panel making 10 degree with the seabed.

4.5 Conclusions

We have shown that the seabed shear stress associated with the flow through and around a netting panel is dependent on its height above the seabed, its angle of attack, and its length, solidity and towing speed, whereas the hydrodynamic lift and drag coefficients are primarily influenced only by the angle of attack and solidity, and that height above the seabed is of little importance. Further we have demonstrated, for the specific cases examined, that the magnitude of the shear stress under normal operating conditions can be large enough to mobilise and suspend sediments from fine silt to coarse sands. Accordingly, in order to make accurate estimates of the quantity and particle size distribution of the sediment that is disturbed into the water column during the fishing process, all of these parameters need to be taken into account. This is particularly important, as to date, estimates of the amount of sediment mobilised by trawl netting have been relatively crude, and are based on relationships between netting drag and empirical measurements of the quantity of sediment mobilised, that have been established for gear components that are in contact with the seabed. We have shown here that for netting materials towed above the seabed, there is not such a direct relationship between netting drag and the bed shear stresses responsible for sediment mobilisation.

Thus, our results will permit a better assessment of the environmental impact of towed fishing gears. Trawling can increase turbidity, alter the integrity and particle size distribution of the seabed, smother benthic organisms and release sequestered nutrients [78]. Our improved understanding will permit the development of gears that have a reduced physical impact on the seabed. This is important, because in many jurisdictions, there is an increased focus on the environmental impact of fishing, and access to specific fishing grounds can be dependent on the type of gear used. Additionally, our study will support some of the recent developments in the real time monitoring and control of fishing gears using underwater images of the fishing process. These images are often occluded by the sediment put into the water column by the gear, and our results here will help in relation to camera placement and sediment suppression ([79]).

Chapter 5

Conclusions and Future Work

This chapter summarizes the work developed during this thesis and presents the conclusions. In addition, the future work is also discussed.

5.1 Conclusions

As described in chapter 1, the motivation of this thesis was to contribute to the developments in the computational fluid dynamics (CFD) simulation of fishing gears. Being able to predict the behavior of fishing gears such as trawls is important for improving the fishing industry to make it more efficient and environment friendly. Netting is one of the most important components in a fishing gear, and one of the most complex to simulate. Fishing nets are also used in aquaculture and many studies were carried out in this area for predicting the behaviour of fishing nets in water. It is computationally expensive to model the net panel as knots and twines to apply traditional no-slip conditions in a fluid simulation. Hence, a porous media approach has been recently proposed to represent the net panels as thin porous solids in CFD simulations, which proved to be an efficient alternative to detailed models of knots and twines.

In chapter 2 a new method is proposed to model net panels as porous surfaces instead of thin porous solids, aiming at simplifying the modelling of net configurations with complex shapes, as seen in the real life fishing gears. The proposed method was validated against experimental results from [1]. The results of the CFD simulations agree very well with the experimental measurements, and the flow fields obtained are also very similar to those obtained using the traditional method based on thin porous solids. It was also shown that the results are independent of the thickness of the generated porous zones, allowing for the use of only one or two layers of cells with no significant errors. To demonstrate the algorithm's ability to deal with complex net geometries, the proposed method was used to simulate a complex net configuration with curved nets and intersections. Improvements achieved comparing to the traditional thin solid method in areas such as: modelling curved nets, dealing with multiple nets with intersections, easier control over the thickness of the porous media without any additional pre-processing, easier control over the size and number of porous zones created for a curved net and finally ability to deal with net panels having large deflection.

In chapter 3 a new a method to estimate the resistance coefficients of the porous media model used in this thesis is presented. A regression model based on a full 2D CFD model is used in this method. A parametric study is used to calculate the flow through a layer of porous media and interpolated to create an efficient regression model, which is then used to estimate the porous resistance coefficients by comparing with experimental results. This method uses a regression model based on a full 2D CFD model of the flow through a layer of porous media and is pre-calculated by a parametric study and interpolated to build an efficient regression model and then is used to compare with experimental results for estimating the porous resistance coefficients. The methods allows to estimate both the viscous and the inertial resistance coefficients or just the inertial ones, as proposed by some authors. It was applied to different net panels and results were compared with existing methods. The methods were compared to the previously used ones by evaluating the goodness of fitting using the coefficient of determination $\bar{R}^2$. It is discovered that estimating both the inertial and viscous resistance coefficients yields better results than estimating only the inertial coefficients, and that using both simplifies the implementation of the proposed method. Because the method employs a CFD model of porous media, it can be used to estimate the resistance coefficients of a wide variety of netting and other materials that can be modeled as porous media. The methods for such materials should be validated in future research.

This developed methods were efficiently used in a real life problem of learning the impact of fishing nets on sediment transport while demersal trawling (chapter 4). Demersal trawling, often referred to as bottom trawling is one of the major fishing technique practised across the world. While trawling the fishing gear through the seabed, there are many environmental issues which has to be addressed including destruction of benthic environment, very high bycatch among some of them. The previous studies on sediment impact while demersal trawling focus mainly on the parts of fishing gears such as trawl doors for the hydrodynamic impact and ground gears for the direct impact. Fishing nets are a major part of the fishing gear and even though they don't come in direct contact with the seabed, trawling them close to the seabed will have an impact on sediment entrainment. There were no data on the sediment mobilization due to a fishing net towed close to the seabed. Extensive numerical study was carried out for evaluating different parameters and their effect on hydrodynamic forces and sediment mobilization while trawling.

Simulations were carried out for a rigid net panel to be towed close to a seabed using the model proposed in the thesis in chapter 2. The study demonstrated the impact of parameters like distance for the netting panel to the seabed, length of the netting panel, type of the net used (solidity of the net), angle of attack made by the panel to the seabed and the velocity of trawling on moving or mobilising sediments of type fine silt to coarse sand. This study helps to provide a starting point in the investigations on impact of fishing nets on sediment transport while trawling and good understanding on the importance on the above mentioned variables.

5.2 Future Work

During this thesis, net is considered rigid and a new method is proposed to simulate the fluid flow through them. Behaviour of net in a fishing gear is not a fluid only problem but a fluid-structure interaction problem. The structural solvers should predict the shape of the flexible fishing nets for the particular flow field. And a coupling between these fluid and structural solver should be done in order to capture the right movement of flexible nets in a fishing gear. There are already studies on coupling the porous media model with solid Finite Element Method (FEM) solvers. Since some of the structural solvers use triangulated meshes to represent nets [14], this proposed way of modelling net panels will facilitate a better coupling between the solid and fluid solvers. This has to be applied and investigated in the future for completing the simulation of flexible fishing nets.

Another improvement which can be done in the future is developing methods for finding the porous resistance coefficients, which is an important part as far as the porous media approach is concerned. The fishing nets are at very small angle of attack to the flow in most part of the fishing gear and calculating the resistance coefficients effectively for smaller angles of attack is essential for improving the accuracy of simulations of fishing gears. In the recent years [30] proposed a new experimental setup different from the other researchers aiming at improving the estimation of hydrodynamic coefficients at small angles of attack. Investigations on these methods for estimating the porous resistance coefficients is a future line of work that needs attention.

Finally, the model developed in this thesis needs to be applied to different types of complex-shaped, real-life fishing gears and validated against experimental data.

Bibliography

[1] Ø. Patursson, M. R. Swift, I. Tsukrov, K. Simonsen, K. Baldwin, D. W. Fredriksson, and B. Celikkol, "Development of a porous media model with application to flow through and around a net panel," *Ocean Engineering*, vol. 37, pp. 314–324, Feb. 2010.

[2] H. Rudi, G. Løland, and I. Furunes, "Experiments with nets; forces on and flow through net panels and cage systems, technical report mt 51 f88-0215, marintek, trondheim, norway. (in norwegian).," 1988.

[3] J. M. Zhan, X. P. Jia, Y. S. Li, M. G. Sun, G. X. Guo, and Y. Z. Hu, "Analytical and experimental investigation of drag on nets of fish cages," *Aquacultural Engineering*, vol. 35, pp. 91–101, June 2006.

[4] T. Cashion, D. Al-Abdulrazzak, D. Belhabib, B. Derrick, E. Divovich, D. K. Moutopoulos, S.-L. Noël, M. L. D. Palomares, L. C. L. Teh, D. Zeller, and D. Pauly, "Reconstructing global marine fishing gear use: Catches and landed values by gear type and sector," *Fisheries Research*, vol. 206, pp. 57–64, Oct. 2018.

[5] European Parliament, "Regulation (eu) no 1380/2013 of the european parliament and of the council of 11 december 2013 on the common fisheries policy, amending council regulations (ec) no 1954/2003 and (ec) no 1224/2009 and repealing council regulations (ec) no 2371/2002 and (ec) no 639/2004 and council decision 2004/585/ec," *Official Journal of the European Union*, vol. L 354, pp. 22–61, 2013.

[6] M. Krishnamurthy, "Computation of drag force acting on fishing nets," in *OCEANS '77 Conference Record*, pp. 697–701, Oct. 1977.

[7] F. O'Neill, "Differential equations governing the geometry of a diamond mesh cod-end of a trawl net," *Journal of Applied Mechanics, Transactions ASME*, vol. 64, no. 1, pp. 7–13, 1997.

[8] F. O'Neill, "Axisymmetric trawl cod-ends made from netting of a generalized mesh shape," *IMA Journal of Applied Mathematics (Institute of Mathematics and Its Applications)*, vol. 62, no. 3, pp. 245–262, 1999.

[9] C.-W. Lee, J.-H. Lee, B.-J. Cha, H.-Y. Kim, and J.-H. Lee, "Physical modeling for underwater flexible systems dynamic simulation," *Ocean Engineering*, vol. 32, no. 3, pp. 331–347, 2005.

[10] Y.-C. Li, Y.-P. Zhao, F.-K. Gui, and B. Teng, "Numerical simulation of the hydrodynamic behaviour of submerged plane nets in current," *Ocean Engineering*, vol. 33, no. 17, pp. 2352–2368, 2006.

[11] A. de la Prada and M. González, "Nonlinear stiffness models of a net twine to describe mesh resistance to opening of flexible net structures," *Proceedings of the Institution of Mechanical Engineers, Part M: Journal of Engineering for the Maritime Environment*, vol. 230, no. 1, pp. 33–44, 2016.

[12] B. Vincent, J. Simon, and N. Di Cesare, "Development of a model for flexural rigidity of fishing net with a spring mass approach and its inverse identification by metaheuristic parametric optimization," *Ocean Engineering*, vol. 203, p. 107166, 2020.

[13] I. Tsukrov, O. Eroshkin, D. Fredriksson, M. Swift, and B. Celikkol, "Finite element modeling of net panels using a consistent net element," *Ocean Engineering*, vol. 30, no. 2, pp. 251–270, 2003.

[14] D. Priour, "Calculation of net shapes by the finite element method with triangular elements," *Communications in Numerical Methods in Engineering*, vol. 15, no. 10, pp. 755–763, 1999.

[15] J. Lee, L. Karlsen, and C. Lee, "A method for improving the dynamic simulation efficiency of underwater flexible structures by implementing non-active points in modelling," *ICES Journal of Marine Science*, vol. 65, no. 9, pp. 1552–1558, 2008.

[16] A. de la Prada and M. González, "Assessing the suitability of gradient-based energy minimization methods to calculate the equilibrium shape of netting structures," *Computers & Structures*, vol. 135, pp. 128–140, 2014.

[17] A. Sala, F. O'Neill, G. Buglioni, A. Lucchetti, V. Palumbo, and R. Fryer, "Experimental method for quantifying resistance to the opening of netting panels," *ICES Journal of Marine Science*, vol. 64, no. 8, pp. 1573–1578, 2007.

[18] H. Moe, A. Olsen, O. Hopperstad, Ø. Jensen, and A. Fredheim, "Tensile properties for netting materials used in aquaculture net cages," *Aquacultural Engineering*, vol. 37, no. 3, pp. 252–265, 2007.

[19] A. de la Prada and M. Gonzalez, "Quantifying mesh resistance to opening of netting panels: experimental method, regression models, and parameter estimation strategies," *ICES Journal of Marine Science*, vol. 72, no. 2, pp. 697–707, 2015.

[20] I. Mnassri, D. Le Touzé, B. Vincent, and B. Alessandrini, "A numerical investigation for underwater fluid-netting interaction problem," in *Contributions on the Theory of Fishing Gears and Related Marine Systems*, pp. 117–130, 10 2011.

[21] Y.-P. Zhao, C.-W. Bi, G.-H. Dong, F.-K. Gui, Y. Cui, C.-T. Guan, and T.-J. Xu, "Numerical simulation of the flow around fishing plane nets using the porous media model," *Ocean Engineering*, vol. 62, pp. 25–37, 2013.

[22] C.-W. Bi, Y.-P. Zhao, G.-H. Dong, T.-J. Xu, and F.-K. Gui, "Numerical simulation of the interaction between flow and flexible nets," *Journal of Fluids and Structures*, vol. 45, pp. 180–201, Feb. 2014.

[23] K. Breddermann, *Filtration performance of plankton nets used to catch micro- and mesozooplankton*. PhD thesis, Universitat Rostock, 10 2016.

[24] P. Druault and G. Germain, "Analysis of hydrodynamics of a moving trawl codend and its fluttering motions in flume tank," *European Journal of Mechanics - B/Fluids*, vol. 60, pp. 219–229, Nov. 2016.

[25] M. Devilliers, B. Vincent, and I. Mnassri, "A new adaptive mesh refinement to model water flow around fishing nets," *Ocean Engineering*, vol. 113, pp. 34–43, Feb. 2016.

[26] B. T. Nyatchouba Nsangue, H. Tang, L. Xu, F. Hu, S. Dong, N. P. Achille, and B. Zou, "Comparison between physical model testing and numerical simulation using two-way fluid-structure interaction approach of new trawl design for coastal bottom trawl net," *Ocean Engineering*, vol. 233, p. 109112, Aug. 2021.

[27] F. Le Bris and D. Marichal, "Numerical and experimental study of submerged supple nets: Applications to fish farms," *Journal of Marine Science and Technology*, vol. 3, pp. 161–170, Dec. 1998.

[28] N. N. Bruno Thierry, H. Tang, X. Liuxiong, X. You, F. Hu, N. P. Achile, and R. Kindong, "Hydrodynamic performance of bottom trawls with different materials, mesh sizes, and twine thicknesses," *Fisheries Research*, vol. 221, p. 105403, Jan. 2020.

[29] B. Zou, N. N. B. Thierry, H. Tang, L. Xu, S. Dong, and F. Hu, "The deformation characteristics and flow field around knotless polyethylene netting based on fluid structure interaction (FSI) one-way coupling," *Aquaculture and Fisheries*, vol. 7, no. 1, pp. 89–102, 2022.

[30] H. Tang, F. Hu, L. Xu, S. Dong, C. Zhou, and X. Wang, "Variations in hydrodynamic characteristics of netting panels with various twine materials, knot types, and weave patterns at small attack angles," *Scientific Reports*, vol. 9, p. 1923, Dec. 2019.

[31] H. Tang, N. N. B. Thierry, A. N. Pandong, Q. Sun, L. Xu, F. Hu, and B. Zou, "Hydrodynamic and turbulence flow characteristics of fishing nettings made of three twine materials at small attack angles and low Reynolds numbers," *Ocean Engineering*, vol. 249, p. 110964, 2022.

[32] B. Buck, M. Troell, G. Krause, D. Angel, B. Grote, and T. Chopin, "State of the art and challenges for offshore integrated multi-trophic aquaculture (imta)," *Frontiers in Marine Science*, vol. 5, no. MAY, 2018. cited By 50.

[33] P. Klebert, P. Lader, L. Gansel, and F. Oppedal, "Hydrodynamic interactions on net panel and aquaculture fish cages: A review," *Ocean Engineering*, vol. 58, pp. 260–274, 2013.

[34] G. Loland, "Current forces on, and water flow through and around, floating fish farms," *Aquaculture International*, vol. 1, pp. 72–89, Sept. 1993.

[35] C. Balash, B. Colbourne, N. Bose, and W. Raman-Nair, "Aquaculture Net Drag Force and Added Mass," *Aquacultural Engineering*, vol. 41, pp. 14–21, July 2009.

[36] H. D'arcy, *Les fontaines publiques de la ville de dijon*. V. Dalmont (Paris), 1856.

[37] P. Forchheimer, *Wasserbewegung durch boden. Zeitschrift des Vereines Deutscher Ingenieure 45, 1782 - 1788*. Verein, 1901.

[38] I. Tsukrov, A. Drach, J. DeCew, M. Robinson Swift, and B. Celikkol, "Characterization of geometry and normal drag coefficients of copper nets," *Ocean Engineering*, vol. 38, pp. 1979–1988, Dec. 2011.

[39] C.-W. Bi, Y.-P. Zhao, G.-H. Dong, T.-J. Xu, and F.-K. Gui, "Numerical simulation of the interaction between flow and flexible nets," *Journal of Fluids and Structures*, vol. 45, pp. 180–201, Feb. 2014.

[40] H. Chen and E. Christensen, "Development of a numerical model for fluid-structure interaction analysis of flow through and around an aquaculture net cage," *Ocean Engineering*, vol. 142, pp. 597–615, 2017.

[41] B. Jensen, N. G. Jacobsen, and E. D. Christensen, "Investigations on the porous media equations and resistance coefficients for coastal structures," *Coastal Engineering*, vol. 84, pp. 56–72, Feb. 2014.

[42] H. Chen and E. Christensen, "Simulating the hydrodynamic response of a floater–net system in current and waves," *Journal of Fluids and Structures*, vol. 79, pp. 50–75, 2018.

[43] H. Chen and E. D. Christensen, "Investigations on the porous resistance coefficients for fishing net structures," *Journal of Fluids and Structures*, vol. 65, pp. 76–107, Aug. 2016.

[44] F. O'Neill and K. Mutch, "Selectivity in trawl fishing gears," *Scottish Marine and Freshwater Science*, vol. 8, no. 1, 2017. Publisher: Marine Scotland Science.

[45] M. Krishnamurthy, "Computation of drag force acting on fishing nets," in *OCEANS '77 Conference Record*, pp. 697–701, 1977.

[46] C.-W. Bi, Y.-P. Zhao, G.-H. Dong, Y.-N. Zheng, and F.-K. Gui, "A numerical analysis on the hydrodynamic characteristics of net cages using coupled fluid-structure interaction model," *Aquacultural Engineering*, vol. 59, pp. 1–12, Mar. 2014.

[47] C.-W. Bi, Y.-P. Zhao, G.-H. Dong, Y. Cui, and F.-K. Gui, "Experimental and numerical investigation on the damping effect of net cages in waves," *Journal of Fluids and Structures*, vol. 55, pp. 122–138, May 2015.

[48] T. Martin, A. Kamath, and H. Bihs, "A Lagrangian approach for the coupled simulation of fixed net structures in a Eulerian fluid model," *Journal of Fluids and Structures*, vol. 94, p. 102962, Apr. 2020.

[49] H. Cheng, M. C. Ong, L. Li, and H. Chen, "Development of a coupling algorithm for fluid-structure interaction analysis of submerged aquaculture nets," *Ocean Engineering*, vol. 243, p. 110208, Jan. 2022.

[50] B. E. Launder and D. B. Spalding, "The numerical computation of turbulent flows," *Computer Methods in Applied Mechanics and Engineering*, vol. 3, pp. 269–289, Mar. 1974.

[51] OpenFOAM, "Openfoam, opensource cfd toolkit."

[52] A. Fredheim, *Current Forces on Net Structure*. Fakultet for ingeniørvitenskap og teknologi, 2005.

[53] K. Breddermann and M. Paschen, "On the way to plankton net calibration," in *Contributions on the Theory of Fishing Gears and Related Marine Systems*, pp. 153–168, 10 2011.

[54] H. E. Hafsteinsson, "Porous media in openfoam," 2009.

[55] European Parliament. Directorate General for Parliamentary Research Services., *Understanding fisheries technical rules: an illustrated guide for non experts : in depth analysis*. Publications Office, 2015.

[56] X. You, F. Hu, Y. Takahashi, D. Shiode, and S. Dong, "Resistance performance and fluid-flow investigation of trawl plane netting at small angles of attack," *Ocean Engineering*, vol. 236, p. 109525, Sept. 2021.

[57] H. Moe-Føre, P. Lader, E. Lien, and O. Hopperstad, "Structural response of high solidity net cage models in uniform flow," *Journal of Fluids and Structures*, vol. 65, pp. 180–195, 2016.

[58] MATLAB, *MATLAB version 9.12.0 (R2022a)*. The Mathworks, Inc., Natick, Massachusetts, 2022.

[59] P. Virtanen, R. Gommers, T. E. Oliphant, M. Haberland, T. Reddy, D. Cournapeau, E. Burovski, P. Peterson, W. Weckesser, J. Bright, S. J. van der Walt, M. Brett, J. Wilson, K. J. Millman, N. Mayorov, A. R. J. Nelson, E. Jones, R. Kern, E. Larson, C. J. Carey, İ. Polat, Y. Feng, E. W. Moore, J. VanderPlas, D. Laxalde, J. Perktold, R. Cimrman, I. Henriksen, E. A. Quintero, C. R. Harris, A. M. Archibald, A. H. Ribeiro, F. Pedregosa, P. van Mulbregt, and SciPy 1.0 Contributors, "SciPy 1.0: Fundamental Algorithms for Scientific Computing in Python," *Nature Methods*, vol. 17, pp. 261–272, 2020.

[60] J. C. Lagarias, J. A. Reeds, M. H. Wright, and P. E. Wright, "Convergence properties of the nelder–mead simplex method in low dimensions," *SIAM Journal on Optimization*, vol. 9, no. 1, pp. 112–147, 1998.

[61] F. G. O'Neill and A. Ivanović, "The physical impact of towed demersal fishing gears on soft sediments," *ICES Journal of Marine Science*, vol. 73, pp. i5–i14, 2016.

[62] A. Palanques, P. Puig, J. Guillén, M. Demestre, and J. Martín, "Effects of bottom trawling on the ebro continental shelf sedimentary system (nw mediterranean)," *Continental Shelf Research*, vol. 72, pp. 83–98, 2014.

[63] F. K. Oberle, C. D. Storlazzi, and T. J. Hanebuth, "What a drag: Quantifying the global impact of chronic bottom trawling on continental shelf sediment," *Journal of Marine Systems*, vol. 159, pp. 109–119, 2016.

[64] A. D. Rijnsdorp, J. Depestele, O. R. Eigaard, N. T. Hintzen, A. Ivanovic, P. Molenaar, F. G. O'Neill, H. Polet, J. J. Poos, and T. van Kooten, "Mitigating seafloor disturbance of bottom trawl fisheries for north sea sole solea solea by replacing mechanical with electrical stimulation," *PLOS ONE*, vol. 15, pp. 1–17, 11 2020.

[65] B. Mengual, P. Le Hir, F. Cayocca, and T. Garlan, "Bottom trawling contribution to the spatio-temporal variability of sediment fluxes on the continental shelf of the bay of biscay (france)," *Marine Geology*, vol. 414, pp. 77–91, 2019.

[66] F. G. O'Neill and K. Summerbell, "The mobilisation of sediment by demersal otter trawls," *Marine Pollution Bulletin*, vol. 62, pp. 1088–1097, May 2011.

[67] O. R. Eigaard, F. Bastardie, M. Breen, G. E. Dinesen, N. T. Hintzen, P. Laffargue, L. O. Mortensen, J. R. Nielsen, H. C. Nilsson, F. G. O'Neill, H. Polet, D. G. Reid, A. Sala, M. Sköld, C. Smith, T. K. Sørensen, O. Tully, M. Zengin, and A. D. Rijnsdorp, "Estimating seabed pressure from demersal trawls, seines, and dredges based on gear design and dimensions," *ICES Journal of Marine Science*, vol. 73, pp. i27–i43, 06 2015.

[68] A. D. Rijnsdorp, J. Depestele, P. Molenaar, O. R. Eigaard, A. Ivanović, and F. G. O'Neill, "Sediment mobilization by bottom trawls: a model approach applied to the Dutch North Sea beam trawl fishery," *ICES Journal of Marine Science*, vol. 78, pp. 1574–1586, 04 2021.

[69] F. G. O'Neill and K. Summerbell, "The hydrodynamic drag and the mobilisation of sediment into the water column of towed fishing gear components," *Journal of Marine Systems*, vol. 164, pp. 76–84, 2016.

[70] T. Takagi, T. Shimizu, K. Suzuki, T. Hiraishi, and K. Yamamoto, "Validity and layout of "nala": a net configuration and loading analysis system," *Fisheries Research*, vol. 66, no. 2, pp. 235–243, 2004.

[71] F. G. O'Neill and R. D. Neilson, "A Dynamic Model of the Deformation of a Diamond Mesh Cod-End of a Trawl Net," *Journal of Applied Mechanics*, vol. 75, 01 2008. 011018.

[72] J. Bessonneau and D. Marichal, "Study of the dynamics of submerged supple nets (applications to trawls)," *Ocean Engineering*, vol. 25, no. 7, pp. 563–583, 1998.

[73] C.-W. Lee, J.-H. Lee, B.-J. Cha, H.-Y. Kim, and J.-H. Lee, "Physical modeling for underwater flexible systems dynamic simulation," *Ocean Engineering*, vol. 32, no. 3, pp. 331–347, 2005.

[74] S.-K. Karumathil and M. Gonzalez, "Simulation of fluid flow across net structures with a porous media approach," in *Contributions on the Theory of Fishing Gears and Related Marine Systems*, vol. 11, 2019.

[75] A. Shields, "Application of similarity principles, and turbulence research to bed-load movement," 1936.

[76] A. D. Rijnsdorp, J. J. Poos, F. J. Quirijns, R. HilleRisLambers, J. W. De Wilde, and W. M. Den Heijer, "The arms race between fishers," *Journal of Sea Research*, vol. 60, no. 1, pp. 126–138, 2008. Dynamics of Fish and Fishers.

[77] F. G. O'Neill and T. Noack, "The geometry and dynamics of Danish anchor seine ropes on the seabed," *ICES Journal of Marine Science*, vol. 78, pp. 125–133, 12 2020.

[78] S. A. Breimann, F. G. O'Neill, K. Summerbell, and D. J. Mayor, "Quantifying the resuspension of nutrients and sediment by demersal trawling," *Continental Shelf Research*, vol. 233, p. 104628, 2022.

[79] M. Sokolova, F. G. O'Neill, E. Savina, and L. A. Krag, "Test and development of a sediment suppressing system for catch monitoring in demersal trawls," *Fisheries Research*, vol. 251, p. 106323, 2022.

Appendices

Appendix A

Resumen extendido

Introducción

Los peces y otros organismos vivos en el mar juegan un papel importante como fuente de alimento para la población mundial. En diferentes partes del mundo existen muchas formas de capturar y también criar peces del mar. Las técnicas de pesca de arrastre de fondo y cerco representan el 53 % de la captura mundial de peces y el arrastre de fondo causa más del 60 % de los descartes de pescado [4]. Las últimas décadas fueron cruciales tanto para la industria pesquera como para la acuícola, ya que la demanda de pescado ha aumentado exponencialmente así como la necesidad de hacer que estas industrias sean más ecológicas. La FAO impuso regulaciones de desembarque exigiendo a los pescadores mejorar la selectividad de sus artes de pesca para conservar y revitalizar las pesquerías [5]. Mejorar la selectividad de los equipos de pesca y encontrar regulaciones para estos de acuerdo con las especies objetivo requiere de mucha investigación, incluidos experimentos en canales de ensayo y senderos marinos para los cambios que se hacen en cada equipo de pesca. Hay desarrollos notables en el poder computacional disponible durante las últimas décadas y, por lo tanto, invitan a más investigaciones sobre simulación computacional de equipos de pesca para mejorar la selectividad y reducir el impacto ambiental asociado a las diferentes técnicas de pesca. La red de pesca es la parte principal de un arte de pesca, siendo de naturaleza flexible es una parte difícil de simular en la pesca de arrastre.

Esta tesis pretende mejorar los métodos existentes para la simulación de redes de pesca utilizando dinámica de fluidos computacional, con el fin de tratar con formas complejas lo que observamos en las artes de pesca de la vida real. Las investigaciones anteriores sobre simulación de redes de pesca se centraron principalmente en jaulas de acuicultura y utilizaron un método que modela la red como un sólido delgado. Aplicar ese método en artes de pesca complejas requiere mucho trabajo de procesamiento previo y es propenso a errores humanos. En esta tesis, se desarrolla un nuevo método para modelar paneles de redes como superficies porosas como una solución para tratar estas formas complejas que se encuentran en artes de pesca.

Objectivos

El principal objetivo de esta tesis es desarrollar un método para simular numéricamente el flujo a través de las redes de pesca que pueda ser aplicado a artes de pesca a escala real utilizados en diferentes pesquerías alrededor del mundo. Este objetivo principal se puede desglosar en las siguientes partes:

- Simular las redes de pesca modelando la red como una superficie porosa para manejar formas complejas de redes que se pueden ver en los artes de pesca.
- Investigar sobre las formas de encontrar los coeficientes de porosidad de un determinado tipo de red de pesca.
- Validar los métodos desarrollados utilizando investigaciones y experimentos previos.
- Aplicar el método desarrollado en problemas relacionados con la pesca y comprender la influencia hidrodinámica de las redes de pesca en las técnicas de pesca.

Dados los objetivos anteriores, las principales contribuciones de este trabajo se resumen a continuación:

- Un método para modelar la red como una superficie para aplicar modelos de medios porosos para simular artes de pesca, validado con datos experimentales.
- Un enfoque nuevo y eficiente para encontrar los coeficientes de resistencia de los medios porosos de una red de pesca dada utilizando mediciones experimentales y simulaciones CFD 2D.
- Un estudio en profundidad sobre el efecto de las redes de pesca arrastradas cerca del lecho marino para comprender y mejorar la pesca de arrastre demersal utilizando experimentos numéricos utilizando el enfoque de modelado de superficie.

Estructura de la tesis

Esta tesis se ha organizado en 5 capítulos con los tres capítulos principales (2,3,4) escritos como documentos independientes que incluyen la metodología, los resultados y las conclusiones:

Capítulo 1 presenta la introducción a la tesis incluyendo los antecedentes del estudio, el estado del arte discutiendo el desarrollo reciente en el área y la motivación de la tesis y los objetivos que se desean completar con la tesis.

Capítulo 2 describe la implementación de un modelo de superficie porosa y la validación con experimentos de investigaciones anteriores.

Capítulo 3 describe un nuevo método para calcular los coeficientes de resistencia de un medio poroso a partir de datos experimentales.

Capítulo 4 muestra el uso del modelo descrito en 2 para investigaciones y una mejor comprensión del efecto de arrastrar la red de pesca cerca del lecho marino y el estudio de sedimentos arrastre debido al arrastre de la red de pesca cerca del lecho marino.

Capítulo 5 concluye los trabajos realizados en la tesis y también propone las futuras líneas de investigación.

Modelado de red como superficies porosas

La industria pesquera y los campos de la acuicultura se enfrentan a más desafíos en los últimos años, lo que requiere una predicción precisa de la respuesta de las redes de pesca flexibles en el agua. Esta red flexible en el agua es un problema de interacción de estructuras fluidas. Un modelado detallado de la red como una estructura sólida con cordeles y nudos para resolver la parte fluida de este problema de interacción de estructura fluida es computacionalmente costoso de simular. Como consecuencia necesaria, se usa un enfoque de medios porosos para interpretar el efecto causado por la red, con la red modelada como un medio poroso sólido delgado y la caída de presión a través de la red evaluada usando el modelo de medios porosos de Darcy-Forchheimer. Para las redes de pesca a escala real, el modelado de redes como un medio poroso sólido y delgado sigue siendo computacionalmente costoso y difícil de modelar para formas de redes complejas. En esta investigación se implementa un nuevo método donde la red se modela como una superficie y las celdas cercanas a las superficies se agrupan según su orientación para aplicar la resistencia del medio poroso. Este enfoque de modelado de superficies no solo minimiza las dificultades para modelar formas complejas, sino que también reduce el gasto computacional al no tener que hacer mallas muy finas a lo largo del grosor de la red. También ayuda a un fácil acoplamiento entre el solver sólido y el solver fluido ya que las redes se modelan como superficies trianguladas. El método actual ha sido validado con investigaciones experimentales pasadas y se obtuvo un buen ajuste entre los resultados.

Se exige la simulación computacional de redes de pesca para comprender la hidrodinámica de los artes de pesca y las jaulas de acuicultura. Recientemente se ha propuesto un enfoque de medios porosos para representar los paneles de red como sólidos porosos delgados en simulaciones CFD, que demostró ser una alternativa eficiente a los modelos detallados de nudos y cordeles con condiciones de contorno tradicionales sin deslizamiento. En este estudio, se propone un nuevo método para modelar los paneles de red como superficies porosas en lugar de sólidos porosos delgados, con el objetivo de simplificar el modelado de configuraciones de red con formas complejas, como se ve en los artes de pesca de la vida real.

En el ejemplo 1 (Sección 2.4.1), el método propuesto se validó con los resultados experimentales de [1]. Los resultados de las simulaciones CFD muestran una muy buena concordancia con las medidas experimentales, y los campos de flujo obtenidos también son muy similares a los obtenidos con el método tradicional basado en sólidos porosos delgados. También hemos encontrado que los resultados son independientes del grosor de las zonas porosas generadas, lo que permite utilizar incluso una o dos capas de células sin causar errores significativos. En el ejemplo 2 (Sección

2.4.2), se utilizó el método propuesto para simular una configuración de red compleja con intersecciones y redes curvas. Demostró que el método es capaz de lidiar con geometrías de red tan complejas. Las mejoras logradas con el enfoque propuesto son:

- Modelado de redes curvas. El enfoque tradicional requiere que el usuario los aproxime mediante una colección de sólidos delgados que no se superponen y que calcule las direcciones principales de los coeficientes de resistencia porosa para cada sólido, lo que requiere mucho tiempo y es propenso a errores. Con el enfoque propuesto, las redes curvas se describen mediante una malla triangular, que se genera fácilmente a partir de modelos CAD, y el proceso de generación de zonas porosas está completamente automatizado y, por lo tanto, es más rápido y libre de errores humanos.

- Modelado de múltiples redes con intersecciones. Nuevamente, el enfoque tradicional requiere que el usuario tenga cuidado para evitar la interferencia entre los sólidos delgados que modelan cada panel de red. El enfoque propuesto se ocupa automáticamente de las intersecciones y genera zonas porosas que no se superponen en esas regiones.

- Control más fácil del espesor de las zonas porosas. En el enfoque tradicional, el grosor se define implícitamente por el tamaño y la forma de los sólidos delgados que se utilizan para representar los paneles de la red: cambiar el grosor requiere modificar el modelo CAD y, probablemente, mallar nuevamente para lograr una malla de buena calidad alrededor de los sólidos. En el enfoque propuesto, el grosor es un parámetro del algoritmo: se puede modificar fácilmente sin cambiar las mallas triangulares de entrada utilizadas para describir los paneles de red o la malla computacional.

- Control más fácil del tamaño y número de zonas porosas. En el enfoque tradicional, el tamaño y el número dependen de cómo se aproximan las redes curvas por una colección de sólidos delgados. Aumentar el número de sólidos permite capturar mejor la curvatura de la red y obtener un modelo CFD más preciso, pero requiere mucho trabajo de preprocesamiento, como se explica en los puntos anteriores.

  En el enfoque propuesto, el tamaño y número de zonas porosas se controla fácilmente con el ángulo de umbral utilizado para agrupar triángulos con orientación similar en la malla de triángulos que describe la red. Nuevamente, se puede modificar fácilmente sin cambiar las mallas triangulares de entrada o la malla computacional.

- La capacidad de lidiar con grandes desviaciones. Como se mencionó en investigaciones anteriores [40, 48], modelar redes como sólidos de medios porosos delgados puede crear complicaciones y celdas faltantes al simular grandes desviaciones. Con el enfoque propuesto, se crean zonas porosas continuas alrededor de las superficies que representan las redes, sin que falten celdas a pesar del nivel de deflexión de la red. Las celdas faltantes solo pueden ocurrir en costuras entre paneles de red que forman ángulos lejos de 180°.

Además, el enfoque propuesto puede facilitar la comunicación con un solucionador estructural en caso de problemas de interacción fluido-estructura, ya que algunos modelos estructurales para redes se basan en una malla triangular [14].

Estimación de coeficientes de resistencia de medios porosos

Modelar paneles de red como medios porosos delgados es un enfoque muy efectivo para llevar a cabo simulaciones de dinámica de fluidos computacional (CFD) de redes de pesca a gran escala y jaulas de acuicultura. Esta técnica requiere estimar a partir de datos experimentales los coeficientes de resistencia de la ecuación de D'arcy-Forchheimer para medios porosos. Existen dos métodos para esto, ambos basados en modelos analíticos simplificados que relacionar los coeficientes de arrastre y sustentación del panel de red con sus coeficientes de resistencia, y utilizar el análisis de regresión para estimar dichos coeficientes. En lugar de eso, proponemos un nuevo método que utiliza un modelo CFD completo del flujo a través de una capa de medios porosos, el mismo tipo de modelo utilizado para simular paneles de red a escala real en aplicaciones de pesca y acuicultura. Para aumentar el rendimiento computacional del análisis de regresión, la respuesta del modelo se calcula previamente mediante un estudio paramétrico e interpolados para construir un modelo de regresión eficiente. El método propuesto se aplica a diferentes paneles de red y los resultados se comparan con los métodos existentes. También investigamos: (i) la diferencia entre estimar los coeficientes de resistencia inercial y viscosa o estimando sólo las inerciales, como proponen algunos autores; (ii) el efecto de usar diferentes funciones de error en el análisis de regresión. Los resultados muestran que el método propuesto logra resultados similares o mejores que los métodos anteriores. Además, es más fácil de implementar y se puede utilizar para estimar los coeficientes de resistencia de materiales distintos de los paneles de red. Estimación de los coeficientes de resistencia inercial y viscosa siempre proporciona mejores resultados que estimar solo los coeficientes de inercia y no complica demasiado el análisis de regresión con el método propuesto. No está claro qué función de error proporciona mejores resultados, por lo tanto, recomendamos hacer el análisis de regresión con diferentes funciones de error y seleccionando el que funciona mejor para un conjunto de datos experimentales en particular.

Aplicación a la pesca de arrastre demersal

La pesca demersal y su impacto en la alteración de los fondos marinos es un área que necesita atención urgente. Los artes de arrastre y su impacto en la movilización de sedimentos se estudian ampliamente en los últimos años, aunque aún no se ha investigado la contribución de las redes de pesca en la movilización de sedimentos. En esta investigación, llevamos a cabo simulaciones numéricas de paneles de redes cerca del lecho marino para comprender el impacto de las redes de pesca en el arrastre de sedimentos durante la pesca de arrastre. Se ha llevado a cabo un estudio

exhaustivo para comprender la importancia de diferentes parámetros que son variables habituales en la pesca de arrastre demersal, incluida la velocidad de arrastre, los ángulos de ataque que hace la red con el fondo marino, la distancia desde el fondo marino, el tipo de red de pesca, la longitud de la pesca. net entre algunos de ellos. Los resultados muestran la dependencia de estos parámetros del transporte de sedimentos y también de las fuerzas hidrodinámicas, lo que contribuye a la eficiencia del remolque y permitirá una mejor evaluación del impacto ambiental de los artes de pesca remolcados.

Hemos demostrado que el esfuerzo cortante del lecho marino asociado con el flujo a través y alrededor de un panel de red depende de su altura sobre el lecho marino, su ángulo de ataque y su longitud, solidez y velocidad de remolque, mientras que los coeficientes hidrodinámicos de sustentación y arrastre son principalmente influenciado únicamente por el ángulo de ataque y la solidez, y que la altura sobre el fondo del mar es de poca importancia. Además, hemos demostrado, para los casos específicos examinados, que la magnitud del esfuerzo cortante en condiciones normales de operación puede ser lo suficientemente grande como para movilizar y suspender sedimentos desde limo fino hasta arena gruesa. En consecuencia, para realizar estimaciones precisas de la cantidad y la distribución del tamaño de las partículas del sedimento que se altera en la columna de agua durante el proceso de pesca, es necesario tener en cuenta todos estos parámetros. Esto es particularmente importante, ya que hasta la fecha, las estimaciones de la cantidad de sedimento movilizado por la red de arrastre han sido relativamente toscas y se basan en relaciones entre la resistencia de la red y las mediciones empíricas de la cantidad de sedimento movilizado, que se han establecido para los componentes del arte que están en contacto con el fondo del mar. Hemos demostrado aquí que para los materiales de red remolcados sobre el lecho marino, no existe una relación tan directa entre la resistencia de la red y los esfuerzos cortantes del lecho responsables de la movilización de sedimentos.

Conclusiones y trabajo futuro

Estos métodos desarrollados se utilizaron de manera eficiente en un problema de la vida real de conocer el impacto de las redes de pesca en el transporte de sedimentos durante la pesca de arrastre demersal (capítulo 4). La pesca de arrastre demersal, a menudo denominada arrastre de fondo, es una de las principales técnicas de pesca practicadas en todo el mundo. Mientras se arrastra el arte de pesca a través del lecho marino, hay muchos problemas ambientales que deben abordarse, incluida la destrucción del medio ambiente béntico, entre algunos de ellos, la captura incidental muy alta. Los estudios anteriores sobre el impacto de los sedimentos durante la pesca de arrastre demersal se centran principalmente en las partes de los artes de pesca, como las puertas de arrastre para el impacto hidrodinámico y los artes de fondo para el impacto directo. Las redes de pesca son una parte importante de los artes de pesca y, aunque no entren en contacto directo con el lecho marino, arrastrarlas cerca del lecho marino tendrá un impacto en el arrastre de sedimentos. No hubo datos sobre la movilización de sedimentos debido a una red de pesca remolcada cerca del fondo marino. Se llevó a cabo un extenso estudio numérico para evaluar

diferentes parámetros y su efecto sobre las fuerzas hidrodinámicas y la movilización de sedimentos durante la pesca de arrastre.

Se realizaron simulaciones de un panel de red rígida para ser remolcado cerca de un fondo marino utilizando el modelo propuesto en la tesis en el capítulo 2. El estudio demostró el impacto de parámetros como la distancia del panel de la red al fondo marino, la longitud del panel de la red, el tipo de red utilizada (solidez de la red), el ángulo de ataque del panel al fondo marino y la velocidad de arrastre. sobre el movimiento o movilización de sedimentos del tipo limo fino a arena gruesa. Este estudio ayuda a proporcionar un punto de partida en las investigaciones sobre el impacto de las redes de pesca en el transporte de sedimentos durante la pesca de arrastre y buena comprensión y sobre la importancia de las variables antes mencionadas.

Durante esta tesis, las redes se consideran rígidas y se propone un nuevo método para simular el flujo de fluidos a través de ellas. El comportamiento de la red en un arte de pesca no es solo un problema de fluido sino un problema de interacción fluido-estructura. Los solucionadores estructurales deben predecir la forma de las redes de pesca flexibles para el campo de flujo particular. Y se debe realizar un acoplamiento entre estos fluidos y el solucionador estructural para poder capturar el movimiento correcto de las redes flexibles en un arte de pesca. Ya hay estudios sobre el acoplamiento del modelo de medios porosos con solucionadores de FEM sólidos. Dado que algunos de los solucionadores estructurales usan mallas trianguladas para representar redes [14], esta forma propuesta de modelar paneles de red facilitará un mejor acoplamiento entre los solucionadores de sólidos y fluidos. Esto debe aplicarse e investigarse en el futuro para completar la simulación de redes de pesca flexibles.